THE CONTROL OF CHAOS: THEORY AND APPLICATIONS

S. BOCCALETTI[a], C. GREBOGI[b], Y.-C. LAI[c], H. MANCINI[a], D. MAZA[a]

[a] *Department of Physics and Applied Mathematics, Institute of Physics, Universidad de Navarra, Irunlarrea s/n, 31080 Pamplona, Spain*
[b] *Institute for Plasma Research, Department of Mathematics, and Institute for Physical Science and Technology, University of Maryland, College Park, MD 20742, USA*
[c] *Dept. of Math. and Electrical Engineering, Center for Systems Science and Engineering Research, Arizona State University, Tempe, AZ 85287*

ELSEVIER

AMSTERDAM – LAUSANNE – NEW YORK – OXFORD – SHANNON – TOKYO

ELSEVIER

Physics Reports 329 (2000) 103–197

PHYSICS REPORTS

www.elsevier.com/locate/physrep

The control of chaos: theory and applications

S. Boccaletti[a], C. Grebogi[b], Y.-C. Lai[c], H. Mancini[a], D. Maza[a]

[a]*Department of Physics and Applied Mathematics, Institute of Physics, Universidad de Navarra, Irunlarrea s/n, 31080 Pamplona, Spain*

[b]*Institute for Plasma Research, Department of Mathematics, and Institute for Physical Science and Technology, University of Maryland, College Park, MD 20742, USA*

[c]*Dept. of Math and Electrical Engineering, Center for Systems Science and Engineering Research, Arizona State University, Tempe, AZ 85287, USA*

Received June 1999; editor: I. Procaccia

Contents

PII: S0370-1573(99)00096-4

Abstract

Control of chaos refers to a process wherein a tiny perturbation is applied to a chaotic system, in order to realize a desirable (chaotic, periodic, or stationary) behavior. We review the major ideas involved in the control of chaos, and present in detail two methods: the Ott–Grebogi–Yorke (OGY) method and the adaptive method. We also discuss a series of relevant issues connected with chaos control, such as the targeting problem, i.e., how to bring a trajectory to a small neighborhood of a desired location in the chaotic attractor in both low and high dimensions, and point out applications for controlling fractal basin boundaries. In short, we describe procedures for stabilizing desired chaotic orbits embedded in a chaotic attractor and discuss the issues of communicating with chaos by controlling symbolic sequences and of synchronizing chaotic systems. Finally, we give a review of relevant experimental applications of these ideas and techniques.

PACS: 05.45. + b

1. Introduction

1.1. The control of chaos: exploiting the critical sensitivity to initial conditions to play with chaotic systems

A deterministic system is said to be *chaotic* whenever its evolution sensitively depends on the initial conditions. This property implies that two trajectories emerging from two different closeby initial conditions separate exponentially in the course of time. The necessary requirements for a deterministic system to be chaotic are that the system must be nonlinear, and be at least three dimensional.

The fact that some dynamical model systems showing the above necessary conditions possess such a critical dependence on the initial conditions was known since the end of the last century. However, only in the last thirty years, experimental observations have pointed out that, in fact, chaotic systems are common in nature. They can be found, for example, in Chemistry (Belouzov–Zhabotinski reaction), in Nonlinear Optics (lasers), in Electronics (Chua–Matsumoto circuit), in Fluid Dynamics (Rayleigh–Bénard convection), etc. Many natural phenomena can also be characterized as being chaotic. They can be found in meteorology, solar system, heart and brain of living organisms and so on.

Due to their critical dependence on the initial conditions, and due to the fact that, in general, experimental initial conditions are never known perfectly, these systems are instrinsically unpredictable. Indeed, the *prediction* trajectory emerging from a *bonafide* initial condition and the *real* trajectory emerging from the *real* initial condition diverge exponentially in course of time, so that the error in the prediction (the distance between prediction and real trajectories) grows exponentially in time, until making the system's real trajectory completely different from the predicted one at long times.

For many years, this feature made chaos undesirable, and most experimentalists considered such characteristic as something to be strongly avoided. Besides their critical sensitivity to initial conditions, chaotic systems exhibit two other important properties. Firstly, there is an infinite number of unstable periodic orbits embedded in the underlying chaotic set. In other words, the skeleton of a chaotic attractor is a collection of an infinite number of periodic orbits, each one being unstable. Secondly, the dynamics in the chaotic attractor is ergodic, which implies that during its temporal evolution the system ergodically visits small neighborhood of every point in each one of the unstable periodic orbits embedded within the chaotic attractor.

A relevant consequence of these properties is that a chaotic dynamics can be seen as shadowing some periodic behavior at a given time, and erratically jumping from one to another periodic orbit. The idea of controlling chaos is then when a trajectory approaches ergodically a desired periodic orbit embedded in the attractor, one applies small perturbations to stabilize such an orbit. If one switches on the stabilizing perturbations, the trajectory moves to the neighborhood of the desired periodic orbit that can now be stabilized. This fact has suggested the idea that the critical sensitivity of a chaotic system to changes (perturbations) in its initial conditions may be, in fact, very desirable in practical experimental situations. Indeed, if it is true that a small perturbation can give rise to a very large response in the course of time, it is also true that a judicious choice of such a perturbation can direct the trajectory to wherever one wants in the attractor, and to produce a series of *desired* dynamical states. This is exactly the idea of targeting.

The important point here is that, because of chaos, one is able to produce an infinite number of desired dynamical behaviors (either periodic and not periodic) using *the same* chaotic system, with the only help of *tiny* perturbations chosen properly. We stress that this is not the case for a nonchaotic dynamics, wherein the perturbations to be done for producing a desired behavior must, in general, be of the same order of magnitude as the unperturbed evolution of the dynamical variables.

The idea of chaos control was enunciated at the beginning of this decade at the University of Maryland [1]. In Ref. [1], the ideas for controlling chaos were outlined and a method for stabilizing an unstable periodic orbit was suggested, as a proof of principle. The main idea consisted in waiting for a natural passage of the chaotic orbit close to the desired periodic behavior, and then applying a small judiciously chosen perturbation, in order to stabilize such periodic dynamics (which would be, in fact, unstable for the unperturbed system). Through this mechanism, one can use a given laboratory system for producing an infinite number of different periodic behavior (the infinite number of its unstable periodic orbits), with a great flexibility in switching from one to another behavior. Much more, by constructing appropriate goal dynamics, compatible with the chaotic attractor, an operator may apply small perturbations to produce any kind of desired dynamics, even not periodic, with practical application in the coding process of signals.

1.2. From the Ott–Grebogi–Yorke ideas and technique to the other control methods

It is reasonable to assume that one does not have complete knowledge about the system dynamics since our system is typically complicated and has experimental imperfections. It is better, then, to work in the space of solutions since the equations, even if available, are not too useful due to the sensitivity of the dynamics to perturbations. One gets solutions by obtaining a time series of one dynamically relevant variable. The right perturbation, therefore, to be applied to the system is selected after a learning time, wherein the dependence of the dynamics on some external control is tested experimentally. Such perturbation can affect either a control parameter of the system, or a state variable. In the former case, a perturbation on some available control parameter is applied, in the latter case a feedback loop is designed on some state variable of the system.

The first example of the former case is reported in Ref. [1]. Let us draw the attention on a chaotic dynamics developing onto an attractor in a D-dimensional phase space. One can construct a section of the dynamics such that it is perpendicular to the chaotic flow (it is called Poincaré section). This $(D-1)$-dimensional section retains all the relevant information of the dynamics, which now is seen as a mapping from the present to the next intersection of the flow with the Poincare' section. Any periodic behavior is seen here as a periodic cycling among a discrete number of points (the number of points determines the periodicity of the periodic orbit). Since all periodic orbits in the unperturbed dynamics are unstable, also the periodic cycling in the map will be unstable. Furthermore, since, by ergodicity, the chaotic flow visits closely all the unstable periodic orbits, this implies that also the mapping in the section will visit closely all possible cycles of points corresponding to a periodic behavior of the system. Let us then consider a given periodic cycle of the map, such as period one. A period one cycle corresponds to a single point in the Poincaré section, which repeats itself indefinitely. Now, because of the instability of the corresponding orbit, this point in fact possesses a stable manifold and an unstable manifold. For stable (unstable) manifold we mean the collection of directions in phase space through which the trajectory

approaches (diverges away from) the point geometrically. The control of chaos idea consists in perturbing a control parameter when the natural trajectory is in a small neighborhood of the desired point, such that the next intersection with the Poincaré section puts the trajectory on the stable manifold. In this case, all divergences are cured, and the successive natural evolution of the dynamics, except for nonlinearities and noise, converges to the desired point (that is, it stabilizes the desired periodic behavior). Selection of the perturbation is done by means of a reconstruction from experimental data of the local linear properties of the dynamics around the desired point.

In some practical situations, however, it may be desirable to perform perturbations on a state variable accessible to the operator. This suggests the development of some alternative approaches. The first was introduced in Ref. [2]. It consists in designing a proper feedback line through which a state variable is directly perturbed such as to control a periodic orbit. This second method requires the availability of a state variable for experimental observation and for the perturbations. In such a case, a negative feedback line can be designed which is proportional to the difference between the actual value of the state variable, and the value delayed of a time lag T. The idea is that, when T coincides with the period of one unstable periodic orbit of the unperturbed system, the negative feedback pushes to zero the difference between the present and the delayed dynamics, and the periodic orbit is stabilized. Furthermore, as soon as the control becomes effective, this difference goes effectively to zero, so that the feedback perturbation vanishes. Moreover, as before, a preliminary learning time is needed, for learning the periods of the unstable periodic orbits. In the above mechanism, the proportionality constant entering in the feedback loop is given in Ref. [3] where an adaptive technique has been introduced which automatically selects this constant by adaptively exploiting the local dynamics of the system.

Many other techniques have been introduced with the aim of establishing control over chaos that will be referred to and described along this Report. Among the many available reviews, books, and monographies on this matter, here we address the reader the most recent ones, contained in Refs. [4–8]. In face of this huge number of theoretical studies, experimental realizations of chaos control have been achieved with a magnetoelastic ribbon [9], a heart [10,11], a thermal convection loop [12,13], a yttrium iron garnet oscillator [14], a diode oscillator [15], an optical multimode chaotic solid-state laser [16], a Belousov–Zhabotinski reaction diffusion chemical system [17], and many other experiments.

While control of chaos has been successfully demonstrated experimentally in many situations, the control of patterns in space-extended systems is still an open question. This is the reason why most of the interest has moved actually from the control of periodic behaviors in concentrated systems, to the control of periodic patterns in space-extended systems, with the aim of controlling infinite dimensional chaos, or even space–time chaos. The applications would be enormous, ranging from the control of turbulent flows, to the parallel signal transmission and computation to the parallel coding-decoding procedure, to the control of cardiac fibrillation, and so forth.

1.3. Targeting desirable states within chaotic attractors

One of the major problems in the above process is that one can switch on the control only when the system is sufficiently close to the desired behavior. This is warranted by the ergodicity of chaos regardless of the initial condition chosen for the chaotic evolution, but it may happen that the small neighborhood of a given attractor point (target) may be visited only infrequently, because

of the locally small probability function. Thus the unperturbed dynamics may take a long time to approach a given target, resulting in an unacceptably large waiting time for the operator to apply the control of chaos process.

Efficient targeting methods can, instead, reduce the waiting time by orders of magnitude, and so they can be seen as a preliminary task for chaos control, independent of the particular control algorithm that one applies. In this Report, we devote Section 4 to the problem of targeting of chaos, since it is crucial for the realization of the control procedure, and summarize the different proposed methods for directing chaotic trajectories to target points in the attractor.

1.4. The control of chaotic behaviors, and the communication with chaos

Another section of this Report is devoted to the problem of the control of desired chaotic behaviors and its major applications. The critical sensitivity to initial conditions of a chaotic system can, indeed, be exploited not only to produce a large number of possible periodic behaviors (the different unstable periodic orbit), but, much more generally, any desired behavior compatible with the natural evolution of the system. Therefore, one can imagine to select suitable perturbations to slave the chaotic system toward a particular "desired" chaotic behavior.

Among the practically unlimited possible applications of the control of chaotic behavior, herewith we concentrate on two applications, which have attracted considerable attention in the scientific community over the past few years; namely the control of chaotic behavior for communicating with chaos and for the synchronization of chaotic systems for various communication schemes. In the first case, a chaotic system is conveniently perturbed, in order to give rise to a particular chaotic trajectory carrying a given message. In the second case, the process of chaos synchronization is applied to a communication line between a message sender and a message receiver, allowing the synchronization between them.

There is a simple connection between chaos and communication theory. Chaotic systems can be viewed, indeed, as information sources that naturally produce digital communication signals. The formal connection between chaotic dynamics and information theory began with the introduction of the concept of measure-theoretic entropy in ergodic theory [18–20]. Chaotic systems are, indeed, characterized by having positive entropies and thus they are information sources. By assigning a discrete alphabet to the system state space using the formalism of symbolic dynamics, the chaotic system becomes a symbol source, and because it is a continuous-time waveform source, it is also a digital signal source. A chaotic system is, therefore, a natural source of digital communication signals. This concept has been recently shown to be more than formal [24]. Controlling the output of an oscillator via small guiding current pulses allows for the transmission of a desired message without effectively altering the time-evolution equations for the system. As an example, a very simple chaotic electrical oscillator can produce a seemingly random sequence of positive and negative (bipolar) voltage peaks [21]. If these bipolar peaks are assigned binary symbols 0 and 1, respectively, then the signal can be viewed as a binary communication waveform. We can furthermore encode any desired message into the waveform by using small perturbing pulses to control the sequence of peaks representing the symbols 0 and 1. More sophisticated waveforms and encodings are possible, but this example suffices to convey the basic concept. In this Report, we also

summarize the most relevant achievements in communicating with chaos, and we suggest some problems still unsolved.

The control of chaotic behavior has another important application, namely, the synchronization of chaotic systems. If one consider two identical chaotic systems starting from different initial conditions, then the critical sensitivity to initial conditions implies that their difference grows exponentially in time, and that they will evolve in an unsynchronized manner. The feeding of the right signal from one system to another can, however, reduce to zero such difference, and push the two systems into a synchronized manifold, wherein the chaotic motion is now developed so as the system are in step during the course of time. This proposal was intensively pushed forward at the beginning of this decade [22]. In the present Report, we simply summarize a possible application of synchronization of chaos, consisting in making secure the transmission of a signal between a message sender and a receiver along a communication line.

1.5. The experimental verifications of chaos control

Finally, we devote a section to summarize the most relevant experimental applications of the above ideas and techniques. Since it would be unrealistic to cover the whole body of experimental implementations of chaos control, herewith we limit ourselves to focus on few prototypical experiments, and we suggest to the interested reader to the most relevant literature.

The OGY ideas found experimental applications in several different fields, such as mechanical oscillations (magnetoelastic ribbon), electronic circuits (diode resonator), chemical systems (Belouzov–Zhabotinski reaction), nonlinear optics (multimode laser). Different control techniques were also experimentally tested on fluid dynamical systems leading to the control of convective instabilities, and on biomechanical systems for the control of the cardiac activity in a rabbit heart, and of the neuronal activity of an hippocampal slice. In every experimental example, we point out the relevance of the achievements, the difficulties for the practical realization of the theoretical proposals, and the perspective opened by such implementations.

1.6. Outline of the Report

The present Report is organized as follows.

In Section 2, the OGY method is illustrated with applications to one-dimensional and two-dimensional mappings. The pole placement technique is then discussed for the control of higher-dimensional situations. In Section 3, we discuss alternative schemes for chaos control, and we describe in detail the adaptive strategy with application to delayed dynamical systems, since it constitutes a bridge between concentrated and spatially extended systems. Section 4 is devoted to the discussion of the targeting problem. We show how the OGY criterion and adaptivity can provide suitable tools for directing the chaotic trajectories to desired targets. Furthermore, we show a possible application for the control of fractal basin boundaries. In Section 5, we discuss the issue of stabilizing desirable chaotic trajectories, and we point out two main applications: the communication with chaos, and communication through chaos synchronization. Section 6 summarizes the main experimental work in chaos control, and points out the perspective open in different fields by this process.

2. The OGY method of controlling chaos

2.1. The basic idea

Besides the occurrence of chaos in a large variety of natural processes, chaos may also occur because one may wish to design a physical, biological or chemical experiment, or to project an industrial plant to behave in a chaotic manner. The idea of Ott, Grebogi, and Yorke (OGY) is that chaos may indeed be desirable since it can be controlled by using small perturbation to some accessible parameter [1,23] or to some dynamical variable of the system [24].

The major key ingredient for the control of chaos [1,23] is the observation that a chaotic set, on which the trajectory of the chaotic process lives, has embedded within it a large number of unstable low-period periodic orbits. In addition, because of ergodicity, the trajectory visits or accesses the neighborhood of each one of these periodic orbits. Some of these periodic orbits may correspond to a desired system's performance according to some criterion. The second ingredient is the realization that chaos, while signifying sensitive dependence on small changes to the current state and henceforth rendering unpredictable the system state in the long time, also implies that the system's behavior can be altered by using small perturbations [1,23]. Then, the accessibility of the chaotic systems to many different periodic orbits combined with its sensitivity to small perturbations allows for the control and the manipulation of the chaotic process. Specifically, the OGY approach is then as follows. One first determines some of the unstable low-period periodic orbits that are embedded in the chaotic set. One then examines the location and the stability of these orbits and chooses one which yields the desired system performance. Finally, one applies small control to stabilize this desired periodic orbit. However, all this can be done from data [1,23] by using nonlinear time series analysis for the observation, understanding and control of the system. This is particularly important since chaotic systems are rather complicated and the detailed knowledge of the equations of the process is often unknown.

In what follows, we first give a pedagogical example of controlling chaos by using a simple one-dimensional map. We describe a general method for two-dimensional maps. Issues of noise and the average time of achieve control will also be discussed. We then describe the pole-placement method for controlling high-dimensional chaos, and we discuss how controlling chaos can be done when the equations of the systems are not available.

2.2. A one-dimensional example

The basic idea of controlling chaos can be understood [25] by considering the following one-dimensional logistic map, one of the best studied chaotic systems:

$$x_{n+1} = f(x_n, r) = r x_n (1 - x_n) \,, \tag{1}$$

where x is restricted to the unit interval [0,1], and r is a control parameter. It is known that this map develops chaos via the period-doubling bifurcation route. For $0 < r < 1$, the asymptotic state of the map (or the attractor of the map) is $x = 0$; for $1 < r < 3$, the attractor is a nonzero fixed point $x_F = 1 - 1/r$; for $3 < r < 1 + \sqrt{6}$, this fixed point is unstable and the attractor is a stable period-2 orbit. As r is increased further, a sequence of period-doubling bifurcations occurs in which

successive period-doubled orbits become stable. The period-doubling cascade accumulates at $r = r_\infty \approx 3.57$, after which chaos can arise.

Consider the case $r = 3.8$ for which the system is apparently chaotic. An important characteristic of a chaotic attractor is that there exists *an infinite number of unstable periodic orbits embedded within it*. For example, there are a fixed point $x_F \approx 0.7368$ and a period-2 orbit with components $x(1) \approx 0.3737$ and $x(2) = 0.8894$, where $x(1) = f(x(2))$ and $x(2) = f(x(1))$.

Now suppose we want to avoid chaos at $r = 3.8$. In particular, we want trajectories resulting from a randomly chosen initial condition x_0 to be as close as possible to the period-2 orbit, assuming that this period-2 orbit gives the best system performance. Of course, we can choose the desired asymptotic state of the map to be any of the infinite number of unstable periodic orbits. Suppose that the parameter r can be finely tuned in a small range around the value $r_0 = 3.8$, i.e., r is allowed to vary in the range $[r_0 - \delta, r_0 + \delta]$, where $\delta \ll 1$. Due to the nature of the chaotic attractor, a trajectory that begins from an arbitrary value of x_0 will fall, with probability one, into the neighborhood of the desired period-2 orbit at some later time. The trajectory would diverge quickly from the period-2 orbit if we do not intervene. Our task is to program the variation of the control parameter so that the trajectory stays in the neighborhood of the period-2 orbit as long as the control is present. In general, the small parameter perturbations will be time dependent. We emphasize that it is important to apply only small parameter perturbations. If large parameter perturbations are allowed, then obviously we can eliminate chaos by varying r from 3.8 to 2.0 for example. Such a large change is not interesting.

The logistic map in the neighborhood of a periodic orbit can be approximated by a linear equation expanded around the periodic orbit. Denote the target period-m orbit to be controlled as $x(i)$, $i = 1, \ldots, m$, where $x(i+1) = f(x(i))$ and $x(m+1) = x(1)$. Assume that at time n, the trajectory falls into the neighborhood of component i of the period-m orbit. The linearized dynamics in the neighborhood of component $i+1$ is then:

$$\begin{aligned} x_{n+1} - x(i+1) &= \frac{\partial f}{\partial x}[x_n - x(i)] + \frac{\partial f}{\partial r}\Delta r_n \\ &= r_0[1 - 2x(i)][x_n - x(i)] + x(i)[1 - x(i)]\Delta r_n \ , \end{aligned} \tag{2}$$

where the partial derivatives are evaluated at $x = x(i)$ and $r = r_0$. We require x_{n+1} to stay in the neighborhood of $x(i+1)$. Hence, we set $x_{n+1} - x(i+1) = 0$, which gives

$$\Delta r_n = r_0 \frac{[2x(i) - 1][x_n - x(i)]}{x(i)[1 - x(i)]} \ . \tag{3}$$

Eq. (3) holds only when the trajectory x_n enters a small neighborhood of the period-m orbit, i.e., when $|x_n - x(i)| \ll 1$, and hence the required parameter perturbation Δr_n is small. Let the length of a small interval defining the neighborhood around each component of the period-m orbit be 2ε. In general, the required maximum parameter perturbation δ is proportional to ε. Since ε can be chosen to be arbitrarily small, δ also can be made arbitrarily small. As we will see, the average transient time before a trajectory enters the neighborhood of the target periodic orbit depends on ε (or δ). When the trajectory is outside the neighborhood of the target periodic orbit, we do not apply any parameter perturbation, so the system evolves at its nominal parameter value r_0. Hence

we set $\Delta r_n = 0$ when $\Delta r_n > \delta$. Note the parameter perturbation Δr_n depends on x_n and is time dependent.

The above strategy for controlling the orbit is very flexible for stabilizing different periodic orbits at different times. Suppose we first stabilize a chaotic trajectory around a period-2 orbit. Then we might wish to stabilize the fixed point of the logistic map, assuming that the fixed point would correspond to a better system performance at a later time. To achieve this change of control, we simply turn off the parameter control with respect to the period-2 orbit. Without control, the trajectory will diverge from the period-2 orbit exponentially. We let the system evolve at the parameter value r_0. Due to the nature of chaos, there comes a time when the chaotic trajectory enters a small neighborhood of the fixed point. At this time we turn on a new set of parameter perturbations calculated with respect to the fixed point. The trajectory can then be stabilized around the fixed point [25].

In the presence of external noise, a controlled trajectory will occasionally be 'kicked' out of the neighborhood of the periodic orbit. If this behavior occurs, we turn off the parameter perturbation and let the system evolve by itself. With probability one the chaotic trajectory will enter the neighborhood of the target periodic orbit and be controlled again. The effect of the noise is to turn a controlled periodic trajectory into an intermittent one in which chaotic phases (uncontrolled trajectories) are interspersed with laminar phases (controlled periodic trajectories) [1,23]. It is easy to verify that the averaged length of the laminar phase increases as the noise amplitude decreases [25].

It is interesting to ask how many iterations are required on average for a chaotic trajectory originating from an arbitrarily chosen initial condition to enter the neighborhood ε of the target periodic orbit. Clearly, the smaller the value of ε, the more iterations that are required. In general, the average transient time $\langle\tau\rangle$ before turning on control scales with δ as:

$$\langle\tau\rangle \sim \delta^{-\gamma} , \tag{4}$$

where $\gamma > 0$ is a scaling exponent. For one-dimensional maps, the probability that a trajectory enters the neighborhood of a particular component (component i) of the periodic orbit is given by

$$P(\varepsilon) = \int_{x(i)-\varepsilon}^{x(i)+\varepsilon} \rho[x(i)]\,\mathrm{d}x \approx 2\varepsilon\rho[x(i)] , \tag{5}$$

where ρ is the frequency that a chaotic trajectory visits a small neighborhood of the point x on the attractor. We have $\langle\tau\rangle = 1/P(\varepsilon) \sim \varepsilon^{-1} \sim \delta^{-1}$, and therefore $\gamma = 1$. For higher-dimensional chaotic systems, the exponent γ can be related to the eigenvalues of the periodic orbit to be controlled.

A major advantage of the controlling chaos idea [1,23] is that it can be applied to experimental systems in which a priori knowledge of the system is usually not known. A time series found by measuring one of the system's dynamical variables in conjunction with the time delay embedding method [26,27], which transforms a scalar time series into a trajectory in phase space, is sufficient to determine the desired unstable periodic orbits to be controlled and the relevant quantities required to compute parameter perturbations [1,23]. The theoretical issue of using delay-coordinate embedding technique to control chaos will be detailed in Section 2.4. Another advantage of the OGY paradigm of controlling chaos is its flexibility in choosing the desired periodic orbit to be controlled, as we have detailed in the example of the logistic map.

2.3. Controlling chaos in two dimensions

The general algorithm for controlling chaos for two-dimensional invertible maps (or three-dimensional autonomous flows that can be reduced to two-dimensional maps on the Poincaré surface of section) can be formulated in a similar way. Consider the following map:

$$\boldsymbol{x}_{n+1} = \boldsymbol{F}(\boldsymbol{x}_n, p) \ , \tag{6}$$

where $\boldsymbol{x}_n \in \mathbf{R}^2$, $\boldsymbol{F}$ is a smooth function of its variables, and $p \in \mathbf{R}$ is an externally accessible control parameter. We restrict parameter perturbations to be small:

$$|p - \bar{p}| < \delta \ , \tag{7}$$

where $\bar{p}$ is some nominal parameter value, and $\delta \ll 1$ defines the range of parameter variation. We wish to program the parameter p so that a chaotic trajectory is stabilized when it enters an ε-neighborhood of the target periodic orbit. In the sequel, we first discuss the simple case of stabilizing a fixed point of the map $\boldsymbol{F}$. We then give a method for stabilizing higher-period periodic orbits.

2.3.1. Stabilizing a fixed point

2.3.1.1. A linear control law. Let $\boldsymbol{x}_F(\bar{p})$ be one of the fixed points of the map (6) at the nominal parameter value $\bar{p}$ that we wish to stabilize. In general, the location of the fixed point in the phase space depends on the control parameter p. Upon application of a small perturbation Δp, we have $p = \bar{p} + \Delta p$. Since Δp is small, we expect $\boldsymbol{x}_F(p)$ to be close to $\boldsymbol{x}_F(\bar{p})$. We write

$$\boldsymbol{x}_F(p) \approx \boldsymbol{x}_F(\bar{p}) + \boldsymbol{g}\,\Delta p \ , \tag{8}$$

where the vector $\boldsymbol{g}$ is given by

$$\boldsymbol{g} \equiv \left.\frac{\partial \boldsymbol{x}_F}{\partial p}\right|_{p=\bar{p}} \approx \frac{\boldsymbol{x}_F(p) - \boldsymbol{x}_F(\bar{p})}{\Delta p} \ . \tag{9}$$

The vector $\boldsymbol{g}$ needs to be determined before a control law can be derived to stabilize the fixed point $\boldsymbol{x}_F(\bar{p})$.

The simplest way to formulate an applicable control law is to make use of the fact that the dynamics of any smooth nonlinear system is approximately linear in a small ε-neighborhood of a fixed point. Thus, near $\boldsymbol{x}_F(\bar{p})$, we can use the linear approximation for the map:

$$[\boldsymbol{x}_{n+1} - \boldsymbol{x}_F(p)] \approx \boldsymbol{M}[\boldsymbol{x}_F(p)] \cdot [\boldsymbol{x}_n - \boldsymbol{x}_F(p)] \ , \tag{10}$$

where $\boldsymbol{M}[\boldsymbol{x}_F(p)]$ is the 2×2 Jacobian matrix of the map $\boldsymbol{F}(\boldsymbol{x}, p)$ evaluated at the fixed point $\boldsymbol{x}_F(p)$, which is defined as follows:

$$\boldsymbol{M}[\boldsymbol{x}_F(p)] = \left.\frac{\partial \boldsymbol{F}}{\partial \boldsymbol{x}}\right|_{\boldsymbol{x}_F(p)} \approx \boldsymbol{M}[\boldsymbol{x}_F(\bar{p})] + \left.\frac{\partial \boldsymbol{M}}{\partial p}\right|_{p=\bar{p}} \Delta p \ . \tag{11}$$

Note that $\Delta p \sim \varepsilon$ and $|[\boldsymbol{x}_n - \boldsymbol{x}_F(p)]| \sim \varepsilon$, where ε is the size of the small neighborhood in which the linear approximation (10) is valid. Writing $\boldsymbol{x}_F(p) \approx \boldsymbol{x}_F(\bar{p}) + \boldsymbol{g}\,\Delta p$ [from Eq. (9)], substituting this

relation and Eq. (11) into Eq. (10), and keeping only terms which are first-order in ε, we obtain

$$\boldsymbol{x}_{n+1} - \boldsymbol{x}_F(\bar{p}) \approx \boldsymbol{g}\,\Delta p + \boldsymbol{M}[\boldsymbol{x}_F(\bar{p})]\cdot[\boldsymbol{x}_n - \boldsymbol{x}_F(\bar{p}) - \boldsymbol{g}\,\Delta p]\ . \tag{12}$$

In Eq. (12), the Jacobian matrix $\boldsymbol{M}$ is evaluated at the fixed point $\boldsymbol{x}_F(\bar{p})$ of the unperturbed system, which is the one to be stabilized. Since $\boldsymbol{x}_F(\bar{p})$ is embedded in the chaotic attractor, it is unstable and it has one stable and one unstable direction [28]. Let $\boldsymbol{e}_s$ and $\boldsymbol{e}_u$ be the stable and unstable unit eigenvectors at $\boldsymbol{x}_F(\bar{p})$, respectively, and let $\boldsymbol{f}_s$ and $\boldsymbol{f}_u$ be two unit vectors that satisfy $\boldsymbol{f}_s\cdot\boldsymbol{e}_s = \boldsymbol{f}_u\cdot\boldsymbol{e}_u = 1$ and $\boldsymbol{f}_s\cdot\boldsymbol{e}_u = \boldsymbol{f}_u\cdot\boldsymbol{e}_s = 0$, which are the relations by which the vectors $\boldsymbol{f}_s$ and $\boldsymbol{f}_u$ can be determined from the eigenvectors $\boldsymbol{e}_s$ and $\boldsymbol{e}_u$. The vectors $\boldsymbol{f}_s$ and $\boldsymbol{f}_u$ are the *contravariant* basis vectors associated with the eigenspace $\boldsymbol{e}_s$ and $\boldsymbol{e}_u$ [1,23]. The Jacobian matrix $\boldsymbol{M}[\boldsymbol{x}_F(\bar{p})]$ can then be written as:

$$\boldsymbol{M}[\boldsymbol{x}_F(\bar{p})] = \lambda_u\boldsymbol{e}_u\boldsymbol{f}_u + \lambda_s\boldsymbol{e}_s\boldsymbol{f}_s\ , \tag{13}$$

where λ_s and λ_u are the stable and unstable eigenvalues in the eigendirections $\boldsymbol{e}_s$ and $\boldsymbol{e}_u$, respectively.

When the trajectory point $\boldsymbol{x}_n$ falls into the small ε neighborhood of the desired fixed point $\boldsymbol{x}_F(\bar{p})$ so that Eq. (10) applies, a small parameter perturbation Δp_n can be applied at time n to make the fixed point shift slightly so that at the next iteration $(n+1)$, $\boldsymbol{x}_{n+1}$ falls on the stable direction of $\boldsymbol{x}_F(\bar{p})$. That is, we choose the parameter control Δp_n such that

$$\boldsymbol{f}_u\cdot[\boldsymbol{x}_{n+1} - \boldsymbol{x}_F(\bar{p})] = 0\ . \tag{14}$$

If $\boldsymbol{x}_{n+1}$ falls on the stable direction of $\boldsymbol{x}_F(\bar{p})$, we can then set the control perturbation to zero, and the trajectory for subsequent time will approach the fixed point at the geometrical rate λ_s. Thus for sufficiently small $[\boldsymbol{x}_n - \boldsymbol{x}_F(\bar{p})]$, we can substitute Eq. (12) into Eq. (14) to obtain $\Delta p_n = c_n$:

$$c_n = \frac{\lambda_u\boldsymbol{f}_u\cdot[\boldsymbol{x}_n - \boldsymbol{x}_F(\bar{p})]}{(\lambda_u - 1)\boldsymbol{f}_u\cdot\boldsymbol{g}} \equiv \boldsymbol{C}\cdot[\boldsymbol{x}_n - \boldsymbol{x}_F(\bar{p})]\ . \tag{15}$$

We assume in the above that the generic condition $\boldsymbol{g}\cdot\boldsymbol{f}_u \neq 0$ is satisfied so that $c_n \sim |\boldsymbol{x}_n - \boldsymbol{x}_F(\bar{p})|$, which is small. The considerations above apply only to a local small neighborhood of $\boldsymbol{x}_F(\bar{p})$. Globally, one can specify the parameter perturbation Δp_n by setting $\Delta p_n = 0$ if $|c_n|$ is too large, since the range of the parameter perturbation is limited by Eq. (7). Thus, practically, we can take Δp_n to be given by

$$\Delta p_n = \begin{cases} c_n & \text{if } |c_n| < \delta\ , \\ 0 & \text{if } |c_n| \geq \delta\ , \end{cases} \tag{16}$$

where in the definition of c_n in Eq. (15), it is not necessary to restrict the quantity $|\boldsymbol{x}_n - \boldsymbol{x}_F(\bar{p})|$ to be small.

Eqs. (15) and (16) are one formulation of the OGY-idea of controlling chaos [1,23]. There are several practical factors which must be considered when applying this formulation in practical situations. Among these are the following:

(a) The control situation is possible only if the quantity c_n defined in Eq. (15) satisfies $|c_n| < \delta$. This condition may be violated when the fixed point of the system is such that the vectors $\boldsymbol{g}$ and $\boldsymbol{f}_u$ are nearly orthogonal to each other. Such fixed points are therefore uncontrollable by using

small perturbations. In principle, the magnitude of the control $|c_n|$ can be made arbitrarily small since $|\boldsymbol{x}_n - \boldsymbol{x}_F(\bar{p})|$ can be made arbitrarily small by waiting for the trajectory $\boldsymbol{x}_n$ to be sufficiently close to the desired fixed point $\boldsymbol{x}_F(\bar{p})$. However, the average waiting time for this to occur can be significantly longer. There is thus a trade-off between the magnitude of the perturbations and the average waiting time. There are also nonlinear corrections to Eq. (10) which are typically quadratic in $[\boldsymbol{x}_n - \boldsymbol{x}_F(\bar{p})]$. The quadratic corrections are important in determining the average waiting time, which is, the average length of the chaotic transient experienced typically by trajectories before control is achieved.

(b) In real systems there is often noise present.

(c) There may be errors present in the measurements of the system states used in identifying the system. The location of the coordinates of the fixed point we wish to control may thus differ from its true coordinates. Similarly, the quantities $\boldsymbol{f}_u, \boldsymbol{f}_s, \lambda_u$, and λ_s which are required to compute the parameter perturbations may contain some error.

2.3.1.2. Time to achieve control. Let $\xi_n \equiv (\boldsymbol{x}_n - \boldsymbol{x}_F(\bar{p}))$. We note that the control in Eq. (16) is activated (i.e., $\Delta p_n \neq 0$) only when $|c_n| < \delta$, which in turn, determines a narrow strip region, in the phase space, along the stable direction of the fixed point to be stabilized:

$$|\xi_n^u| < \xi_* \ , \tag{17}$$

where $\xi_n^u \equiv \boldsymbol{f}_u \cdot \xi_n$, $\xi_n^s \equiv \boldsymbol{f}_s \cdot \xi_n$, and ξ_* can be determined by setting $c_n = \delta$. We obtain

$$\xi_* = \delta|(1 - \lambda_u^{-1})\boldsymbol{g} \cdot \boldsymbol{f}_u| \ . \tag{18}$$

Thus, for small δ, a typical trajectory resulting from a random initial condition will execute a chaotic motion, unchanged from the uncontrolled case, until ξ_n falls in the strip (Eq. (17)). Even then, due to the nonlinearity not included in the linear expansion (10), the control may not be able to bring the trajectory to the desired fixed point. In this case, the trajectory will leave the strip and continue to wander chaotically as if there was no control. Since the trajectory on the uncontrolled chaotic attractor is ergodic, which means that the trajectory will visit the neighborhood of every point on the attractor in the course of time evolution, at some time the trajectory will eventually come sufficiently close to the desired fixed point to satisfy $|c_n| < \delta$ so that control is achieved. Thus, in ideal situations (no noise and no imperfect identification in the system parameter), applying control creates a stable orbit, but, for a typical initial condition, it is preceded in time by a chaotic transient in which the orbit is similar to orbits on the uncontrolled chaotic attractor. The lengths of the chaotic transients are different for different initial conditions, and they can be regarded as realizations of a random variable τ with an exponential probability distribution:

$$P(\tau) \sim \exp[-\tau/\langle\tau\rangle] \ , \tag{19}$$

where $\langle\tau\rangle$ is the average length of the chaotic transient. When δ decreases, the size of the control strip (Eq. (17)) decreases, so the average time to achieve control, or $\langle\tau\rangle$, increases.

To understand the exponential distribution (19), imagine we choose a large number of points on the chaotic attractor according to the natural measure [29,30]. Regarding the strip area surrounding the desired fixed point $\boldsymbol{x}_F(\bar{p})$ as an "escaping" region, we see that under the dynamics, each

initial condition enters the escaping region in different times. These times can be considered as the lifetimes for trajectories to stay outside the escaping region. To find the probability distribution for these lifetimes, we iterate the escaping region backward in time under the inverse dynamics. The inverse images intersect the chaotic attractor along the stable foliations, creating a set of infinite number of gaps on the chaotic attractor (there are an infinite number of inverse images) and leaving behind a fractal set of points which never enters the escaping region. This fractal set is nonattracting because a point in the vicinity of the set will eventually leave it and enter one of the gaps. Since almost all points on the chaotic attractor fall into gaps, we see that the lifetimes for those points are in fact the escaping times that the points leave the nonattracting fractal set. It is known that the distribution of escaping times from a nonattracting fractal set is exponential [31,32]. Apparently, different choice of the control strip leads to different fractal sets. There are, in fact, an infinite number of nonattracting fractal sets embedded in the chaotic attractor. Such nonattracting fractal sets are also called *chaotic saddles* [33,34].

Following Refs. [1,23], we now derive the scaling law (4) and give a formula for the scaling exponent γ. Dotting the linearized map for ξ_{n+1}, (Eq. (12)), with $\boldsymbol{f}_{\mathrm{u}}$ and then with $\boldsymbol{f}_{\mathrm{s}}$, and using Eqs. (13) and (15) which is appropriate for $|\xi_n^{\mathrm{u}}| < \xi_*$, we obtain the following two relations for the size of the controlling strip:

$$\xi_{n+1}^{\mathrm{u}} \approx 0 \ , \tag{20}$$

$$\xi_{n+1}^{\mathrm{s}} \approx \lambda_0 \xi_n^{\mathrm{u}} + \lambda_{\mathrm{s}} \xi_n^{\mathrm{s}} \ , \tag{21}$$

where

$$\lambda_0 \equiv (1 - \lambda_{\mathrm{s}}) \frac{\lambda_{\mathrm{u}} \boldsymbol{g} \cdot \boldsymbol{f}_{\mathrm{s}}}{(\lambda_{\mathrm{u}} - 1) \boldsymbol{g} \cdot \boldsymbol{f}_{\mathrm{u}}} \ .$$

Eqs. (20) and (21) are linearizations, and typically the lowest-order corrections to them are quadratic. In particular, ξ_n^{s} is not restricted by $|\xi_n^{\mathrm{u}}| < \xi_*$ and thus may not be small when the control condition is satisfied. Thus we expect the correction that is quadratic in ξ_n^{s} to be most significant. Including such a correction in Eq. (20), we have

$$\xi_{n+1}^{\mathrm{u}} \approx \kappa (\xi_n^{\mathrm{s}})^2 \ , \tag{22}$$

where κ is a constant. Thus, if $|\kappa|(\xi_n^{\mathrm{s}})^2 > \xi_*$, then $|\xi_{n+1}^{\mathrm{u}}| > \xi_*$, and control is not achieved even though $|\xi_n^{\mathrm{u}}| < \xi_*$. Control is achieved when the trajectory falls in the small *control parallelogram* P_{c} given by

$$|\xi_n^{\mathrm{u}}| < \xi_* \ , \tag{23}$$

$$|\xi_n^{\mathrm{s}}| < \sqrt{\xi_*/|\kappa|} \ . \tag{24}$$

For very small ξ_*, a trajectory will wander on the uncontrolled chaotic attractor for a long time before it falls into the control parallelogram P_{c}. At any given time step, the probability of falling in P_{c} is approximately the natural measure [29,30] of the uncontrolled chaotic attractor contained in P_{c}. If one distributes a large number of initial conditions on the chaotic attractor according to the natural measure and then follows the trajectories resulting from these initial conditions, this probability $\mu(P_{\mathrm{c}})$ gives the rate at which these orbits fall into the control parallelogram. Let $N(n)$ be the uncontrolled orbits remaining at time n. If the chaotic transient is long, we can treat the discrete

time approximately as continuous. We obtain

$$\frac{\mathrm{d}N(n)}{\mathrm{d}n} = -\mu(P_c)N(n) \ .$$

Thus $\mu(P_c)$ is the inverse of the exponential decay time for $N(n)$ so that we have

$$\langle\tau\rangle^{-1} = \mu(P_c) \ . \tag{25}$$

To obtain the natural measure $\mu(P_c)$, we make use of the definition of the pointwise dimensions [29]. For the control parallelogram P_c, since its sizes along the stable and unstable directions of desired fixed point $\boldsymbol{x}_F(\bar{p})$ are $\sqrt{\xi_*/|\kappa|}$ and ξ_*, respectively, we obtain the following scaling of $\mu(P_c)$ with ξ_*:

$$\mu(P_c) \sim (\xi_*)^{d_u}(\sqrt{\xi_*/|\kappa|})^{d_s} \sim \xi_*^{d_u+(1/2)d_s} \sim (\xi_*)^{d_u+(1/2)d_s} \ ,$$

where d_s and d_u are the pointwise dimensions for the uncontrolled chaotic attractor at $\boldsymbol{x}_F(\bar{p})$ in the stable and unstable directions, respectively. Since $\xi_* \sim \Delta p$, we obtain the scaling relation (4), where the scaling exponent is given by

$$\gamma = d_u + \tfrac{1}{2}d_s \ . \tag{26}$$

Usually, the chaotic attractor is effectively smooth in the unstable direction [29], which implies $d_u = 1$. The pointwise dimension in the stable direction is given in terms of the stable and unstable eigenvalues at $\boldsymbol{x}_F(\bar{p})$ as, $d_s = (\ln|\lambda_u|/(\ln|\lambda_s|^{-1}))$. Thus

$$\gamma = 1 + \frac{1}{2}\frac{\ln|\lambda_u|}{\ln(1/|\lambda_s|)} \ . \tag{27}$$

The above scaling for the average time to achieve control is obtained under the assumption that the control is off for $|\xi_n^u| > \xi_*$. It is possible, in some situations, to greatly reduce $\langle\tau\rangle$ by applying small controls to the orbit in the region outside the control parallelogram. This is an example of another general type of chaos control problem, the so-called *target acquisition problem* [35–38]. In particular, the goal is to apply small perturbations to a chaotic trajectory so as to bring it from its initial condition to a target region in which the desired fixed point (or periodic orbits) located in the shortest possible time.

Note that in the above, the small neighborhood of the desired fixed point for turning on the control is assumed to have the shape of a parallelogram. One can also consider a small circular area around the desired fixed point. That is, the control is turned on when $|\xi_n| < \xi_*$. This again yields the algebraic scaling (4) but with a different exponent: in this case the exponent is the pointwise dimension $(d_u + d_s)$. Note that this value of the exponent is larger than that given by Eq. (26) due to the fact that the area of the circular region $|\xi_n| < \xi_*$ is much smaller than the control parallelogram P_c and is contained in P_c. Thus, the times to achieve control become longer and, hence, in practice it is more advantageous to consider the control parallelogram for turning on the control.

2.3.1.3. Effect of noise. To study the effect of noise on control, we add a term $\varepsilon\delta_n$ to the right-hand side of the linearized equations for ξ_{n+1}, (Eq. (12)), where δ_n is a random variable and ε is a small parameter specifying the intensity of the noise. To mimic environmental noise in a typical experimental setting, we take the random variable δ_n to have zero mean ($\langle\delta_n\rangle = 0$), be independent

($\langle \delta_n \delta_m \rangle = 0$ for $m \neq n$), have mean squared value unity ($\langle \delta_n^2 \rangle = 1$), and have a probability density independent of n (stationary random variable). Due to noise, the quantity ξ_{n+1}^{u}, which is the dot product between $\boldsymbol{f}_u$ and ξ_{n+1} (Eq. (12)), no longer vanishes when high-order nonlinear terms are neglected. Instead, we have

$$\xi_{n+1}^{u} = \varepsilon \delta_n^{u} , \tag{28}$$

where $\delta_n^{u} \equiv \boldsymbol{f}_u \cdot \delta_n$. If the noise is bounded, i.e., $|\delta_n^{u}| < \delta_{max}$, then the control will hardly be affected by noise if δ_{max} is smaller than the width of the control parallelogram ξ_*, i.e., if

$$\varepsilon \delta_{max} < \xi_* . \tag{29}$$

If Eq. (29) is not satisfied or if the noise is unbounded ($\delta_{max} = \infty$), then the noise can kick a controlled trajectory which is in the control parallelogram P_c into the region outside P_c.

A situation often encountered in practice is that the probability for large noise intensity is extremely low, such as the case where the noise distribution is Gaussiana. In this case, the loss of control due to noise-induced kick-outs (out of P_c) are rare because they are caused by low-probability tails on the probability density and, hence, the average time $\langle T \rangle$ for a controlled trajectory to be kicked out of P_c will be long. Thus a trajectory will typically alternate between epochs of chaotic motion of average time $\langle \tau \rangle$ in which it is far from the desired fixed point, and epochs of average length $\langle T \rangle$ in which the orbit is effectively controlled and lies in the control parallelogram. If $\langle T \rangle$ is much greater than $\langle \tau \rangle$, then the trajectory spends most of its time in the controlled epochs, and the control can be regarded as being effective.

The average time $\langle T \rangle$ for which control is maintained can be computed as follows. Let the probability density of the random variable δ_n^{u} be $P(\delta_n^{u})$. The quantity $\langle T \rangle$ is then the time for δ_n^{u} to become larger than $\delta_* \equiv \xi_*/\varepsilon$, which is the inverse of the probability for δ_n^{u} to lie outside the strip $|\delta_*|$. Thus, we have

$$\langle T \rangle = \left[\int_{-\infty}^{-\delta_*} P(\delta_n^{u}) \, d\delta_n^{u} + \int_{\delta_*}^{\infty} P(\delta_n^{u}) \, d\delta_n^{u} \right]^{-1} . \tag{30}$$

If $P(\delta_n^{u})$ is Gaussian and if δ_* is several times the standard deviation, then the kick-outs will correspond to δ_n^{u} in the far tails of the probability density. In this case, $\langle T \rangle$ will be large.

2.3.2. Stabilizing a periodic orbit of higher period

Let the desired period-m orbit be $\boldsymbol{x}(1, \bar{p}) \to \boldsymbol{x}(2, \bar{p}) \to \cdots \to \boldsymbol{x}(m, \bar{p}) \to \boldsymbol{x}(m+1, \bar{p}) = \boldsymbol{x}(1, \bar{p})$. The linearized dynamics in the neighborhood of component $i+1$ of the period-m orbit is

$$\boldsymbol{x}_{n+1} - \boldsymbol{x}(i+1, \bar{p}) = \boldsymbol{A} \cdot [\boldsymbol{x}_n - \boldsymbol{x}(i, \bar{p})] + \boldsymbol{B} \, \Delta p_n , \tag{31}$$

where $\Delta p_n = p_n - \bar{p}$, $\Delta p_n \leq \delta$, $\boldsymbol{A}$ is a 2×2 Jacobian matrix, and $\boldsymbol{B}$ is a two-dimensional column vector:

$$\begin{aligned} \boldsymbol{A} &= \boldsymbol{D}_x \boldsymbol{F}(\boldsymbol{x}, p)_{|x = x(i), p = \bar{p}} , \\ \boldsymbol{B} &= \boldsymbol{D}_p \boldsymbol{F}(\boldsymbol{x}, p)_{|x = x(i), p = \bar{p}} . \end{aligned} \tag{32}$$

In two dimensions, there exist a stable and an unstable directions at *each* component (point) of an unstable periodic orbit. The stable (unstable) direction is a direction along which points

approach (leave) the periodic orbit exponentially. (For higher-dimensional maps, there may be several stable and unstable directions.) Intuitively, the existence of both a stable and an unstable directions at each point of a periodic orbit can be seen as follows. Choose a small circle of radius ε around an orbit point $\boldsymbol{x}(i)$. This circle can be written as $\mathrm{d}x^2 + \mathrm{d}y^2 = \varepsilon^2$ in the Cartesian coordinate system whose origin is at $\boldsymbol{x}(i)$. The image of the circle under $\boldsymbol{F}^{-1}$ can be expressed as $A\,\mathrm{d}x'^2 + B\,\mathrm{d}x\,\mathrm{d}y' + C\,\mathrm{d}y'^2 = 1$, an equation for an ellipse in the Cartesian coordinate system whose origin is at $\boldsymbol{x}(i-1)$. The coefficients A, B and C are functions of elements of the inverse Jacobian matrix at $\boldsymbol{x}(i)$. This deformation from a circle to an ellipse means that the distance along the major axis of the ellipse at $\boldsymbol{x}(i-1)$ contracts as a result of the map. Similarly, the image of a circle at $\boldsymbol{x}(i-1)$ under $\boldsymbol{F}$ is typically an ellipse at $\boldsymbol{x}(i)$, which means that the distance along the inverse image of the major axis of the ellipse at $\boldsymbol{x}(i)$ expands under $\boldsymbol{F}$. Thus the major axis of the ellipse at $\boldsymbol{x}(i-1)$ and the inverse image of the major axis of the ellipse at $\boldsymbol{x}(i)$ approximate the stable and unstable directions at $\boldsymbol{x}(i-1)$. We note that typically the stable and unstable directions are not orthogonal to each other, and in rare situations they can be identical (nonhyperbolic dynamical systems) [34,39].

The stable and unstable directions at each point of an unstable periodic orbit can be computed using the algorithm developed in Ref. [34]. This algorithm can be applied to cases where the period of the orbit is arbitrarily large. To find the stable direction at a point $\boldsymbol{x}$, one first iterates this point forward N times under the map $\boldsymbol{F}$ and obtains the trajectory $\boldsymbol{F}^1(\boldsymbol{x}), \boldsymbol{F}^2(\boldsymbol{x}), \ldots, \boldsymbol{F}^N(\boldsymbol{x})$. Now imagine that a circle of small radius ε is placed at the point $\boldsymbol{F}^N(\boldsymbol{x})$. If this circle is iterated backward once, it becomes an ellipse at the point $\boldsymbol{F}^{N-1}(\boldsymbol{x})$, with the major axis along the stable direction of the point $\boldsymbol{F}^{N-1}(\boldsymbol{x})$. One can iterate this ellipse backwards continuously, while at the same time rescaling the ellipse's major axis to be order ε. When the ellipse is iterated back to the point $\boldsymbol{x}$, it becomes very thin with its major axis along the stable direction at the point $\boldsymbol{x}$, if N is sufficiently large. For a short period-m orbit, one can choose, say $N = km$, where k an integer. In practice, instead of using a small circle, one takes a unit vector at the point $\boldsymbol{F}^N(\boldsymbol{x})$, since the Jacobian matrix of the inverse map $\boldsymbol{F}^{-1}$ rotates a vector in the tangent space of $\boldsymbol{F}$ towards the stable direction. Hence one iterates a unit vector backward to the point $\boldsymbol{x}$ by multiplying by the Jacobian matrix of the inverse map at each point on the already existing orbit. The vector is rescaled after each multiplication to unit length. For sufficiently large N, the unit vector so obtained at $\boldsymbol{x}$ is a good approximation to the stable direction at $\boldsymbol{x}$.

Similarly, to find the unstable direction at point $\boldsymbol{x}$, one first iterates $\boldsymbol{x}$ backward under the inverse map N times to obtain a backward orbit $\boldsymbol{F}^{-j}(\boldsymbol{x})$ with $j = N, \ldots, 1$. One then chooses a unit vector at point $\boldsymbol{F}^{-N}(\boldsymbol{x})$ and iterates this unit vector forward to the point $\boldsymbol{x}$ along the already existing orbit by multiplying by the Jacobian matrix of the map N times. (Recall that the Jacobian matrix of the forward map rotates a vector towards the unstable direction.) The vector is rescaled to unit length at each step. The final vector at point $\boldsymbol{x}$ is a good approximation to the unstable direction at that point if N is sufficiently large.

The above method is efficient. For instance, the error between the calculated and real stable or unstable directions [34] is on the order of 10^{-10} for chaotic trajectories in the Hénon map [40] if $N = 20$.

Let $\boldsymbol{e}_{\mathrm{s},i}$ and $\mathrm{e}_{\mathrm{u},i}$ be the stable and unstable directions at $\boldsymbol{x}(i)$, and let $\boldsymbol{f}_{\mathrm{s},i}$ and $\boldsymbol{f}_{\mathrm{u},i}$ be the corresponding contravariant vectors that satisfy the conditions $\boldsymbol{f}_{\mathrm{u},i} \cdot \boldsymbol{e}_{\mathrm{u},i} = \boldsymbol{f}_{\mathrm{s},i} \cdot \boldsymbol{e}_{\mathrm{s},i} = 1$ and $\boldsymbol{f}_{\mathrm{u},i} \cdot \boldsymbol{e}_{\mathrm{s},i} = \boldsymbol{f}_{\mathrm{s},i} \cdot \boldsymbol{e}_{\mathrm{u},i} = 0$. To stabilize the orbit, we require that the next iteration of a trajectory point,

after falling into a small neighborhood about $\boldsymbol{x}(i)$, along the stable direction at $\boldsymbol{x}(i+1,\bar{p})$:

$$[\boldsymbol{x}_{n+1} - \boldsymbol{x}(i+1,\bar{p})]\cdot\boldsymbol{f}_{\mathrm{u},i+1} = 0\ . \tag{33}$$

Taking the dot product of both sides of Eq. (33) with $\boldsymbol{f}_{\mathrm{u},i+1}$ and use Eq. (31), we obtain the following expression for the parameter perturbations:

$$\Delta p_n = \frac{\{\boldsymbol{A}\cdot[\boldsymbol{x}_n - \boldsymbol{x}(i,\bar{p})]\}\cdot\boldsymbol{f}_{\mathrm{u},i+1}}{-\boldsymbol{B}\cdot\boldsymbol{f}_{\mathrm{u},i+1}}\ . \tag{34}$$

The general algorithm for controlling chaos for two-dimensional maps can thus be summarized as follows:

(a) Find the desired unstable periodic orbit to be stabilized.
(b) Find a set of stable and unstable directions, $\boldsymbol{e}_{\mathrm{s}}$ and $\boldsymbol{e}_{\mathrm{u}}$, at each component of the periodic orbit. The set of corresponding contravariant vectors $\boldsymbol{f}_{\mathrm{s}}$ and $\boldsymbol{f}_{\mathrm{u}}$ can be found by solving $\boldsymbol{e}_{\mathrm{s}}\cdot\boldsymbol{f}_{\mathrm{s}} = \boldsymbol{e}_{\mathrm{u}}\cdot\boldsymbol{f}_{\mathrm{u}} = 1$ and $\boldsymbol{e}_{\mathrm{s}}\cdot\boldsymbol{f}_{\mathrm{u}} = \boldsymbol{e}_{\mathrm{u}}\cdot\boldsymbol{f}_{\mathrm{s}} = 0$.
(c) Randomly choose an initial condition and evolve the system at the parameter value $\bar{p}$. When the trajectory enters the ε neighborhood of the target periodic orbit, calculate parameter perturbations at each time step according to Eq. (34).

2.4. Pole placement method of controlling chaos in high dimensions

We consider the following discrete-time high-dimensional dynamical system:

$$\boldsymbol{x}_{n+1} = \boldsymbol{F}(\boldsymbol{x}_n, p_n)\ , \tag{35}$$

where $\boldsymbol{x}_n \in \mathbf{R}^N$, $\boldsymbol{F}$ is a smooth vector function, p_n is an accessible parameter that can be externally perturbed. Continuous dynamical systems can be regarded as discrete maps on the Poincaré surface of section. Periodically driven dynamical systems have a natural Poincaré surface of section at the period of the driver. However, for autonomous dynamical systems such a section may not exist, or it may be singular if some of the trajectories take arbitrarily long time to return to it. One might need then, in order to discretize the dynamical process, to select some other kind of section whose choice typically depends on the particular system. We conceive using only small controls, so we restrict p to lie in some small interval, as in the control of low-dimensional chaos:

$$|p_n - \bar{p}| < \delta\ , \tag{36}$$

where $\bar{p}$ is a nominal parameter value. As in the low-dimensional case, if p_n is outside this interval, we set $p_n = \bar{p}$. Assuming that the dynamical system $\boldsymbol{F}(\boldsymbol{x}_n,\bar{p})$ possesses a chaotic attractor, the goal is to vary the parameter p_n within the range $(\bar{p}-\delta,\bar{p}+\delta)$ in such a way that for almost all initial conditions in the basin of the chaotic attractor, the dynamics of the system converges onto a desired time periodic orbit contained in the attractor. To do this we consider a small neighborhood of size comparable to δ of the desired periodic orbit. In this neighborhood, the dynamics is approximately linear. Since linear systems are stabilizable if the controllability assumption is obeyed, it is reasonable to assume that the chosen periodic orbit can be stabilized by feedback control. The ergodic nature of the chaotic dynamics guarantees that the state trajectory enters the

neighborhood. Once inside, we apply the stabilizing feedback control law to keep the trajectory in the neighborhood of the desired orbit.

For simplicity we describe the method as applied to the case where the desired orbit is a fixed point of the map $\boldsymbol{F}$. Consideration of periodic orbits of period larger than one is straightforward [41]. Let $\boldsymbol{x}_*(\bar{p})$ be an unstable fixed point on the attractor. For values of p_n close to $\bar{p}$ and in the neighborhood of the fixed point $\boldsymbol{x}_*(\bar{p})$, the map can be approximated by the linear map:

$$\boldsymbol{x}_{n+1} - \boldsymbol{x}_*(\bar{p}) = \boldsymbol{A}[\boldsymbol{x}_n - \boldsymbol{x}_*(\bar{p})] + \boldsymbol{B}(p_n - \bar{p}) \ , \tag{37}$$

where $\boldsymbol{A}$ is the $N \times N$ Jacobian matrix and $\boldsymbol{B}$ is an N-dimensional column vector:

$$\begin{aligned} \boldsymbol{A} &= \boldsymbol{D}_x \boldsymbol{F}(\boldsymbol{x}, p) \ , \\ \boldsymbol{B} &= \boldsymbol{D}_p \boldsymbol{F}(\boldsymbol{x}, p) \ . \end{aligned} \tag{38}$$

The partial derivatives in $\boldsymbol{A}$ and $\boldsymbol{B}$ are evaluated at $\boldsymbol{x} = \boldsymbol{x}_*$ and $p = \bar{p}$. To calculate the time-dependent parameter perturbation $(p_n - \bar{p})$, we assume that it is a linear function of $\boldsymbol{x}$:

$$p_n - \bar{p} = -\boldsymbol{K}^{\mathrm{T}}[\boldsymbol{x}_n - \boldsymbol{x}_*(\bar{p})] \ , \tag{39}$$

where the $1 \times n$ matrix $\boldsymbol{K}^{\mathrm{T}}$ is to be determined so that the fixed point $\boldsymbol{x}_*$ becomes stable. Substituting Eq. (39) into Eq. (37), we obtain

$$\boldsymbol{x}_{n+1} - \boldsymbol{x}_*(\bar{p}) = (\boldsymbol{A} - \boldsymbol{B}\boldsymbol{K}^{\mathrm{T}})[\boldsymbol{x}_n - \boldsymbol{x}_*(\bar{p})] \ , \tag{40}$$

which shows that the fixed point will be stable if the matrix $(\boldsymbol{A} - \boldsymbol{B}\boldsymbol{K}^{\mathrm{T}})$ is asymptotically stable; that is, all its eigenvalues have modulus smaller than unity.

The solution to the problem of determining $\boldsymbol{K}^{\mathrm{T}}$, such that the eigenvalues of the matrix $(\boldsymbol{A} - \boldsymbol{B}\boldsymbol{K}^{\mathrm{T}})$ have specified values, is known from control systems theory as the "pole placement technique" [42]. In this context, the eigenvalues of the matrix $(\boldsymbol{A} - \boldsymbol{B}\boldsymbol{K}^{\mathrm{T}})$ are called the "regular poles". The following results give a necessary and sufficient condition for a unique solution of the pole placement problem to exist, and also a method for obtaining it (Ackermann's method) [42]: (1) The pole placement problem has a unique solution if and only if the $N \times N$ matrix

$$\boldsymbol{C} = (\boldsymbol{B} \vdots \boldsymbol{A}\boldsymbol{B} \vdots \boldsymbol{A}^2\boldsymbol{B} \vdots \ldots \vdots \boldsymbol{A}^{n-1}\boldsymbol{B}) \ ,$$

is of rank N, where $\boldsymbol{C}$ is the controllability matrix; and (2) the solution of the pole placement problem is given by

$$\boldsymbol{K}^{\mathrm{T}} = (\alpha_N - a_N, \ldots, \alpha_1 - a_1)\boldsymbol{T}^{-1} \ ,$$

where $\boldsymbol{T} = \boldsymbol{C}\boldsymbol{W}$ and

$$\boldsymbol{W} = \begin{pmatrix} a_{N-1} & a_{N-2} & \ldots & a_1 & 1 \\ a_{N-2} & a_{N-3} & \ldots & 1 & 0 \\ \vdots & \vdots & & \vdots & \vdots \\ a_1 & 1 & \ldots & 0 & 0 \\ 1 & 0 & \ldots & 0 & 0 \end{pmatrix} .$$

Here $\{a_1,\ldots,a_N\}$ are the coefficients of the characteristic polynomial of $\boldsymbol{A}$:

$$|s\boldsymbol{I}-\boldsymbol{A}| = s^N + a_1 s^{n-1} + \cdots + a_N \ ,$$

and $\{\alpha_1,\ldots,\alpha_N\}$ are the coefficients of the desired characteristic polynomial $(\boldsymbol{A}-\boldsymbol{B}\boldsymbol{K}^{\mathrm{T}})$.

The condition for the matrix $\boldsymbol{C}$ to be of rank N is too strong as far as stabilizability of a closed loop system is concerned. In fact, the pole placement technique only requires a set of N points, placed symmetrically with respect to the real axis in the complex plane. Then there exists a feedback matrix $\boldsymbol{K}^{\mathrm{T}}$ such that the poles of the closed-loop system are the above set of points. It should be pointed out that there is a large class of control systems, in particular those arising in physical situations, which do not have a controllable linearization as indicated in Eq. (40). One has then to choose another control that obeys the controllability assumption if one wishes to use linear control. In particular, special care should be exercised when dealing with pole placement technique for nonautonomous systems. It should be noted that the control Eq. (39) is based on the linear Eq. (37) and therefore it is only valid in the neighborhood of the desired fixed point $\boldsymbol{x}_*(\bar{p})$. The size of this valid neighborhood is determined by the limitation in the size of the parameter perturbation δ. Combining Eqs. (36) and (39), we obtain

$$|\boldsymbol{K}^{\mathrm{T}}[\boldsymbol{x}_n - \boldsymbol{x}_*(\bar{p})]| < \delta \ . \tag{41}$$

This defines an invariant slab of width $2\delta/|\boldsymbol{K}^{\mathrm{T}}|$ in $\mathbf{R}^N$. We choose to activate the control according to Eq. (41) only when the trajectory falls into the slab, and we leave the control parameter at its nominal value $\bar{p}$ when the trajectory is outside this slab. It should also be noted that the matrix $\boldsymbol{K}^{\mathrm{T}}$ can be chosen in many different ways. In principle, a choice of regulator poles inside the unit circle, which does not violate the controllability condition, works [41]. The OGY method consists of setting the unstable poles equal to zero while leaving the stable ones as they are. With the OGY choice of regulator poles, the trajectory approaches the fixed point geometrically along the stable manifold after the control is turned on.

Since the control is turned on only when the trajectory enters the thin slab about the desired fixed point, one has to wait for some time for this to occur if the trajectory starts from a randomly chosen initial condition. Even then, because of nonlinearity not included in the linearized Eq. (37), the control may not be able to keep the trajectory in the vicinity of the fixed point. In this case the trajectory will leave the slab and continue to wander chaotically as if there was no control. Since a chaotic trajectory on the uncontrolled chaotic attractor is ergodic, at some time it will eventually reenter the slab and also be sufficiently close to the fixed point so that control is achieved. As a result, we create a stable orbit, which, for a typical initial condition, is preceded by a chaotic transient [32,43] in which the orbit is similar to orbits on the uncontrolled chaotic attractor. Of course, there is a probability zero Cantor-like set of initial conditions which never enters the slab. In Ref. [41], it is shown that the OGY choice for the regulator poles yields the shortest chaotic transient or, equivalently, the shortest average time to achieve control.

As a typical higher-dimensional physical system, we consider the double rotor map which is a four-dimensional map describing the time evolution of a mechanical system known as the kicked double rotor [41,44]. The double rotor consists of two thin, massless rods as shown in Fig. 1. The first rod of length l_1 pivots about P_1 (fixed), and the second rod of length $2l_2$, pivots about P_2 which moves. A mass m_1 is attached at P_2, and two masses $m_2/2$ are attached to each end of the second rod. The end of the second rod (P_3) receives vertical periodic impulse kicks of period T and

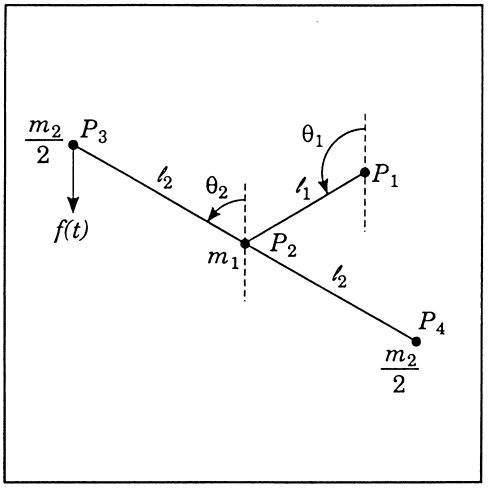

Fig. 1. From Ref. [41]. The double rotor.

strength f_0. The motion is in the horizontal plane so that gravity can be neglected. The double rotor is also subject to friction at P_1 and P_2 which is proportional to the angular velocity $\mathrm{d}\theta_1(t)/\mathrm{d}t$ and $\mathrm{d}\theta_2(t)/\mathrm{d}t - \mathrm{d}\theta_1(t)/\mathrm{d}t$ with proportional constants v_1 and v_2, respectively. Due to the periodic forcing, the set of differential equations describing the double rotor can be reduced to the following four-dimensional map by using the stroboscopic sectioning technique [41,44]:

$$\begin{pmatrix} \boldsymbol{X}_{n+1} \\ \boldsymbol{Y}_{n+1} \end{pmatrix} = \begin{pmatrix} \boldsymbol{M}\boldsymbol{Y}_n + \boldsymbol{X}_n \\ \boldsymbol{L}\boldsymbol{Y}_n + \boldsymbol{G}(\boldsymbol{X}_{n+1}) \end{pmatrix}, \tag{42}$$

where $\boldsymbol{X} = (x^1, x^2)^{\mathrm{T}}$, $\boldsymbol{Y} = (y^1, y^2)^{\mathrm{T}}$, x^1 and x^2 are the angular positions of the rods at the instant of the kth kick, and y^1 and y^2 are the angular velocities of the rods immediately after the kth kick. $\boldsymbol{L}$ and $\boldsymbol{M}$ are constant 2×2 matrices defined by

$$\boldsymbol{L} = \sum_{j=1}^{2} \boldsymbol{W}_j e^{\lambda_j} T, \quad \boldsymbol{M} = \sum_{j=1}^{2} \boldsymbol{W}_j \frac{e^{\lambda_j} T - 1}{\lambda_j}, \tag{43}$$

$$\boldsymbol{W}_1 = \begin{pmatrix} a & b \\ b & d \end{pmatrix}, \quad \boldsymbol{W}_2 = \begin{pmatrix} d & -b \\ -b & a \end{pmatrix},$$

$$a = \tfrac{1}{2}(1 + (v_1/\Delta)), \quad d = \tfrac{1}{2}(1 - (v_1/\Delta)), \quad b = -v_2/\Delta,$$

$$\lambda_{1,2} = -\tfrac{1}{2}(v_1 + v_2 \pm \Delta), \quad \Delta = \sqrt{v_1^2 + 4v_2^2}.$$

The function $\boldsymbol{G}(\boldsymbol{X})$ is given by

$$\boldsymbol{G}(\boldsymbol{X}) = \begin{pmatrix} c_1 \sin x^1 \\ c_2 \sin x^2 \end{pmatrix}, \tag{44}$$

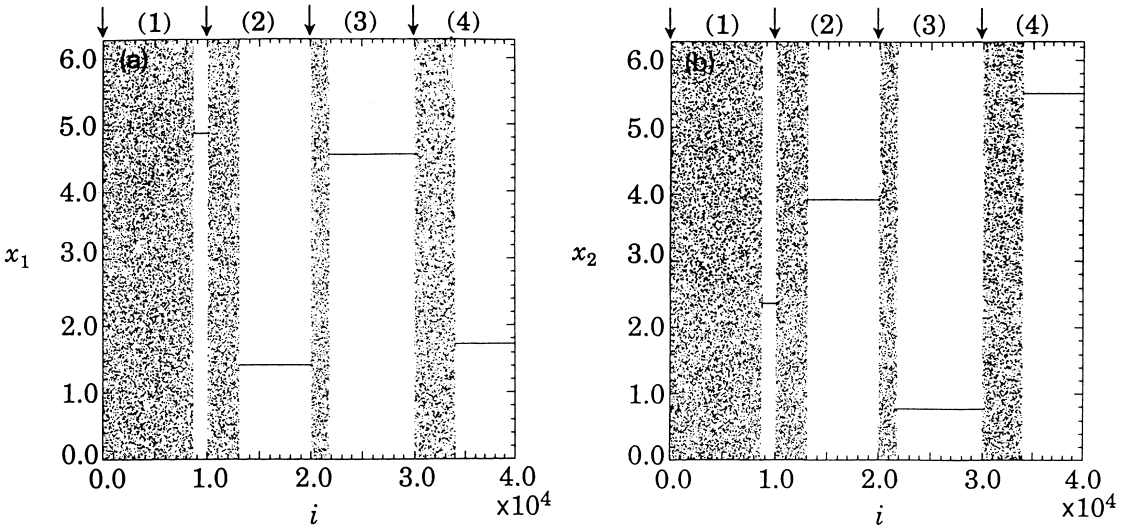

Fig. 2. From Ref. [41]. Double rotor map: successive control of unstable fixed points embedded in the chaotic attractor. The arrows indicate the times of switching.

where $c_1 = f_0 l_1/I$, $c_2 = f_0 l_2/I$, and $I = (m_1 + m_2)l_1^2 = m_2 l_2^2$. For illustrative purposes we fix $v = T = I = m_1 = m_2 = l_2 = 1$ and $l_2 = 1/\sqrt{2}$. For $f_0 = 9.0$, the double rotor map has a chaotic attractor with two positive Lyapunov exponents. There are 32 unstable fixed points embedded in this chaotic attractor [41].

To apply the pole-placement technique, we choose f_0 as the control parameter so it can be varied about its nominal value $\overline{f_0} = 9.0$. Let $(\boldsymbol{X}_*, \boldsymbol{Y}_*)$ be a fixed point to be stabilized. The quantities required in the application of the pole-placement technique are as follows:

$$\boldsymbol{A} = \begin{pmatrix} \boldsymbol{I}_2 & \boldsymbol{M} \\ \boldsymbol{H}(\boldsymbol{X}_*) & \boldsymbol{L} + \boldsymbol{H}(\boldsymbol{X}_*)\boldsymbol{M} \end{pmatrix}, \tag{45}$$

$$\boldsymbol{H}(\boldsymbol{X}_*) = \frac{\overline{f_0}}{I}\begin{pmatrix} l_1 \cos x_*^1 & 0 \\ 0 & l_2 \cos x_*^2 \end{pmatrix},$$

$$\boldsymbol{B}^{\mathrm{T}} = (0, 0, l_1 \sin x_*^1/I, l_2 \sin x_*^2/I)\ ,$$

$$\boldsymbol{C} = (\boldsymbol{B} \vdots \boldsymbol{A}\boldsymbol{B} \vdots \boldsymbol{A}^2\boldsymbol{B} \vdots \ldots \vdots \boldsymbol{A}^{n-1}\boldsymbol{B}), \quad \boldsymbol{T} = \boldsymbol{C}\boldsymbol{W}\ ,$$

$$\boldsymbol{W} = \begin{pmatrix} a_3 & a_2 & a_1 & 1 \\ a_2 & a_1 & 1 & 0 \\ a_1 & 1 & 0 & 0 \\ 1 & 0 & 0 & 0 \end{pmatrix},$$

$$\boldsymbol{K}^{\mathrm{T}} = (\alpha_4 - a_4, \alpha_3 - a_3, \alpha_2 - a_2, \alpha_1 - a_1)\boldsymbol{T}^{-1}\ .$$

Fig. 2(a) and (b) show how the method works to stabilize different unstable fixed points embedded in the chaotic attractor. Control of the first fixed point was turned on when the trajectory enters its

slab defined by (41) with switches to control other fixed points occurring at later times. In the figures, the state variables x^1 and x^2 of an orbit are plotted. The times at which the control is switched from stabilizing one fixed point to stabilizing another are labeled by the arrows in the figures. The magnitude of the parameter perturbation is chosen as $\delta = 1.0$, which is roughly 10% of the nominal f_0 value. A smaller δ would increase the average time to achieve control. The figures clearly illustrate the flexibility offered by the method in controlling different periodic motions embedded in the attractor.

2.4.1. Use of delay coordinates

In most experimental situations, a detailed knowledge of the system's equations is not known. One usually measures a time series of a single scalar state variable, say $u(t)$, and then uses the delay coordinates [26] to represent the system state. A delay-coordinate vector in the m-dimensional embedding space can be formed as follows:

$$\boldsymbol{x}(t) = (u(t), u(t - t_D), u(t - 2t_D), \ldots, u(t - (m-1)t_D)) ,$$

where t is the continuous time variable, and t_D is some conveniently chosen delay time. The embedding theorem [26] guarantees that for $m \geq 2N$, where N is the phase-space dimension of the system, the vector $\boldsymbol{x}$ is generically a global one-to-one representation of the system state. Since we only require $\boldsymbol{x}$ to be one-to-one in the small region near the fixed point, the requirement for the embedding dimension is actually $m = N - 1$ [1,23]. To obtain a map, one can take a Poincaré surface of section. For the often encountered case of periodically driven systems, one can define a "stroboscopic surface of section" by sampling the state at discrete time $t_n = nT + t_0$, where T is the driving period. In this case the discrete state variable is $\boldsymbol{x}_n = \boldsymbol{x}(t_n)$.

As pointed out in Ref. [45], in the presence of parameter variation, delay coordinates lead to a map of a different form than Eq. (1). For example, in the periodically forced case, since the components of $\boldsymbol{x}_n$ are $u(t - it_D)$ for $i = 0, 1, \ldots, (m-1)$, the vector $\boldsymbol{x}_{n+1}$ must depend not only on p_n, but also on all previous values of the parameter that are in effect during the time interval $(t_n - (m-1)t_D) \leq t \leq t_n$. In particular, let r be the smallest integer such that $mt_D < rT$. Then the relevant map is in general of the form:

$$\boldsymbol{x}_{n+1} = \boldsymbol{G}(\boldsymbol{x}_n, p_n, p_{n-1}, \ldots, p_{n-r}) . \tag{46}$$

We now discuss how the OGY method can be applied to the case of delay coordinates. For simplicity we consider $r = 1$. In this case, we have

$$\boldsymbol{x}_{n+1} = \boldsymbol{G}(\boldsymbol{x}_n, p_n, p_{n-1}) . \tag{47}$$

Linearizing as in Eq. (37) and again restricting attention to the case of a fixed point, we have

$$\boldsymbol{x}_{n+1} - \boldsymbol{x}_*(\bar{p}) = \boldsymbol{A}[\boldsymbol{x}_n - \boldsymbol{x}_*(\bar{p})] + \boldsymbol{B}_a(p_n - \bar{p}) + \boldsymbol{B}_b(p_{n-1} - \bar{p}) , \tag{48}$$

where $\boldsymbol{A} = \boldsymbol{D}_x\boldsymbol{G}(\boldsymbol{x}, p, p')$, $\boldsymbol{B}_a = \boldsymbol{D}_p\boldsymbol{G}(\boldsymbol{x}, p, p')$, $\boldsymbol{B}_b = \boldsymbol{D}_{p'}\boldsymbol{G}(\boldsymbol{x}, p, p')$, and all partial derivatives in $\boldsymbol{A}, \boldsymbol{B}_a$, and $\boldsymbol{B}_b$ are evaluated at $\boldsymbol{x} = \boldsymbol{x}_*(\bar{p})$ and $p = \bar{p} = p'$. One can now define a new state variable with one extra component by

$$\bar{\boldsymbol{x}}_{n+1} = \begin{pmatrix} \boldsymbol{x}_{n+1} \\ p_n \end{pmatrix} , \tag{49}$$

and introduce the linear control law

$$p_n - \bar{p} = -\boldsymbol{K}^{\mathrm{T}}[\boldsymbol{x}_n - \boldsymbol{x}_*(\bar{p})] - k(p_{n-1} - \bar{p}) \ . \tag{50}$$

Combining Eqs. (48) and (50), we obtain

$$\bar{\boldsymbol{x}}_{n+1} - \bar{\boldsymbol{x}}_*(\bar{p}) = (\bar{\boldsymbol{A}} - \overline{\boldsymbol{B}\boldsymbol{K}}^{\mathrm{T}})[\bar{\boldsymbol{x}} - \bar{\boldsymbol{x}}_*(\bar{p})] \ , \tag{51}$$

where

$$\bar{\boldsymbol{x}}_*(\bar{p}) = \begin{pmatrix} \boldsymbol{x}_*(\bar{p}) \\ \bar{p} \end{pmatrix}, \quad \bar{\boldsymbol{A}} = \begin{pmatrix} \boldsymbol{A} & \boldsymbol{B}_b \\ \boldsymbol{0} & 0 \end{pmatrix}, \quad \bar{\boldsymbol{B}} = \begin{pmatrix} \boldsymbol{B}_a \\ 1 \end{pmatrix}, \quad \bar{K} = \begin{pmatrix} \boldsymbol{K} \\ k \end{pmatrix} .$$

Since Eq. (51) is now of the same form as Eq. (40), the method of pole placement can be applied. A similar result holds for any $r > 1$. Although the explicit form for the function $\boldsymbol{G}(\boldsymbol{x}_n, p_n, p_{n-1})$ is not known, the quantities required for computing the parameter perturbations in Eq. (51) can usually be extracted directly from the measurement [9]. The location of the periodic orbits are obtained by looking at recurrences in the embedded space [46,47]. The matrix $\boldsymbol{A}$ in Eq. (48) and the corresponding eigenvalues and eigenvectors are obtained by looking at the same recurrences about the desired periodic orbit and fitting an affine transformation $\boldsymbol{x}_{n+1} = \boldsymbol{A}\boldsymbol{x}_n + \boldsymbol{b}$, since the dynamics is approximately linear close to the periodic orbit. The vectors $\boldsymbol{B}_a$ and $\boldsymbol{B}_b$ in Eq. (48) are obtained by perturbing the control parameter of the system [1,23,45,48].

2.5. Discussion

The OGY method described above applies to invertible maps. In general, dynamical systems that can be described by a set of first-order autonomous differential equations are invertible, and the inverse system is obtained by letting $t \to -t$ in the original set of differential equations. Hence, the discrete map obtained on the Poincaré surface of section also is invertible. Most dynamical systems encountered in practice fall into this category. Noninvertible dynamical systems possess very distinct properties from invertible dynamical systems [49,50]. For instance, for two-dimensional noninvertible maps, a point on a chaotic attractor may not have a unique stable (unstable) direction. A method for determining all these stable and unstable directions is not known. If one or several such directions at the target unstable periodic orbit can be calculated, the OGY method can in principle be applied to noninvertible systems by forcing a chaotic trajectory to fall on one of the stable directions of the periodic orbit.

The transient phase where the orbit wanders chaotically before locking into a controlled orbit can be greatly shortened by applying a "targeting" technique [35–38] so that a trajectory can be rapidly brought to a target region on the attractor by using small control perturbations. The idea is that, since chaotic systems are exponentially sensitive to perturbations, careful choice of even small control perturbations can, after some time, have a large effect on the trajectory location and can be used to guide it. Thus the time to achieve control can, in principle, be greatly reduced by properly applying small controls when the orbit is far from the neighborhood of the desired periodic orbit.

We have considered the case where there is only a single control parameter available for adjustment. While generically a single parameter is sufficient for stabilization of a desired periodic orbit, there may be some advantage to utilizing several control variables. Therefore, the single

control parameter p becomes a vector. In particular, the added freedom in having several control parameters might allow better means of choosing the control so as to minimize the time to achieve control, as well as the effects of noise.

We emphasize that full knowledge of the system dynamics is not necessary in order to apply the OGY idea [1,23]. In particular, we only require the location of the desired periodic orbit, the linearized dynamics about the periodic orbit, and the dependence of the location of the periodic orbit on small variation of the control parameter. Delay-coordinate embedding has been successfully utilized in experimental studies to extract such information purely from observations of experimental chaotic orbits on the attractor without any a priori knowledge of the equations of the system, and such information has been utilized to control periodic orbits [9].

The OGY idea of controlling chaos gives flexibility. By switching the small control, one can switch the time asymptotic behavior from one periodic orbit to another. In some situations, where the flexibility offered by the ability to do such switching is desirable, it may be advantageous to design the system so that it is chaotic. In other situations, where one is presented with a chaotic system, the method may allow one to eliminate chaos and achieve greatly improved behavior at relatively low cost.

Finally, we point out that the OGY method is not restricted to the control of unstable periodic orbits. The success of the method relies on the existence of distinct stable and unstable directions at trajectory points. It can be applied to stabilizing any desirable chaotic trajectory embedded in a chaotic attractor [51–53] and, consequently, it is also applicable to pseudo-periodic orbits which are chaotic trajectories coming arbitrarily close to some unstable periodic orbits. This observation has a number of potential applications. One can use this to synchronize two chaotic systems [51], to convert transient chaos into sustained chaos [52], to communicate with chaos by controlling symbolic dynamics [21,24,54–57], and to select a desirable chaotic state from intermittent chaotic signal [53], etc.

3. The adaptive method for control of chaos

3.1. The basic idea

Many alternative approaches to the OGY method have been proposed for the stabilization of the unstable periodic orbits (UPO) [47] of a chaotic dynamics. In general the strategies for the control of chaos can be classified into two main classes, namely: closed loop or feedback methods and open loop or non feedback methods.

The first class includes those methods which select the perturbation based upon a knowledge of the state of the system, and oriented to control a prescribed dynamics. Among them, we here recall (besides OGY) the so called occasional proportional feedback (OPF) simultaneously introduced by Hunt [15] and Showalter [17], the method of Huebler [58], and the method introduced by Pyragas [2], which apply a delayed feedback on one of the system variables. All these methods are model independent, in the sense that the knowledge on the system necessary to select the perturbation can be done by simply observing the system for a suitable learning time.

The second class includes those strategies which consider the effect of external perturbations (independent on the knowledge of the actual dynamical state) on the evolution of the system.

Periodic [59] or stochastic [60] perturbations have been seen to produce drastic changes in the dynamics of chaotic systems, leading eventually to the stabilization of some periodic behavior. These approaches, however, are in general limited by the fact that their action is not goal oriented, i.e. the final periodic state cannot be decided by the operator.

In what follows, we will try to summarize one of the possible closed-loop approach for the stabilization of UPO. Although it belongs to the same class of OGY, it can be considered as alternative, insofar as it consists in perturbing a state variable of the system, instead of a control parameter. This may result preferable in all cases in which the control parameters are strongly influenced by the environmental conditions, and a variation of them is not easy to be performed.

3.2. The algorithm for adaptive chaos control

In the following we will then discuss the general problem of forcing a dynamical system

$$\dot{\boldsymbol{x}} = \boldsymbol{F}(\boldsymbol{x}, \mu) \tag{52}$$

toward a desired goal dynamics $\boldsymbol{g}(t)$, by the use of a feedback perturbation $U(t)$ acting on one of its state variables. Here dot denotes temporal derivative, μ is a vector of control parameters, $\boldsymbol{x}(t) \equiv (x_1(t), x_2(t), \ldots, x_m(t))$ is a m-dimensional vector of the state variables, $\boldsymbol{F}$ is a suitable nonlinear function, and $\boldsymbol{g}(t) \equiv (g_1(t), g_2(t), \ldots, g_m(t))$ is the m-dimensional desired dynamics. The further hypothesis here is that it exists a scalar state variable (e.g., x_1) out from $\boldsymbol{x}$ that is accessible for measurements and perturbations. The problem is to select a suitable additive perturbation to the x_1 equation so that the whole system evolves asymptotically to yield $|\boldsymbol{x}(t) - \boldsymbol{g}(t)| = 0$.

In general $\boldsymbol{g}(t)$ can be any desired dynamics compatible with the natural evolution of the system. However, along this section, we will consider $\boldsymbol{g}(t)$ to equal a particular UPO of period $T(\boldsymbol{g}(t) \equiv \boldsymbol{x}(t - T))$ so that the above condition corresponds to the stabilization of that UPO.

The first attempt to solve this problem was provided by Pyragas [2], who introduced an additive feedback perturbation in the equation for the observable variable x_1 given by

$$U(t) = K(g_1(t) - x_1(t)) = K(x_1(t - T) - x_1(t)) \,, \tag{53}$$

K being a suitable parameter setting up the weight of the perturbation. This perturbation is nothing but a time-delayed continuous feedback on the state variable x_1, with the effect of forcing $x_1(t)$ to follow $g_1(t)$. In practice, the method transform a system of ordinary differential equations into a delayed dynamical system. This implies to increase its dimensionality so as the desired UPO (which was unstable in the original ordinary differential equation system) becomes now stable in the new delayed dynamical system.

The two crucial parameters in Ref. [2] are T and K. The first can be experimentally detected by observing the unperturbed evolution of the system for a while, and applying e.g. the standard topological techniques for the detection of UPOs [61]. Once T has been properly detected, the operator begins with different K values in order to extract the range for which the desired UPO comes out to be stabilized (the so called controllability range).

The above technique has been later elaborated in Refs. [62] and by the same Pyragas in Ref. [63], by redefining the correction perturbation $U(t)$ as a sum of the contributions at all previous multiple pT (p integer) of the UPOs period.

An improvement of the Pyragas' technique has been recently offered, based on an adaptive recognition [64] and control [3] method, allowing a natural selection of the weighting factor K in Eq. (53), which becomes now function of time and it is selected exploiting the local information of the dynamics. The method, originally introduced for the stabilization of UPOs in chaotic systems, has been later extended for solving the problem of chaos synchronization [65], targeting of chaos [66], filtering noise from experimental chaotic data sets [67], and for the control of defects and space-like structures in delayed dynamical systems [68].

The adaptive algorithm can be summarized as follows. In Eq. (52), at each time t_n at which the perturbation must be applied, one measures the distance $\delta(t_n)$ between the dynamics of the observable $x_1(t_n)$ and the goal dynamics $g_1(t_n)$

$$\delta(t_n) = x_1(t_n) - g_1(t_n) \ . \tag{54}$$

Then, one evaluates the local variation rate

$$\lambda(t_n) = \log \left| \frac{\delta(t_n)}{\delta(t_{n-1})} \right| , \tag{55}$$

measuring how the distance between actual and desired dynamics evolves in time, and selects the perturbation as

$$U(t_n) = K(t_n)(g_1(t_n) - x_1(t_n)) \ , \tag{56}$$

where

$$\frac{1}{K(t_n)} = \frac{1}{K_0}(1 - \tanh(\sigma\lambda(t_n))), \quad \sigma > 0, \ K_0 > 0 \ . \tag{57}$$

The adaptive nature of the algorithm is clear when one considers that the strength of the perturbation in Eq. (56) now adaptively depends on the local dynamics of the system. Namely, when $x_1(t)$ naturally tends to shadow the goal pattern $g_1(t)$, this is reflected by a temporal decreasing behavior of $\delta(t)$, implying a negative value of $\lambda(t)$ and therefore a shrinking of the weighting factor $K(t)$ in Eq. (57). On the contrary, whenever the natural evolution of the dynamics tends to push the system away from the goal dynamics, this is reflected by an increasing process for $K(t)$. In other words the perturbation is adapted to the local dynamics, since the far (close) the system is to the goal dynamics, the big (small) is the weight given to the perturbation. It should be remarked that the limit $\sigma \to 0$ of the above algorithm recovers the Pyragas' control method of Ref. [2], implying a constant weighting factor K_0 in Eq. (57), which then equals Eq. (53).

While this process solves the problem of encountering the controllability range (the weighting factor K is now not constant as far as $\sigma \neq 0$ and it is automatically selected by the adaptive algorithm), there are here two crucial parameters, namely σ and K_0.

We have already pointed out that $\sigma \to 0$ leads the adaptive algorithm to be equivalent to the Pyragas' method. On the other hand, a too big σ may cause stability problems in Eq. (57). In order to have a reasonable K dynamics, avoiding undesirable saturation effects of the function tanh, one immediately see that σ should be selected as to be sufficiently smaller than the maximum λ, in order that the product $\sigma\lambda(t_n)$ lies within the linear region of the function tanh for all times t_n.

Therefore, a preliminary observation of the unperturbed dynamics may be in order so as to have statistics of the typical λ values occurring in the unperturbed dynamics, leading to the natural choice of the sensitivity parameter.

As for K_0, while there are no upper limit in the choice, a lower limit should be taken into account. Indeed, Eq. (57) allows variations of $K(t)$ in the range from 0 (when $\lambda = +\infty$) to $2K_0$ (when $\lambda = -\infty$). Therefore one should assure that this range overlaps conveniently the controllability range, through a judicious choice of K_0. Even though one could then be tempted to take a very large K_0, this can result in an undesirably large initial perturbation, leading to practical problems in the implementation of the method. In practice, the optimal K_0 for the adaptive technique can be always easily individuated.

A further remark is in order. Eq. (57) can be rewritten as

$$\begin{aligned} &K(t_n) \equiv 1/\tau(t_n) \\ &\tau(t_n) = \tau_0(1 - \tanh(\sigma\lambda(t_n))) \, . \end{aligned} \tag{58}$$

Since the perturbation is additive on the right-hand side of the model equation, $\tau(t_n)$ and τ_0 must be time intervals. The original adaptive method (Ref. [64]) was indeed introduced for the recognition of chaos, and it consisted in selecting the appropriate time interval in order to minimize the second variations of the dynamics. In that case, the evolution equation for $\tau(t_n)$ was

$$\tau(t_n) = \tau(t_{n-1})(1 - \tanh(\sigma\lambda(t_n))) \, , \tag{59}$$

that is, substituting in Eq. (58) a fixed reference time interval τ_0 with a recursive search in the time intervals. The obtained irregular sequence of time intervals was used to extract suitable chaotic indicators, such as the periods of the UPOs [3] and a discriminator between chaos and stochasticity [67].

It is important to remark that the recursive formula implies a direct choice of the optimal τ in Eq. (58), thus of the optimal K in Eq. (57), while the selection of a fixed reference time interval τ_0 implies an overconstraints to the search for the optimal perturbation. However, the former mechanism can be only applied when the switch on of the process is done close to the UPO to be controlled. In practice, this would imply a preliminary learning task for an initial targeting procedure. We will come back to this point in the following of the present Report.

When, instead, one wants to switch on the control on an arbitrarily selected region of the attractor, then the latter strategy would be preferable, insofar as the former one can have limitations due to initial large fluctuation of the τ_n which can eventually drive the τ sequence away from the controllability range. This, of course, can be cured by a reliable choice of the sensitivity, but the whole process may result quite complicate to implement. This is the main reason for which we will focus on the latter strategy, which, though being less complete, has the merit of being easily implementable.

3.3. Application to high-dimensional systems

While applications to low-dimensional dynamics are straightforward, and we here address the reader to the available literature contained in Ref. [3], in the following we provide an example of the reliability of the above algorithm when used for the stabilization of periodic motions in

high-dimensional systems. The natural framework for this is the application to delayed dynamical systems (DS), which was provided in Ref. [68], and represents an intermediate stage between the control of concentrated systems (CS) and that of space-extended systems (ES).

DS are systems ruled by

$$\dot{y} = \mathscr{F}(y, y_d) \ , \tag{60}$$

where $y = y(t)$ is a m dimensional real vector, dot denotes temporal derivative, $\mathscr{F}$ is a nonlinear function, and $y_d \equiv y(t - T)$, T being a time delay.

Experimental evidence of the analogy between DS and ES was provided for a CO_2 laser with delayed feedback [69] and supported by a theoretical model [70]. Most of the statistical indicators for DS, such as the fractal dimensions, are extensive parameters proportional to T, which thus plays a role analogous to the size for the extended case [71].

The conversion from the DS to ES is based on a two variable time representation, defined by

$$t = \sigma + \theta T \ , \tag{61}$$

where $0 \leq \sigma \leq T$ is a continuous space-like variable and the integer θ plays the role of a discrete temporal variable [69]. By such a representation the long-range interactions introduced by the delay are reinterpreted as short-range interactions along the θ direction, since now $y_d \equiv y(\sigma, \theta - 1)$. In this framework, the formation and propagation of *space–time* structures, as defects and/or spatiotemporal intermittency can be identified [69,70].

When T is sufficiently larger than the oscillating period of the system, the behavior of a delayed system is analogous to that of a one-dimensional extended system. In particular, it may display phase defects, i.e. points where the phase suddenly changes its value and the amplitude goes to zero.

For sake of exemplification, let us make reference to the following particular delayed dynamics:

$$\dot{A} = \varepsilon A + \beta_1 A^2(t - T)A + \beta_2 A^4(t - T)A \ , \tag{62}$$

$$\dot{\varepsilon} = \mu_2 \left(S - \frac{\mu_1}{\mu_2}\varepsilon - kA^2 \right) . \tag{63}$$

Here, all quantities are real. A is an order parameter, ε is a time-dependent linear gain, $\beta_1, \beta_2, \mu_1, k$ are suitable fixed parameters, μ_2 is a measure of the ratio between the characteristic time scales for A and ε, and S is a measure of an external pumping to the system.

Eq. (63) are rather general. For instance, when $T = 0$, $S < 0$, $\beta_1 > 0$, $\beta_2 < 0$, $\mu_2 > 0$, $\mu_1 > 0$, $k > 0$, they model an excitable system, producing the so called *Leontovitch* bifurcation, evidence of which has been shown experimentally on a CO_2 laser with intracavity saturable absorber [72].

For $T \neq 0$, they are similar to the models already used to describe self-sustained oscillations of confined jets [73], or memory induced low frequency oscillations in closed convection boxes [74], or even the pulsed dynamics of a fountain [75]. It should be here remarked that control of Eq. (63) with the OGY method can be complicated because of the extreme high dimensionality of this particular situation, requiring a very high dimensional embedding space wherein reconstructing the local stability properties of the UPOs. This is therefore the typical case in which alternative approaches may provide a less costly strategy for the stabilization of UPOs.

Eq. (63) has been found also a good model for the temperature evolution in a well controlled time-dependent convection experiment [76], done with a cylindrical layer of silicon oil heated from

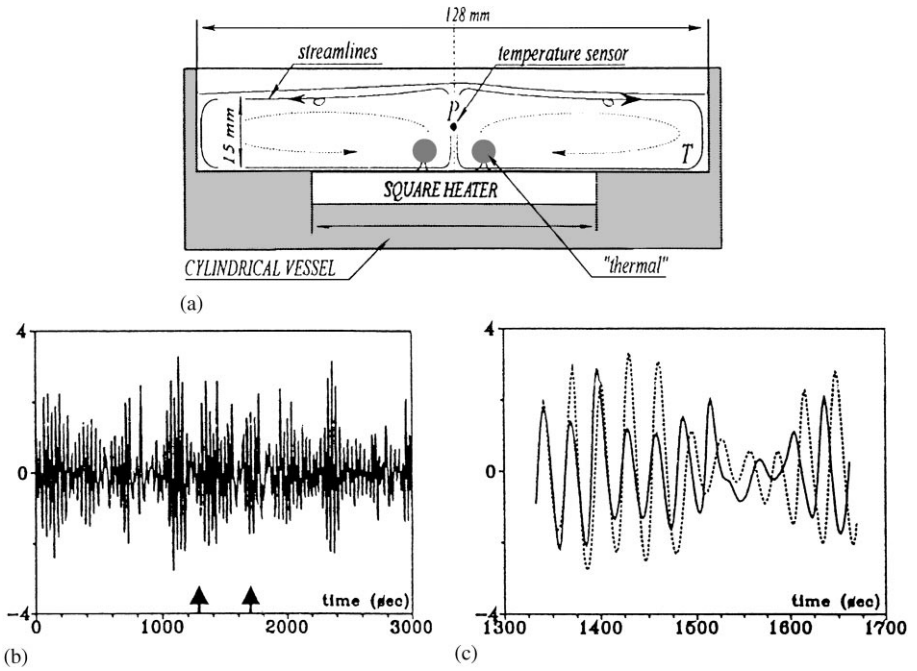

Fig. 3. (a) Cross-section of the experimental setup. A hot drop (thermal) is dragged by the flow and then reinjected into the heating region after having completed a round trip of the cell in a mean time T. P indicates the point where temperature is measured. (b) Experimental time behavior of the temperature at the point P. Vertical axis reports the temperature in arbitrary units, horizontal axis reports the time in seconds ($T = 330$ s). (c) Expanded view of the signal within the arrows which exhibits a phase jump (solid line) and reference signal translated by T (dashed line).

below by a square heater limited to the central part of the container (see Fig. 3a for a scheme of the system). The heater is surrounded by the same insulating material of the vessel. A convective instability driven simultaneously by buoyancy and temperature-dependent surface tension, called Bénard–Marangoni convection, grows as the heating is increased. A steady state is reached and a stationary pattern composed of four convective cells appears in the hot region. Additional details on this experiment can be found in Ref. [76].

By further increasing the heating, a time-dependent regime arises consisting in spatio-temporal modulations, or *thermals*, generated at the bottom boundary layer and then dragged by the flow along the cell as can be seen in Fig. 3a. This configuration provides a natural delayed interaction insofar as it reiterates at each position the local value of the order parameter after a delay T, corresponding to the time lag necessary for the trip of the cell. In this situation, an experimental measurement of the temperature at the point P of Fig. 3a yields the data of Fig. 3b. The vertical axis (temperature) can be taken as representative of the order parameter A. The main feature of this experiment consists of trains of modulated oscillations, interrupted by localized events (phase defects), wherein the phase of the signal changes suddenly and the amplitude decreases to zero.

Therefore, the relaxation oscillations are represented by the normal form of a Hopf bifurcation (Eq. (63)), wherein the saturating terms are delayed to account for the transport of the convective cell. Eq. (63) represents the slow evolution ($\mu_2 < 1$) of the control parameter ε, which is enhanced by

the external pump S and depressed by the convective motion ($-kA^2$) which would naturally uniformize top and bottom temperatures.

Let us now see how phase defects emerge in Eq. (63). If one adjusts pump and delay parameters (S and T) so that the system enters the chaotic region, one realizes that, in fact, chaos appears in the system in two different forms. For low T values, chaos is due to a local chaotic evolution of the phase, whereas no appreciable amplitude fluctuations are observed. This regime was called *phase turbulence* (PT). By increasing T, one observes a transition toward *amplitude turbulence* (AT), wherein the dynamics is dominated by the amplitude fluctuations, and a large number of defects is present. Both PT and AT have counterparts in a one-dimensional complex Ginzburg–Landau equation. Here the parameter space shows a transition from a regime of stable plane waves toward PT (Benjamin–Fair instability), followed by another transition to AT with evidence of space–time defects [77].

We now apply the adaptive method to this particular case. Here, the algorithm can be conveniently reduced to an easily workable form. The application of the method can be summarized by using Eqs. (54)–(57) and substituting $x_1(t)$ with $A(t)$ and $g_1(t)$ with $A(t-T_H)$ (T_H being the Hopf period). The perturbation $U(t)$ is then applied as additive term to the right-hand side of the first of Eq. (63).

A nice approximation holds in this case. Let us refer to Eq. (58), and let $\langle\tau\rangle$ denote the average of the $\{\tau_n\}$ set, then the second of Eq. (58) can be written as

$$\tau_n \simeq \langle\tau\rangle(1-\sigma\lambda_n) \tag{64}$$

where (i) τ_n has been replaced with its ensemble average, and (ii) the tgh function has been linearized. Point (i) corresponds to fixing once forever a reference time scale for the process under study, while point (ii) corresponds to selecting a conveniently small g to keep $g\lambda_{n+1}$ always within the linear region of the tgh function. In the same way, the equation for λ can also be linearized as

$$\lambda(t) \simeq \frac{\dot{A}(t)-\dot{A}(t-T_H)}{A(t)-A(t-T_H)}\,. \tag{65}$$

Combining Eqs. (64) and (65) into Eq. (57), this reduces to

$$U(t) = K_1(A(t-T_H)-A(t)) + K_2(\dot{A}(t-T_H)-\dot{A}(t)) \tag{66}$$

with $K_1 = 1$ and $K_2 = g/\langle\tau\rangle$. The consequences of this approximation are interesting. First of all, it is now evident that the case $K_2 = 0$ ($\sigma = 0$) recovers the Pyragas control method [2]. However, in the present case, K_1 and K_2 can be independently selected, and this introduces an extra degree of freedom with respect to Ref. [2]. Now, the control is more active when the error is increasing and vice versa, so reducing oscillations. Indeed, Eq. (66) performs as a proportional derivative controller, the more usual action for stabilizing feedback linear systems, due to its effect which consists in increasing the phase of the compensated system in a suitable frequency band.

This approximation constitutes the order-one approximation of the adaptive method, and it is very easy to implement, consisting in a double feedback line, one in the observable variable, and one in its derivative. We should point out, however, that not always this approximation leads to positive results, and in some cases (as for example the control of patterns in extended media), one should instead apply the whole adaptive strategy, without any approximation. It is straightforward

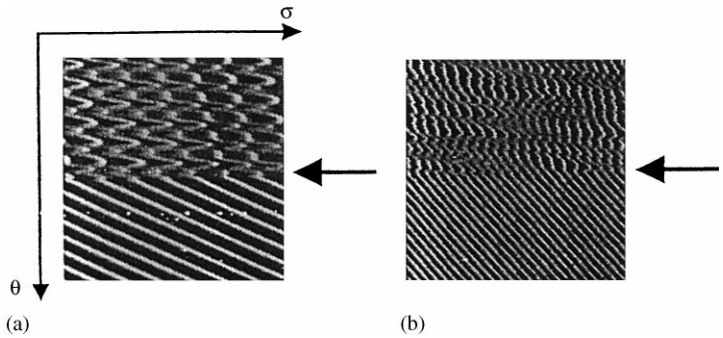

Fig. 4. Space (σ)–time (θ) representation of the controlling process for Eqs. (63). $\beta_1 = 1$, $\beta_2 = -1/16$, $\mu_2 = 0.8$, $\mu_1 = 1$, $k = 11$, $S = 5.5$, $T_H = 1.95$. (a) $T = 15$, PT regime. The chaotic dynamics results in a local turbulent phase of the Hopf oscillation which is corrected by the controlling algorithm. $K_1 = K_2 = 0.2$. Arrow indicates the instant at which control is switched on. (b) $T = 50$, AT regime. The dynamics is dominated by amplitude fluctuations, with the presence of defects. The algorithm ($K_1 = K_2 = 0.2$) suppresses the defects and restores the regular oscillation. Arrow indicates the instant at which control is switched on.

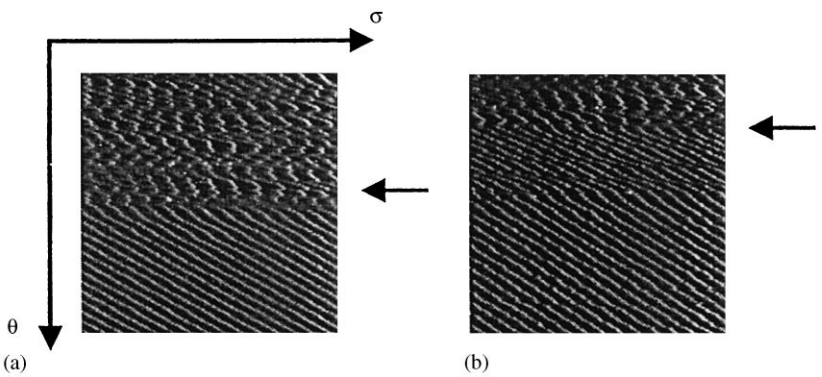

Fig. 5. $T = 50$, AT with 10% noise (a) and 20% noise (b). Control with $K_1 = K_2 = 0.2$. Same stipulations and parameters as in the caption of Fig. 4. Arrows indicate the instant at which control is switched on.

to understand that the range of validity of such approximation is having small λ values, which implies to be sufficiently close to the UPO to be controlled so as linear properties are valid.

In Fig. 4 we report the application of our method to Eq. (63). The desired oscillation, which in the space–time representation gives rise to a roll set, is controlled in PT (Fig. 4a) and in AT (Fig. 4b).

Finally, let us discuss the robustness of our procedure against external noise. For this purpose, we add white noise to the measured A values before the onset of the adaptive feedback control. Notice that the noise does not act additively, insofar as it is reinjected into the nonlinear equations through the control feedback, hence affecting dynamically the evolution of the system. A relevant result is that our method is robust against large amounts of noise. In Fig. 5 the control is achieved within AT for 10% noise (Fig. 5a) and for 20% noise (Fig. 5b). The controlled UPO is slightly distorted by the action of the noise fed back into the system.

4. The problem of targeting

4.1. Targeting and controlling fractal basin boundaries

4.1.1. Introduction

It is common for nonlinear dynamical systems to exhibit multiple coexisting attractors, each with its own basin of attraction [78–83]. The basin of attraction of an attractor is the set of initial conditions in the phase space that asymptote to the attractor. In practical applications, when one of the attractors according to some criteria would yield superior systems performance over the others, it is important to be able to drive most trajectories to the desirable attractor in an efficient and economic way. That is, one wishes to drive trajectories to the desirable attractor rapidly by using only small feedback control to an accessible parameter or state of the system. Previous work has demonstrated that in periodically driven dynamical systems, multiple basins of attraction can be eliminated by replacing the periodic driving by some appropriately chosen, but somewhat large-amplitude chaotic driving [84].

We review a method to drive most trajectories to a desirable attractor by using only small feedback control [85]. We emphasize the need to use small feedback control [1,23] since: (1) we do not wish to alter the system substantially; and (2) large perturbations to the system may be costly. As such, it is only possible to alter the fate of the trajectories resulting from initial conditions in the vicinity of basin boundaries because, for a trajectory deep in the basin of an undesirable attractor, small perturbations cannot change the attractor to which the trajectory is asymptoting. In this regard, it is necessary to distinguish between smooth and fractal basin boundaries [78–83]. Imagine there is an N-dimensional chaotic system. Consider a phase space region that contains part of the basin boundary. Assume that only small perturbations of magnitude ε ($\varepsilon \ll 1$) to an accessible system parameter or state are allowed. If the boundary is smooth, the dimension of the boundary is $D = N - 1$. Thus, the fraction of trajectories whose asymptotic attractors can be altered by small ε perturbation is on the order of magnitude of $\varepsilon^{N-D} = \varepsilon$, which is also very small. If, on the other hand, the basin boundary is fractal with box-counting dimension (capacity) D, where D is a fractional number that satisfies $(N-1) < D < N$, the fraction of trajectories whose fate can be manipulated using small perturbation is $f(\varepsilon) \sim \varepsilon^{\alpha}$, where $\alpha = N - D < 1$ is the uncertainty exponent.[1] Thus, if $\alpha \ll 1, f(\varepsilon)$ can be large. Fractal basin boundaries with $\alpha < 1$ are common in dynamical systems [78–83], and $\alpha \ll 1$ are particularly common in high-dimensional systems [87–89] or in systems with riddled basins[2] [90–96]. Therefore, although the presence of fractal basin boundaries with $\alpha < 1$ poses a fundamental difficulty to predict the asymptotic attractor of the system because of the inevitable error in the specification of initial conditions or system parameters, these boundaries offer a possibility for us to greatly increase the probability that

[1] The relation between the uncertainty exponent and the box-counting dimension, $\alpha = N - D$, was rigorously proven for Axiom-A systems [86]. It was conjectured that the same relation holds for more general dynamical systems [78,79].

[2] It should be noted that a riddled basin has dimension equal to N and its basin boundary is the basin itself. Thus, the boundary also has dimension equal to N. However, its uncertainty exponent is not equal to zero, although in most cases it is close to zero. Therefore, strictly speaking, the relation between the basin boundary dimension and the uncertainty exponent $D = N - \alpha$ does not hold for riddled basins.

typical trajectories can be driven to the desirable attractor by using arbitrarily small perturbations, provided that we are able to harness the system in an intelligent way. It was demonstrated in Ref. [85] that this is indeed possible.

In the sequel, we discuss method of control and present numerical examples for a system with fractal basin boundaries and a system with riddled basins.

4.1.2. Method of control

The setting of the problem is as follows. Let the dynamical system be described by an N-dimensional flow $\mathrm{d}x/\mathrm{d}t = \boldsymbol{F}(\boldsymbol{x}, p)$ or an N-dimensional map $\boldsymbol{x}_{n+1} = \boldsymbol{M}(\boldsymbol{x}_n, p)$, where p is an accessible system parameter. For concreteness, assume there are two distinct attractors for the range of system parameter values of interest. Furthermore, assume that the coexistence of the two attractors is structurally stable, i.e., small change in the parameter changes the behavior of attractors and their basin structures only slightly. Denote the two distinct attractors by $\boldsymbol{A}$ and $\boldsymbol{B}$. For a given region Σ in the phase space that contains part of the basin boundary, a fraction of initial conditions f_A will yield trajectories that asymptote to attractor $\boldsymbol{A}$, and the remaining initial conditions, a fraction of $f_B \equiv (1 - f_A)$, asymptote to attractor $\boldsymbol{B}$. Without loss of generality, assume that f_A and f_B are on the same order of magnitude. Suppose that one of the two attractors yields much superior system performance than the other. We thus wish to increase f_A as much as possible so that most initial conditions asymptote to the attractor with better system performance. This will not occur if no external perturbations to the system are applied. Our goal is to devise an algorithm to increase substantially the fraction of initial conditions that asymptote to the desirable attractor, given that p can be adjusted finely around a nominal value p_0: $p \in [p_0 + \Delta p, p_0 - \Delta p]$, where $\Delta p/p_0 \ll 1$.

The idea is to build a hierarchy or "tree-like" structure of paths to the desirable attractor [36,85]. Specifically, let $\boldsymbol{A}$ be the desirable attractor. We first randomly choose an initial condition in Σ such that it generates a trajectory to $\boldsymbol{A}$. Call this trajectory the "root" path 1 to $\boldsymbol{A}$ and denote it by $\boldsymbol{X}_0, \boldsymbol{X}_1, \ldots, \boldsymbol{X}_A$, where $\boldsymbol{X}_A$ is a point on $\boldsymbol{A}$ (or a point in the vicinity of $\boldsymbol{A}$). We then choose a second trajectory to $\boldsymbol{A}$ from an arbitrary initial condition $\boldsymbol{Y}_0$ in Σ. But for this second path, we examine if it approaches to $\boldsymbol{A}$ directly without coming close to root path 1, in which case we call it root path 2. It is also likely that a point on this trajectory $\boldsymbol{Y}_n$ call fall into a suitably small neighborhood of some point along root path 1 before it comes close to $\boldsymbol{A}$. In this case, we store $\boldsymbol{Y}_n$ together with the path of $(n-1)$ points leading to $\boldsymbol{Y}_n$. We call $\boldsymbol{Y}_0, \boldsymbol{Y}_1, \ldots, \boldsymbol{Y}_n$ the secondary path of the root path 1. This procedure can be repeated for initial conditions chosen on a uniform grid of size δ in Σ. Of course, if a trajectory goes to an undesirable attractor, we simply disregard this trajectory in the tree-building process. Finally, with suitably chosen δ, a hierarchy of paths to $\boldsymbol{A}$ in Σ can be built with, say, N_R root paths. On each root path i, there can be some secondary paths, and on each secondary path there can be third-order paths, etc. We therefore obtain a tree of paths to $\boldsymbol{A}$ in a region that contains the basin boundary, as schematically shown in Fig. 6. In fact, since there can be many root paths, this is more like a "bush" of paths leading to the desirable attractor.[3] A remaining question is

[3] This bush-like structure of paths is somewhat different from the tree structure of paths used in the targeting procedure in Ref. [36]. In that case, there is only one root path to the target point on the attractor, and all paths to the target live on the same chaotic attractor.

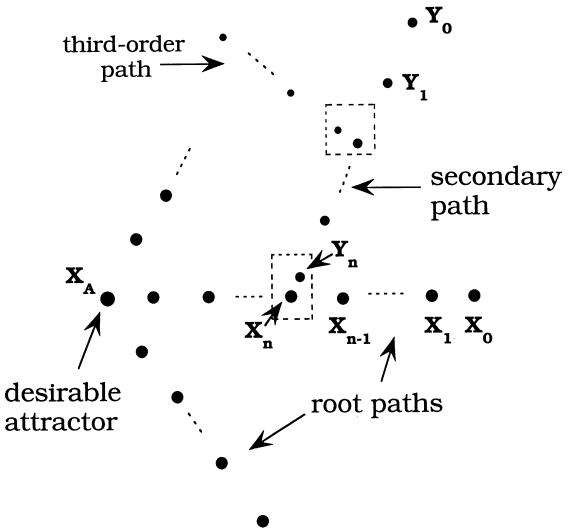

Fig. 6. From Ref. [85]. A schematic illustration of the hierarchy of paths (bush) to the desirable attractor in the phase space.

how fine the grid from which initial conditions are chosen should be. Clearly, the size of the grid δ should be comparable to the magnitude of the allowed parameter perturbation Δp, which is approximately the size of controlling neighborhood around each point on the bush of paths. If $\delta \gg \Delta p$, most trajectories that originally go to the undesirable attractors will not come close to bush of paths and therefore will not be controlled. If $\delta \ll \Delta p$, the bush of paths may have contained too many details and therefore may have used too much computer memory that is unnecessary for realizing the control.

To control a trajectory to direct it to the desirable attractor after it comes close to a path on the bush, we employ a simple feedback scheme. For simplicity we consider the N-dimensional map $\boldsymbol{x}_{n+1} = \boldsymbol{M}(\boldsymbol{x}_n, p)$. Suppose a trajectory originated from a random initial condition $\boldsymbol{x}_0$ falls into an ε-neighborhood of a point $\boldsymbol{y}_n$ on the bush at some later time n, i.e., $|\boldsymbol{x}_n - \boldsymbol{y}_n| \leq \varepsilon$. Let $\boldsymbol{y}_n, \boldsymbol{y}_{n+1}, \ldots, \boldsymbol{y}_A$ be the path on the bush that starts at $\boldsymbol{y}_n$ and ends at $\boldsymbol{y}_A$ which is in the ε-neighborhood of the desirable attractor. In the vicinity of $\boldsymbol{y}_n$, we have the following linearized dynamics: $\Delta \boldsymbol{x}_{n+1} = \boldsymbol{DM}(\boldsymbol{x}_n, p)\Delta \boldsymbol{x}_n + (\partial \boldsymbol{M}/\partial p)\Delta p_n$, where $\Delta \boldsymbol{x}_n = \boldsymbol{x}_n - \boldsymbol{y}_n, \Delta p_n = p_n - p_0$, and the Jacobian matrix $\boldsymbol{DM}(\boldsymbol{x}_n, p)$ and the vector $\partial \boldsymbol{M}/\partial p$ are evaluated at $\boldsymbol{x}_n = \boldsymbol{y}_n$ and $p_n = p_0$. Choosing a unit vector $\boldsymbol{u}$ in the phase space and letting $\boldsymbol{u} \cdot \Delta \boldsymbol{x}_{n+1} = 0$, we obtain for the required parameter perturbation:

$$\Delta p_n = \frac{-\boldsymbol{u} \cdot \boldsymbol{DM}(\boldsymbol{x}_n, p) \cdot \Delta \boldsymbol{x}_n}{\boldsymbol{u} \cdot (\partial \boldsymbol{M}/\partial p)} \ . \tag{67}$$

In principle, the unit vector $\boldsymbol{u}$ can be chosen arbitrarily provided that: (i) it is not orthogonal to $\boldsymbol{x}_{n+1}$; and (ii) the denominator in Eq. (67) is not close to zero. In practice, we define a maximum allowed magnitude for the parameter perturbation $\Delta p_{\max} \sim \varepsilon$. If the computed $|\Delta p_n|$ exceeds $\Delta p_{\max}$, we set $\delta p_n = 0$. Doing this would cause lost of control occasionally. But it was found in numerical

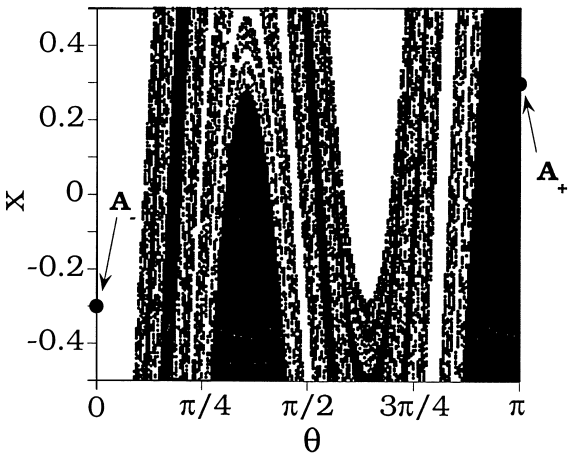

Fig. 7. From Ref. [85]. Basins of attraction for Eq. (68). Black and blank regions are the basins of the A_+ and A_- attractors, respectively. Parameter setting is: $a = 1.32$, $b = 0.9$, and $J_0 = 0.3$.

experiments that robust control can still be achieved since setting $\Delta p_n = 0$ is done only rarely [85]. Because $\Delta \boldsymbol{x}_n$ is small, Δp_n is also small. In the sequel, we present two numerical examples to illustrate the control method.

4.1.3. Example 1: controlling fractal basin boundaries

We consider the following two-dimensional map [78,79]:

$$\begin{aligned} \theta_{n+1} &= \theta_n + a\sin(2\theta_n) - b\sin(4\theta_n) - x_n\sin(\theta_n)\ , \\ x_{n+1} &= -J_0\cos(\theta_n)\ , \end{aligned} \tag{68}$$

where x can be regarded as the radial distance from the center of an annulus, θ is an angle variable so that θ and $\theta + 2\pi$ are equivalent, and a, b and J_0 are parameters. The system is invariant under the symmetry $\theta \to 2\pi - \theta$. The determinant of the Jacobian matrix is $J_0 \sin^2\theta < 1$ (for $J_0 < 1$). At the following parameter setting, $a = 1.32$, $b = 0.9$, $J_0 = 0.3$, there are two attractors, located at $x = -0.3$, $\theta = 0$ (denoted by A_-) and $x = 0.3$, $\theta = \pi$ (denoted by A_+), respectively. The boundaries between basins of the two attractors are fractal, as shown in Fig. 7, where black dots represent the basin of the A_+ attractor. The dimension of the basin boundary is approximately 1.8, corresponding to an uncertainty exponent of $\alpha \approx 0.2$ [78,79].

Now assume that the attractor A_+ corresponds to a better system performance so that it is the desirable attractor. Without control, the fraction of initial conditions that asymptote to A_+ is about 50% for the phase-space region in Fig. 7. Assume a is an accessible parameter which can be perturbed slightly around its nominal value $a_0 = 1.32$. We first build a bush of paths to A_+ by using a grid of 100×100 initial conditions in the region $(0 \le \theta \le \pi,\ -0.5 \le x \le 0.5)$ (corresponding to grid size $\delta \approx 3.3 \times 10^{-2}$). We arbitrarily choose $\boldsymbol{u} = (1/\sqrt{2})(1, 1)$ to compute the parameter perturbation Δa_n from Eq. (67). Fig. 8a shows a controlled trajectory (solid line) to the desirable attractor A_+, where both the size of the controlling neighborhood ε and the maximal allowed parameter perturbation $\Delta p_{\max}$ are set to be 10^{-2}. The trajectory would asymptote to the undesirable attractor without control, as shown by the dotted line in Fig. 8a. When control is applied

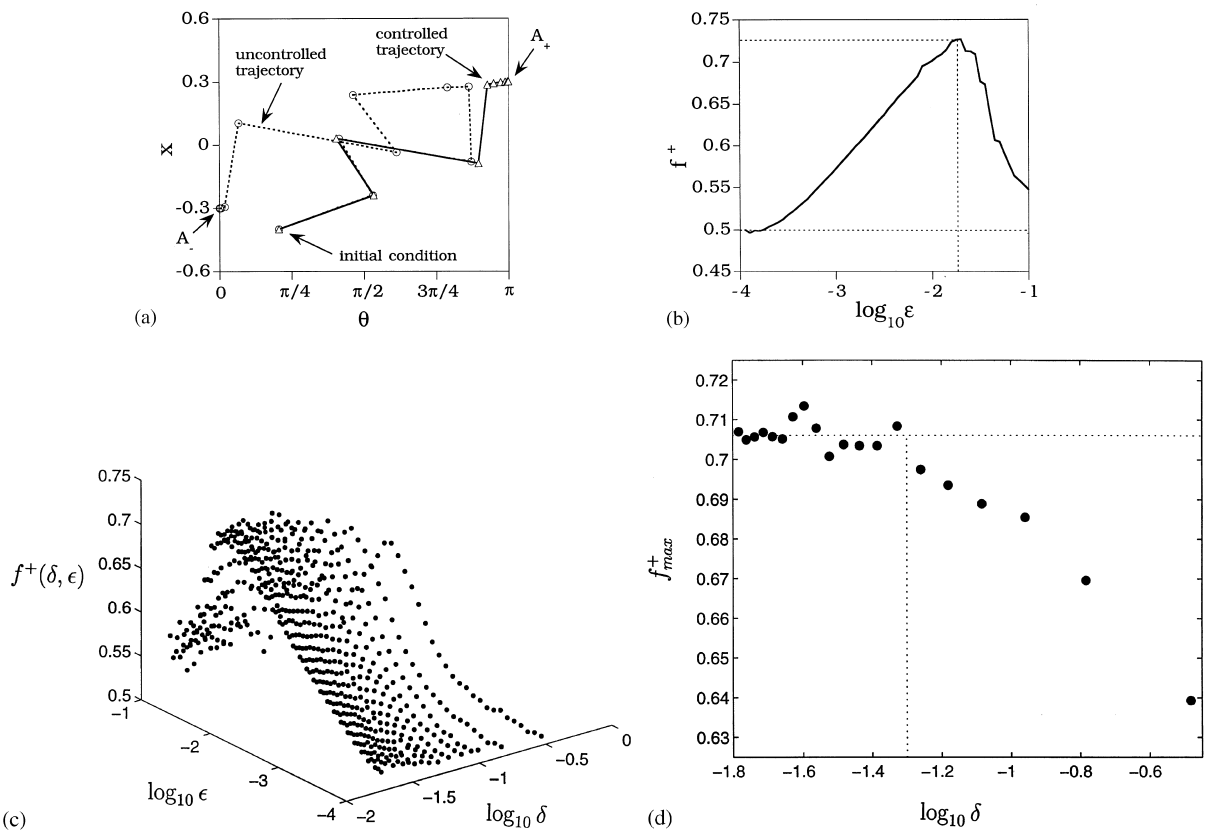

Fig. 8. From Ref. [85]. (a) A controlled trajectory to the desirable attractor A_+, where the size of the controlling neighborhood ε and the maximum allowed parameter perturbation $\Delta p_{\max}$ are both 10^{-2}. The trajectory would asymptote to the undesirable attractor A_- without control. (b) At $\delta \sim 10^{-2}$, the fraction f^+ of initial conditions that asymptote to A_+ versus $\log_{10}\varepsilon$. (c) The three-dimensional plot of f^+ versus $\log_{10}\delta$ and $\log_{10}\varepsilon$. We see that the optimal ε value for which f^+ reaches maximum is about 10^{-2}. (d) The maximum value $f^+_{\max}$ versus $\log_{10}\delta$.

using these values of ε and $p_{\max}$, about 70% of the initial conditions in the region $(0 \le \theta \le \pi,\ -0.5 \le x \le 0.5)$ asymptote to A_+, increased by 20% as compared with the case without control. Let δ be the size of the covering when the bush is built. Clearly, the fraction of initial conditions that asymptote to A_+ depends on both δ and the size of the controlling neighborhood ε. Fig. 8b shows, with the same bush of paths to A_+ as in Fig. 8a, f^+ versus ε ($\Delta p_{\max} = \varepsilon$) for δ fixed at about 3.3×10^{-2} and $10^{-4} \le \varepsilon \le 10^{-1}$. In the figure, for each value of ε, $N_0 = 90\,000$ (300×300) initial conditions uniformly distributed in the region $(0 \le \theta \le \pi,\ -0.5 \le x \le 0.5)$ are chosen and the number of controllable initial conditions N_+, i.e., those asymptote to A_+ via control, are recorded. The fraction f^+ is approximated by N_+/N_0. Since the grid size for building the bush is $\delta \sim 10^{-2}$, we see that when $\varepsilon \ll \delta$, essentially no improvement in f^+ is achieved because it is unlikely for initial conditions originally asymptoting to A_- to fall in the vicinity of points along the bush. When $\varepsilon \sim 10^{-2}$, maximum increase in f^+ is achieved because in this case, it is easy for trajectories to come close to the bush and to be

controlled. However, if $\varepsilon > \delta$, control may be lost for some initial conditions because the linearized dynamics used to derive the parameter perturbation Eq. (67) no longer holds at large values of ε, although in this case it is easy for trajectories to fall in the ε-neighborhood of the bush. Thus, we see that f^+ starts to decrease as ε increases about 10^{-2}. To more clearly see the dependence of f^+ on both δ and ε, we compute f^+ for systematically chosen δ and ε values. Fig. 8c shows the three-dimensional plot of f^+ versus δ and ε for $10^{-2} < \delta < 10^{-0.4}$ and $10^{-4} < \varepsilon < 10^{-1}$. Because of the two-dimensional phase space region used to construct the bush, decreasing δ to values below 10^{-2} leads to huge number of points on the bush and thus to numerical difficults. Nonetheless, it is clear from Fig. 8c that for the range of δ values chosen, maximum improvement in f^+ occurs at $\varepsilon \sim 10^{-2}$.

To understand why the optimal improvement in f^+ occurs at $\varepsilon \sim 10^{-2}$, we note that the maximum value $f^+_{\max}$ of f^+, as ε changes, depends on δ. Generally, $f^+_{\max}$ is small if δ is too large because in this case, the basin boundaries are not adequately covered. As δ decreases, $f^+_{\max}$ increases. But if δ becomes so small that the entire basin boundaries are covered by the bush, decreasing δ further does not help to increase $f^+_{\max}$. Thus, $f^+_{\max}$ saturates as δ decreases through a critical value. This behavior is shown in Fig. 8d, where we see that $f^+_{\max}$ saturates at $\delta \approx 10^{-1.26}$. The saturated value of $f^+_{\max}$ is about 0.706. At this δ value, there are approximately $N_c = 17\,300$ points on the bush. These are the required points to cover the basin boundaries adequately. We ask, how many of these points can be influenced by perturbations of magnitude ε? The answer is $\sim \varepsilon^\alpha N_c$ because the fraction of basin boundary points that are uncertain with respect to perturbation ε scales like ε^α. Since these N_c points on the bush provides a good covering of the basin boundaries, we have $\varepsilon^\alpha_{\text{optimal}} N_c \varepsilon^2_{\text{optimal}} \sim 1$, which gives $\varepsilon_{\text{optimal}} \sim N_c^{-1/(2+\alpha)} \approx 1.2 \times 10^{-2}$. This agrees with the numerical observation in Figs. 8b and c.

4.1.4. *Example 2*: *controlling riddled basins*

We first briefly review the concept of riddled basins. Riddled basins usually occur in dynamical systems with a simple type of symmetry. The existence of symmetry often leads to invariant subspace in the phase space. The description of riddled basins was introduced in Ref. [90] where it was shown that for certain class of dynamical systems with an invariant subspace: (i) if there is a chaotic attractor in the invariant subspace; (ii) if there is another attractor in the phase space; and (iii) if the Lyapunov exponent transverse to the subspace is negative, then the basin of the chaotic attractor in the invariant subspace can be riddled with holes belonging to the basin of the other attractor. That is, for every initial condition that asymptotes to the chaotic attractor in the invariant subspace, there are initial conditions arbitrarily nearby that asymptote to the other attractor. Rigorous results on the dynamics of riddled basins for discrete maps were presented in Refs. [90,91]. The dynamics of riddled basins was subsequently investigated in [92] using a more realistic physical model. A more extreme type of basin structure referred to as "intermingled basins" in which the basins of more than one chaotic attractors are riddled, was also studied using both discrete maps [90] and a more realistic physical system [93]. Riddled basins have been verified in experiments conducted using coupled electrical oscillators [94,95]. The mechanism for riddling to occur, and the basin structure associated with the riddling, were investigated by Ashwin et al. [95,96]. We consider the following two-dimensional map [85]:

$$\begin{aligned} x_{n+1} &= g(x_n) + by_n^2 \,, \\ y_{n+1} &= ax_n y_n + y_n^3 \,, \end{aligned} \tag{69}$$

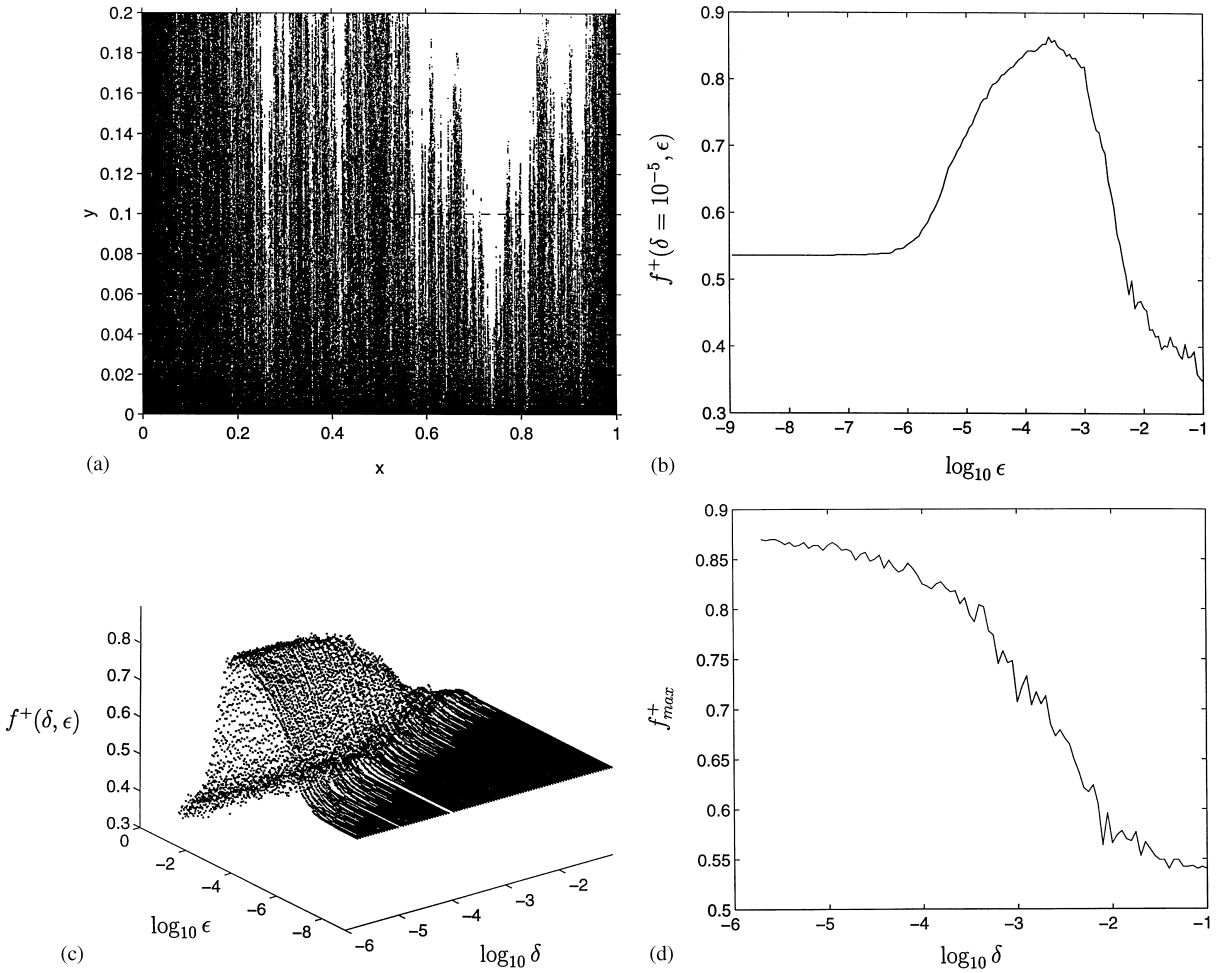

Fig. 9. From Ref. [85]. (a) Riddled basin of the $y = 0$ attractor for Eq. (69). The parameter setting is $r = 3.8$, $a = 1.7$ and $b = 0.1$. (b) For $\delta = 10^{-5}$, f^+ versus $\log_{10}\varepsilon$. (c) The three-dimensional plot of f^+ versus $\log_{10}\delta$ and $\log_{10}\varepsilon$. (d) The maximum value $f^+_{\max}$ versus $\log_{10}\delta$.

where $g(x)$ is a chaotic map, b and a are parameters. The invariant subspace is the one-dimensional line defined by $y = 0$ since if $y_0 = 0$, then $y_n = 0$ for $n \geq 1$. For simplicity we choose $g(x)$ to be the logistic map $g(x) = rx(1 - x)$ with a chaotic attractor. The transverse Lyapunov exponent is given by

$$\Lambda_\perp = \lim_{L\to\infty} \frac{1}{L}\sum_{n=0}^{L} \ln\left|\frac{\partial y_{n+1}}{\partial y_n}\right|_{y_n=0}\right| = \int ax\rho(x)\,\mathrm{d}x\ , \tag{70}$$

where $\rho(x)$ is the invariant density of the chaotic attractor produced by the logistic map. We choose $r = 3.8$ and obtain $a_c \approx 1.725$ where $\Lambda_\perp \geq 0$ for $a \geq a_c$ and $\Lambda_\perp < 0$ for $a < a_c$. For $a < a_c$, there are two attractors, one is $y = 0$ and another is $|y| = \infty$. The basin of the $y = 0$ attractor is riddled.

Fig. 9a shows part of the basin of the $y = 0$ attractor (black dots) for $a = 1.7 < a_c$ and $b = 0.1$, where a grid of 600×600 initial conditions is chosen in the region $0 \le x \le 1$ and $0 < y \le 0.2$. Examination of the figure on finer and finer scales reveals that there are white regions (basin of the $y = \infty$ attractor) near every black dots, a typical feature of riddling.

Now assume that the $y = 0$ chaotic attractor is the desirable attractor and the $y = \infty$ attractor is the undesirable one. To facilitate numerical computation, we choose to control trajectories starting from initial conditions on a line, say, $y = 0.1$. Without control, about 56% of the initial conditions on this line go to the desirable attractor. We build a bush of trajectories starting from $y = 0.1$ with size δ, i.e., we use δ^{-1} points on $y = 0.1$ to determine the points that asymptote to the desirable attractor. A difficulty here is that it typically takes many iterations for a trajectory starting at $y = 0.1$ to reach the desirable attractor (numerically a trajectory is regarded as having $y = 0$ if it says within 10^{-12} of $y = 0$ for certain prescribed number of iterations). Thus, for small grid size the number of points on the bush can be very large. It then becomes computationally difficult to determine whether a trajectory point is close to the bush. To make the computation feasible, we adopt the following strategy. For a random initial condition chosen from the line at $y = 0.1$, we examine whether it falls in an ε-neighborhood of a starting point of a path on the bush. If yes, we control it. Otherwise we let it evolve without control. Assume r in the logistic map is the accessible parameter to be perturbed. The parameter perturbations can be computed from Eq. (67). Fig. 9b shows f^+ versus $\log_{10} \varepsilon$ for $\delta = 10^{-5}$, where f^+ is the fraction of initial conditions that asymptote to the desirable attractor. The plot exhibits similar feature to that of Fig. 8b. We see that no improvement in f^+ is achieved if ε is too small because there are almost no points that come close to the bush. If ε is too large, although many trajectories would fall in the ε-neighborhood of the bush, control can get lost because Eq. (67) is only a linear control law. The optimal ε value for which f^+ reaches maximum is about $10^{-3.5}$, and the maximum possible value of f^+ is about 0.86, a substantial improvement in f^+ compared with the case of no control. Fig. 9c shows the three-dimensional plot of f^+ versus δ and ε. We see that for $\delta < 10^{-2}$, f^+ reaches maximum at $\varepsilon_{\text{optimal}} \approx 10^{-3.5}$. Fig. 9d shows $f^+_{\max}$ versus $\log_{10} \delta$. For $10^{-2} < \delta < 10^{-1}$, $f^+_{\max}$ is about the same as if there were no control. It then increases rapidly as δ is decreased from 10^{-2} and starts to increase slowly as δ decreases through 10^{-4}. Compared with the example of controlling fractal basin boundaries, we see that the maximum value of $f^+_{\max}$ can be higher. This is due to the feature of riddled basins where the uncertainty exponent α is close to zero. The reason that we obtain $\varepsilon_{\text{optimal}} \approx 10^{-3.5}$ can be understood by noting that for $\delta \approx 10^{-4}$, there are about 5560 points on $y = 0.1$ that belong to the bush. Thus we have $\varepsilon^{1+\alpha}_{\text{optimal}} N \sim 1$. Since $\alpha \approx 0$, this gives $\varepsilon_{\text{optimal}} \sim 10^{-3.7}$.

4.1.5. Discussions

We have reviewed an algorithm [85] to drive trajectories to a desirable attractor by using small feedback control for dynamical systems with multiple coexisting attractors. The basic idea is to build a bush-like structure of paths to the target attractor and to stabilize a trajectory around one of the many paths on the bush so that the trajectory asymptotes to the desirable attractor. Such a structure of paths, in principle, can be built up even in more realistic applications. For instance, an experimentalist could run the system first, measure time series resulting from many initial conditions, and build the bush of paths to the desirable attractor in the reconstructed phase space by using the delay-coordinate embedding technique. One can then use techniques such as the direct proportional feedback control [97,98] to compute the required parameter perturbations as it may

be a formidable task to apply Eq. (67) in practice. But of course, at present there is no guarantee that the method can be applied to practical applications. We stress, however, that from a more general theoretical point of view, the success of the method relies on the region in the phase space to which the bush extends. As such, the method is particularly effective when there are fractal basin boundaries with large values of fractal dimension (or small values of the uncertainty exponent α) in the phase space region of interest. In contrast, there is no uncertainty exponent α) in the phase space region of interest. In contrast, there is no appreciable increase in the probability for a trajectory to be driven to the desirable attractor if the basin boundaries are smooth. *One could, therefore, deliberately build into the system fractal basin boundaries or riddled basins in order to drive most initial conditions to the desirable attractor.* While there is a great uncertainty in determining the asymptotic attractor for individual initial conditions when there are fractal basin boundaries or riddled basins, the uncertainty is greatly reduced for a path that consists of a large number of points in the phase space. Therefore, insofar as a trajectory can be stabilized around a path on the bush, the fate of the trajectory is almost certain, i.e., the desirable attractor.

Theoretically, there is no reason for restricting the control to a bush. For instance, one may obtain more optimal results in the following way. Assume that for a map M we have basin of attraction D for a desirable attractor A. For perturbation of magnitude ε, let $B_\varepsilon(D)$ be the union of all ε-balls around all points in D (the ε-parallel body of D). Consider the union of all the preimages of the $B_\varepsilon(D)$. This union would give the largest possible domain (always an open set) for which there exist ε-pseudo orbits of the map that eventually asymptote to the desirable attractor A. If a practical method can be devised to cover this union and to drive trajectories in this union to A, we would expect to achieve an absolute maximum size for the basin of attraction of A under arbitrarily small perturbations. At present, how to cover such a union and how to devise a control algorithm to achieve this theoretical maximum remain unknown.

The central problem in controlling dynamical systems with multiple coexisting attractors is how to maximize the probability of being able to control an arbitrary initial condition. Thus, it is important to assess how this probability varies with the maximum allowed perturbation and the dimension of the basin boundaries. To obtain this information, we now imagine an "ideal" controller. We restrict to situations where only the initial conditions near basin boundaries are accessible to control. For a given initial condition, the ideal controller would evolve the system to see if the asymptotic attractor is the desirable one. If not, small parameter perturbation ε is applied and the system is evolved from the same initial condition. The controller would then check if the initial condition yields the desirable attractor. It could repeat this procedure for a given number of time, insofar as the asymptotic attractor is not the desirable one. In this case, the probability for driving an arbitrary initial condition to the desirable attractor is proportional to the fraction of uncertain initial conditions, which scales with the perturbation as ε^α. Thus, we see that for fixed α, increasing ε would increase the desired probability. For fixed $\varepsilon < 1$, increasing the dimension of the basin boundary, which is equivalent to decreasing the uncertainty exponent α, would increase the desired probability. This, of course, holds only for the ideal controller. In more practical situation, we see that there exists an optimal ε value for achieving the desired probability (see Figs. 8 and 9). This optimal ε value depends on many factors including the dimension of the basin boundaries. Nonetheless, high desired probability can be achieved if the dimension of the basin boundaries is large (or α is small). In cases where the basin-boundary dimension is close to the phase-space

dimension (or α is close to zero, such as in riddled basins), one expects to achieve higher desired probability as in such a case, most initial conditions are near the basin boundaries.

Finally, we emphasize that the control method reviewed here represents *only one possible* approach to solve the general problem of controlling dynamical systems with multiple basins of attraction. There will undoubtedly be better methods that await for future investigation.

4.2. The adaptive targeting of chaos

Targeting of chaos means judiciously perturb a chaotic system with the aim of directing the orbit emerging from a given point to a neighborhood of some other prespecified point (called *target*) on the attractor within a finite and specified time (called target time). As already mentioned in the Introduction, even though ergodicity assures that all point on the attractor are shadowed regardless on the initial conditions chosen for the chaotic evolution, in many cases a small neighborhood of a given attractor point may be visited infrequently; thus, the unperturbed dynamics may take a long time to approach a given target. Thence, the necessity of implementing efficient targeting methods, which can reduce strongly the waiting time [35,36,99–101].

The targeting procedure may be seen as a preliminary task for chaos control, because, as we have already pointed out, the control algorithms (see, e.g. [1–3]) use linearizations of the dynamics that are valid only in a rather small neighborhood of the desired saddle point, and therefore need the system to target such a small neighborhood before the switch on.

The first targeting method was introduced by Shinbrot et al. [35], who have suggested to use the exponential sensitivity of a chaotic process to tiny perturbations in some accessible control parameter. This technique was successfully applied to one-dimensional mappings both theoretically [99] and experimentally [100] and then extended to three-dimensional chaotic flows [101].

Later, Kostelich et al. [36] faced the problem of targeting hyperchaos, that is extending the above procedure to cases where there is more than one positive Lyapunov exponent associated with typical orbits on the attractor. (See Ref. [102] for a review of these procedures.)

The basic algorithm in [36] applies tiny perturbations for performing two successive changes of a control parameter (or one change of two parameters). The perturbations are selected to move the image of the initial condition onto the stable manifold of the target. The robustness of this method against the presence of a small amount of noise or a small modeling error has been proved, and further developments have pointed out how it can help in switching between controlled unstable periodic orbits even in higher-dimensional chaotic situations [103].

However, there are two main limitations for the application of such a technique, namely: (1) the above method is only applicable to invertible mappings, and (2) it needs full a priori information on the stable and unstable manifolds of the target.

The latter requirement can give rise to serious drawbacks in all cases in which the target corresponds to an attractor point whose neighborhood is rarely visited by the natural evolution of the system, insofar as one needs a long data acquisition time to obtain points whose orbits closely visit the target.

Alternative methods have been proposed [104] to increase the number of visits to a target by making small perturbations of the state variables of the system.

The application of the adaptive technique for the targeting of chaos was realized in Ref. [66], either for the case in which all state variables are accessible for detections and perturbations, and

for the case in which the operator may rely on a single state variable, whereas the others are hidden, and not accessible for measurements and perturbations. We summarize herebelow the main results of Ref. [66].

We start from the general problem of considering a chaotic process ruled by

$$\dot{\boldsymbol{x}} = \boldsymbol{f}(\boldsymbol{x}, \mu) \,, \tag{71}$$

where $\boldsymbol{x}$ is a D-dimensional vector ($D \geq 3$), $\boldsymbol{f}$ is a nonlinear function of $\boldsymbol{x}$, dot denotes temporal derivative, and μ is a vector of parameters. The targeting strategy consists of two distinct parts: (1) an algorithm that slaves the chaotic dynamics $\boldsymbol{x}(t)$ to a given goal dynamics $\boldsymbol{g}(t)$ with the only use of small perturbations, and (2) an algorithm detecting and constructing a goal dynamics $\boldsymbol{g}_T(t)$ that brings the trajectory to a small neighborhood of the target within the desired target time starting from a given initial condition $\boldsymbol{g}_T(0) = \boldsymbol{g}_0$ in a way compatible with the unperturbed evolution of the system. The point $\boldsymbol{g}_0$ is chosen so as to lie on the attractor, and typically its neighborhood is visited frequently by the unperturbed dynamics.

While for point (1) one can naturally rely on the existent slaving techniques (and here we will use the adaptive methods of Eqs. (54)–(57)), point (2) has found a solution in Ref. [66].

The main improvement offered by Ref. [66] with respect to other targeting techniques, is that there the extraction of the goal dynamics is done with a *single* visit of the target. This way, one minimizes the learning time, in all cases in which the target is rarely visited by the unperturbed dynamics (which are, indeed, the most interesting cases, since when the target is frequently visited by the natural dynamics, the whole targeting procedure would not be needed).

Let us then consider the following two cases: (i) the system allows detection and perturbation of all its state variables; and (ii) only a single state variable is available for observation.

Let us start with case (i) and discuss the problem of constructing the goal dynamics $\boldsymbol{g}_T(t)$ from a preliminary observation of the unperturbed behavior of the system.

Following Ref. [66], we will describe the targeting procedure with reference to the three-dimensional Rössler system [105]

$$\dot{x} = -z - y, \qquad \dot{y} = x + ay, \qquad \dot{z} = b + z(x - c) \,, \tag{72}$$

with $a = b = 0.2$ and $c = 5.7$. One first constructs a partition of the three-dimensional phase space in parallelograms of sides $\varepsilon \equiv (\varepsilon_1, \varepsilon_2, \varepsilon_3)$. For that purpose, one defines

$$I(x_0, y_0, z_0, \varepsilon) = \{(x, y, z)\colon\ x_0 < x < x_0 + \varepsilon_1,\ y_0 < y < y_0 + \varepsilon_2 \text{ and } z_0 < z < z_0 + \varepsilon_3\} \,. \tag{73}$$

By letting system (72) evolve from the initial condition $x(0) = y(0) = 1$, $z(0) = 4$, a chaotic set is realized, a portion of which is contained in the parallelogram $I_T(4.655146, -6.691886, 0.013528, \varepsilon)$, where $\varepsilon \equiv (0.205382, 0.186303, 0.228361)$.

It is important to remark that this choice of ε corresponds to a box whose sides are 10^{-2} as long as the corresponding sides of the smallest parallelogram containing the attractor for $t > 9743.658203$ (from now on $t = t_T = 9743.658203$ will be the time at which the unperturbed trajectory first enters I_T).

By registering the natural evolution of the system from the above initial conditions up to the first visit to the target, and by using this portion of the natural trajectory, one constructs a web of paths compatible with the unperturbed dynamics, each of which connecting different parallelograms to

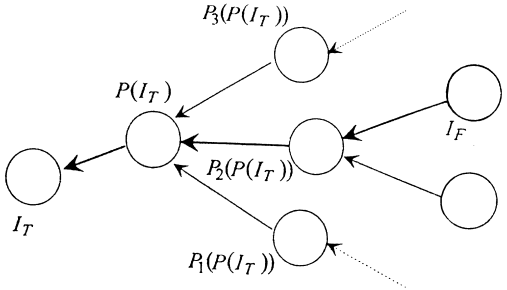

Fig. 10. Procedure for the construction of the goal dynamics $\boldsymbol{g}(t)$. Each bubble represents the neighborhood of a point in the phase space. I_T: target; $P(I_T)$: unique preimage of the target; $P_j(P(I_T))$, $j = 1, 2, 3$: multiple preimages of $P(I_T)$; I_F: most frequently visited neighborhood. The selected path is shown as a thick line.

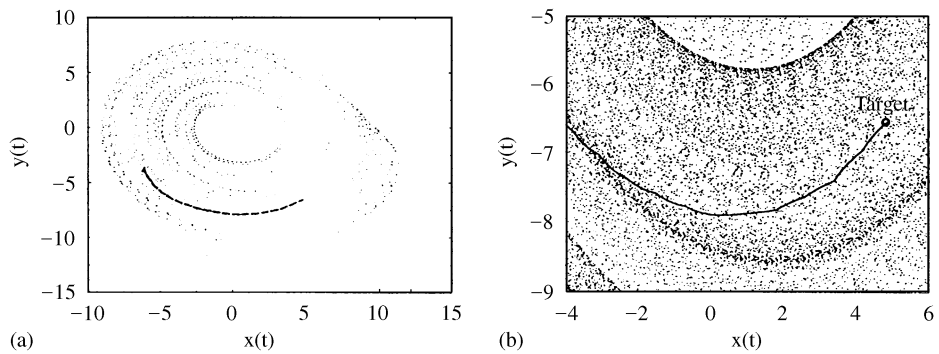

Fig. 11. (a) An (x, y) projection of the unperturbed Rössler dynamics (dots) and path followed by the perturbed dynamics to reach the target (thick dashed line). The path is inside the chaotic attractor. (b) Zoom of (a): the path (solid line) moves from high probability regions of the attractor toward lower probability regions, until reaching I_T (indicated as Target in the figure). Initial conditions and control parameters as in the text.

I_T. Precisely, one follows few trajectories for a given observation interval. Suppose to call $P(I_T)$ the preimage of I_T. Since the recorded trajectory visits the target only once, $P(I_T)$ is univocally determined. One then records the portions of the observed trajectories that lie in I_T and $P(I_T)$ and determines successive preimages of $P(I_T)$, which, in most cases, have been visited previously by the portions of the observed trajectories.

Going backward in time, one selects from the observations a path starting from the most frequently visited parallelogram I_F and leading to the box I_T. Fig. 10 schematically illustrates the obtained web of paths. At the end of this process, one can make use of the observed path from I_F to I_T, as goal function for the application of the adaptive control procedure. Since the natural measure of I_F is large (that is, it is frequently visited by the unperturbed dynamics), the target can be reached quickly regardless of the initial conditions.

Fig. 11a reports the results of applying the adaptive method of Eqs. (54)–(57) to the system of Eqs. (72), using as goal dynamics the reconstructed path. I_F is reached by the unperturbed dynamics for the first time when $t = 30.9$ s, and then I_T is reached by the perturbed dynamics only

1.6 s later. Thus, the total waiting time required to reach I_T is reduced from 9743 to 32.5 s, implying a total speedup of two orders of magnitude.

Fig. 11b illustrates the mechanism that leads the system to the target: the trajectory followed by the perturbed evolution moves from high probability sections of the attractor toward lower and lower probability sections, up to the target.

What described above requires that all state variables be accessible for measurements and perturbations. Therefore, its applicability can be seriously limited in experimental situations, where often only a single state variable of the system is accessible, whereas the others are in general hidden, or not accessible. It is convenient then to reformulate the adaptive targeting strategy in the more realistic case, in which measurements can be done only to one of the state variables of the Rössler system (say the x variable) and perturbations can be applied only to the first of Eqs. (72).

In this case, one immediately realizes that the problem is to retrieve a suitable scalar goal dynamics $g(t)$ from the observations compatible with the unperturbed evolution of the system and coming at least once within a suitable neighborhood of the target. To do this, one can make use of the time delay embedding technique [26], allowing to reconstruct the attractor from a time series of measurements of a single variable, say $x(t)$, from Eqs. (72).

The above problem was solved again in Ref. [66], by selecting a suitable delay time $\tilde{\tau}$, and considering the D-dimensional embedding space of the vectors $\boldsymbol{x}(t) = (x(t), x(t-\tilde{\tau}), \ldots, x(t-(D-1)\tilde{\tau}))$ ($D = 3$ in the present case). One of the main feature of the embedding technique is to retain the basic metric properties of the original phase space description. In other words, this means that points that are neighbors in the original phase space with respect to a given metric M_R remain neighbors in the embedding space with respect to some new metric M_E.[4] $\tilde{\tau} = 5.71157$ was chosen in Ref. [66], corresponding to the inverse frequency of the largest peak in the power spectrum of the signal $x(t)$. The target point in the original phase space is now mapped into the point $\boldsymbol{x}_T = (x_T(t_T), x_T(t_T-\tilde{\tau}), x_T(t_T-2\tilde{\tau})) = (4.727415, 4.295067, 4.929038)$. The idea is to retrieve a scalar goal dynamics $g(t)$ with the following properties: $g(t_0) = x_T(t_T-2\tilde{\tau})$, $g(t_0+\tilde{\tau}) = x_T(t_T-\tilde{\tau})$, and $g(t_0+2\tilde{\tau}) = x_T(t_T)$. Here t_0 is the instant at which the unperturbed $x(t)$ first satisfies $x_T(t_T-2\tilde{\tau}) - \varepsilon_1/2 < x(t) < x_T(t_T-2\tilde{\tau}) + \varepsilon_1/2$ ($\varepsilon_1 = 0.205382$).

By these requirements, one immediately realizes that the perturbations move the trajectory to the target within the target time $t_0 + 2\tilde{\tau}$, regardless on the particular initial conditions for the evolution of the dynamics.

The simplest choice of the goal function would be the recorded unperturbed evolution of x from $t_T - 2\tilde{\tau}$ to t_T. But this choice is not the optimal one. Indeed, since in the present case the observations are limited to a one-dimensional subspace, there is no certainty that at $t = t_0$ the other hidden variables are within a sufficiently small distance from their values at $t_T - 2\tilde{\tau}$. The process could therefore result in an unacceptably large initial perturbation, and another choice of g would be necessary. For instance, the evolution of $x(t)$ could be exploited more thoroughly by constructing two successive webs of 1-dimensional paths, the first connecting $x_T(t_T-2\tilde{\tau})$ to $x_T(t_T-\tilde{\tau})$, and the second connecting $x_T(t_T-\tilde{\tau})$ to $x_T(t_T)$.

But here the selection of a goal dynamics is further complicated by the requirement that paths reach from a given point to another given point within a specified time. This constraint motivates

[4] In most cases, and also in ours, M_R and M_E both coincide with the metric defining the Euclidean distance between points.

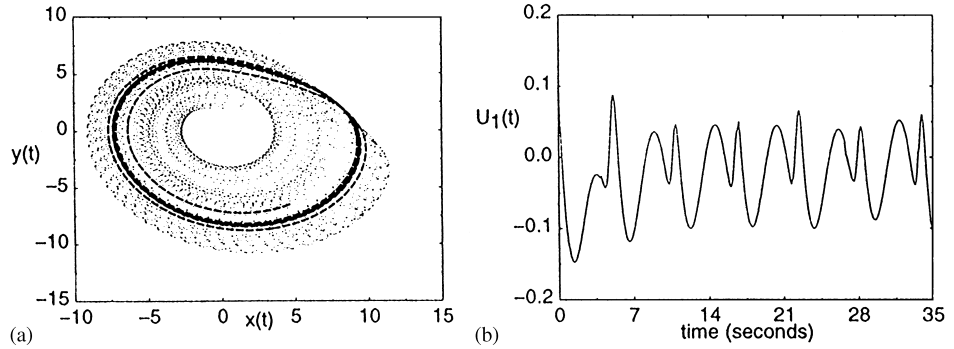

Fig. 12. From Ref. [66]. (a) An (x, y) projection of the unperturbed Rössler dynamics (dots) and path followed by the perturbed dynamics to reach the target (thick dashed line). In this case the perturbation acts only on the x variable of Eqs. (72). Again, the path is inside the chaotic attractor; thus it is compatible with the natural evolution of the system and it goes from higher to lower probability regions. (b) Temporal evolution of the perturbation during the targeting process. The range spanned by U is less than 1% of the range spanned by the x dynamics. Initial conditions and control parameters as in the text.

the choice of $\tilde{\tau}$ in Ref. [66] as the reciprocal of the frequency of the main peak in the power spectrum. This time is, more or less equivalent to the return time of the system onto its Poincaré section. For sufficiently long observations, ergodicity of chaos assures a covering of all the states and guarantees the existence of at least one path from any initial state to any final state within observation interval.

However, these concerns are largely obviated by a suitable choice of $\sigma \neq 0$ in the adaptive control algorithm. In the present case, it is sufficient to choose $g(t)$ as the unperturbed dynamics from $t_T - N\tilde{\tau}$ to t_T $(N > 2)$. While the integer N should be selected as small as possible to minimize the waiting time, larger values of N improve the robustness of the method. Fig. 12a reports the new phase space results for $N = 6$.

The system is left unperturbed from $t = 0$ (same initial conditions as before) until $t = t_0 = 12.9$. Here t_0 is the instant at which the unperturbed dynamics first enters the ε_1 interval containing $x(t_T - 6\tilde{\tau})$. The adaptive scalar perturbation assures a convergence to the target within a target time of $t_0 + 6\tilde{\tau}$, which again is more than two orders of magnitude smaller than t_T.

It is important to visualize accuracy of the adaptive method in targeting the desired I_T in the real phase space, even with this simple choice of g. Fig. 12b shows the range of fluctuations of the perturbations, and Fig. 12a shows the range spanned by the unperturbed x dynamics.

5. Stabilizing desirable chaotic trajectories and application

5.1. Stabilizing desirable chaotic trajectories

5.1.1. Overview

We consider the following situation: suppose there is a nonlinear dynamical system whose trajectories lie on a chaotic attractor. Suppose further that one of the uncountably infinite number of chaotic orbits embedded in the chaotic attractor corresponds to a desirable operational state of

the system. Our goal is to apply only small feedback control to keep trajectories originating from random initial conditions in the vicinity of the desirable *chaotic* orbit. In what follows, we present a general method to achieve this goal and demonstrate that the idea can be applied to synchronization of chaotic systems.

Our method to stabilize a desirable chaotic orbit is based on OGY's method of controlling chaos. We first select the desirable orbit (the target) according to our needs. Different methods can be used to construct such a target orbit in different contexts. We then stabilize a trajectory originated from a random initial condition around the target orbit. This can in fact be achieved if the target chaotic orbit is a trajectory generated by the evolution equations of the dynamical system. Such target orbit possesses a local hyperbolic structure of stable and unstable directions at almost all points, which is rather typical for chaotic orbits. Finally, we apply small feedback control to stabilize the target chaotic orbit. The construction of such a target orbit is, therefore, a crucial step in the controlling method. This will be detailed in numerical examples.

5.1.2. Method for stabilizing a desirable chaotic orbit

Our method for stabilizing a desirable chaotic orbit is based on the OGY idea of stabilizing a desirable unstable periodic orbit. Intuitively, the orbit to be stabilized has a period equal to the length of the orbit. Consider chaotic systems described by two-dimensional maps on the Poincaré surface of section:

$$\boldsymbol{x}_{n+1} = \boldsymbol{F}(\boldsymbol{x}_n, p) \ , \tag{74}$$

where $\boldsymbol{x}_n \in \mathbf{R}^2$, p is an externally controllable parameter. In the spirit of the OGY ideas, we require that the parameter perturbations be small:

$$|\Delta p| \equiv |p - p_0| < \delta \ , \tag{75}$$

where p_0 is some nominal parameter value, δ is a small number defining the range of parameter perturbations. Let $\{\boldsymbol{y}_n\}$ $(n = 0, 1, 2, \ldots, N)$ be the target chaotic orbit. Now generate a trajectory $\{\boldsymbol{x}_n\}$ to be stabilized around the target orbit. Randomly pick an initial condition $\boldsymbol{x}_0$, assume that the trajectory point $\boldsymbol{x}_n$ $(n \geq 0)$ falls in a small neighborhood of the point $\boldsymbol{y}_k$ of the target orbit at time step n. Without loss of generality, we set $k = n$ on the target orbit. In this small neighborhood, linearization of Eq. (74) is applicable. We have

$$\boldsymbol{x}_{n+1}(p_n) - \boldsymbol{y}_{n+1}(p_0) = \boldsymbol{J} \cdot [\boldsymbol{x}_n(p_0) - \boldsymbol{y}_n(p_0)] + \boldsymbol{K}\,\Delta p_n \ , \tag{76}$$

where $\Delta p_n = p_n - p_0$, $|\Delta p_n| \leq \delta$, $\boldsymbol{J}$ is the 2×2 Jacobian matrix and $\boldsymbol{K}$ is a two-dimensional column vector:

$$\boldsymbol{J} = \boldsymbol{D}_x \boldsymbol{F}(\boldsymbol{x}, p)|_{\boldsymbol{x}=\boldsymbol{y}_n, p=p_0}, \quad \boldsymbol{K} = \boldsymbol{D}_p \boldsymbol{F}(\boldsymbol{x}, p)|_{\boldsymbol{x}=\boldsymbol{y}_n, p=p_0} \ . \tag{77}$$

Without control, i.e., $\Delta p_n = 0$, the trajectory $\boldsymbol{x}_i$ $(i = n+1, \ldots)$ diverges from the target orbit $\boldsymbol{y}_i$ $(i > n)$ geometrically. The task is to program the parameter perturbations Δp_n so that $|\boldsymbol{x}_i - \boldsymbol{y}_i| \to 0$ for subsequent iterates $i > n$.

For almost all points on the target orbit, there exist both a stable and an unstable direction [34]. These directions can be calculated by using the numerical method in Ref. [34]. The calculated stable and unstable directions are stored together with the target orbit, and this information is used

to compute the parameter perturbations applied at each orbit point for $i > n$. Let $\boldsymbol{e}_{s(n)}$ and $\boldsymbol{e}_{u(n)}$ be the stable and unstable directions at $\boldsymbol{y}_n$, and $\boldsymbol{f}_{s(n)}$ and $\boldsymbol{f}_{u(n)}$ be two dual vectors orthogonal to $\boldsymbol{e}_{u(n)}$ and $\boldsymbol{e}_{s(n)}$, respectively. The vectors $\boldsymbol{f}_{s(n)}$ and $\boldsymbol{f}_{u(n)}$ satisfy $\boldsymbol{f}_{u(n)} \cdot \boldsymbol{e}_{u(n)} = \boldsymbol{f}_{s(n)} \cdot \boldsymbol{e}_{s(n)} = 1$ and $\boldsymbol{f}_{u(n)} \cdot \boldsymbol{e}_{s(n)} = \boldsymbol{f}_{s(n)} \cdot \boldsymbol{e}_{u(n)} = 0$. To stabilize $\{\boldsymbol{x}_n\}$ around $\{\boldsymbol{y}_n\}$, we require the next iteration of $\boldsymbol{x}_n$, after falling into a small neighborhood around $\boldsymbol{y}_n$, to lie on the stable direction at $\boldsymbol{y}_{(n+1)}(p_0)$:

$$[\boldsymbol{x}_{n+1}(p_n) - \boldsymbol{y}_{(n+1)}(p_0)] \cdot \boldsymbol{f}_{u(n+1)} = 0 \ . \tag{78}$$

Substituting Eq. (76) into Eq. (78), we obtain the following expression for the parameter perturbation:

$$\Delta p_n = \frac{\{\boldsymbol{J} \cdot [\boldsymbol{x}_n(p_0) - \boldsymbol{y}_n(p_0)]\} \cdot \boldsymbol{f}_{u(n+1)}}{-\boldsymbol{K} \cdot \boldsymbol{f}_{u(n+1)}} \ , \tag{79}$$

where if $\Delta p_n > \delta$, we set $\Delta p_n = 0$.

In stabilizing unstable periodic orbits, the average transient ("waiting") time to achieve the control scales with the maximum allowed parameter perturbation δ as $\tau \sim \delta^{-\gamma}$, where the scaling exponent γ can be computed in terms of the stable and unstable eigenvalues of the unstable periodic orbits [1,23]. For cases where $\gamma > 1$, the transient time can be significantly reduced if somewhat larger parameter perturbations are allowed. The problem of transient time is *much less severe* here, since the target orbit is long. In principle, when the trajectory enters the neighborhood of any one of the points on the target orbit, parameter control based on Eq. (79) can be applied. Thus, even if the size of every neighborhood around the target orbit is small, the transient time required can be significantly reduced by increasing the length of the target orbit.

5.1.3. Synchronization of low-dimensional chaotic systems by control

Chaos is characterized by a sensitive dependence of system's dynamical variables on initial conditions. Trajectories starting with slightly different initial conditions diverge from each other geometrically. Consequently, synchronization seems unlikely even for two perfectly identical chaotic systems, if trajectories start from initial conditions that differ slightly. Moreover, in practical applications the existence of noise (both external and internal) and system imperfect identification makes the hope of synchronizing two chaotic systems even more remote. Nonetheless, it was demonstrated by Pecora and Carroll [22] that synchronization of chaotic dynamical systems is not only possible but it is believed to have potential applications in communication [22,106–108].

In the feedback control approach to synchronize chaotic systems [51], as opposed to the open loop synchronization method in Refs. [22,106–108], it is not required that the system under study be divided into subsystems, and both noise and a small amount of system parameter mismatch are allowed. Specifically, the OGY strategy is extended to stabilize a *chaotic trajectory* of one system about a *chaotic orbit* of the other system to achieve synchronization of the two systems. It should be noted that the idea of stabilizing chaotic orbits by using OGY method was also proposed by Metha and Henderson [109]. Their approach is to construct an artificial dynamical system evolving errors between the system's output and the target chaotic orbit. If the artificial system has a zero fixed point, parameter perturbations based on the OGY algorithm are then applied to stabilize the artificial system around its zero fixed point, which means that the original system's output is brought to the desired chaotic orbit. They illustrated their method by using one-dimensional

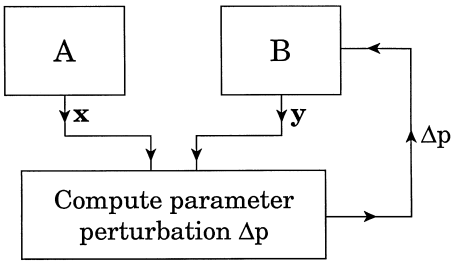

Fig. 13. From Ref. [51]. A schematic illustration of the strategy to synchronize two chaotic systems. Some dynamical variables of two systems are measured, based on which temporal parameter perturbations are calculated and applied to the system B. We assume that before the synchronization, some information about the geometrical structure of the chaotic attractor (e.g., the Jacobian matrices along a long chaotic trajectory that practically covers the whole attractor) has been obtained.

maps. Construction of the artificial map for more general dynamical systems may be nontrivial. In Ref. [51], on the other hand, parameter perturbations are applied *directly to the original dynamical system* and the method makes use of the geometrical structure of the chaotic trajectory.

To synchronize two chaotic systems which we call A and B, we imagine that some parameter of one system (assume B) is externally adjustable. The strategy is illustrated schematically in Fig. 13, where we assume that some state variables of both systems A and B can be measured. Based on this measurement and our knowledge about the system (we can, for example, observe and learn the system first), when it is determined that the state variables of A and B are close, we calculate a small parameter perturbation based on the OGY algorithm and apply it to system B. Two systems can then be synchronized, although their trajectories are still chaotic. Under the influence of external noise, there is a finite probability that the two already synchronized trajectories may lose synchronization. However, with probability one (due to the ergodicity of chaotic trajectories), after a finite amount of transient time, the trajectories of A and B will get close and are synchronized again. In this sense, the synchronization method is robust against small external noise.

We consider two *almost identical* chaotic systems that are described by two-dimensional maps on the Poincaré surface of section:

$$\boldsymbol{x}_{n+1} = \boldsymbol{F}(\boldsymbol{x}_n, p_0)\,[A], \quad \boldsymbol{y}_{n+1} = \boldsymbol{F}(\boldsymbol{y}_n, p)\,[B] \tag{80}$$

where $\boldsymbol{x}_n, \boldsymbol{y}_n \in \mathbf{R}^2$, $\boldsymbol{F}$ is a smooth function in its variables, p_0 for system A is a fixed parameter value and, p for system B is an externally controllable parameter. For the purpose of synchronization, we require that the dynamics should not be substantially different for systems A and B. Equivalently, we require that the parameter perturbations be small, i.e., $|p - p_0| < \delta$, where δ is a small number defining the range of parameter variation. Suppose that the two systems start with different initial conditions. In general, the resulting chaotic trajectories are completely uncorrelated. However, due to ergodicity, the two trajectories can get arbitrarily close to each other at some later time n_c. Without control, the two trajectories will separate from each other exponentially again. We then program the parameter p using the method in Section 2 so that $|\boldsymbol{y}_n - \boldsymbol{x}_n| \to 0$ for $n \geq n_c$, which means that A and B are synchronized for $n \geq n_c$.

We now illustrate the synchronization algorithm by using the Hénon map: $(x, y) \to (a - x^2 + 0.3y, x)$, where a is the control parameter. Consider two such Hénon systems. One has fixed

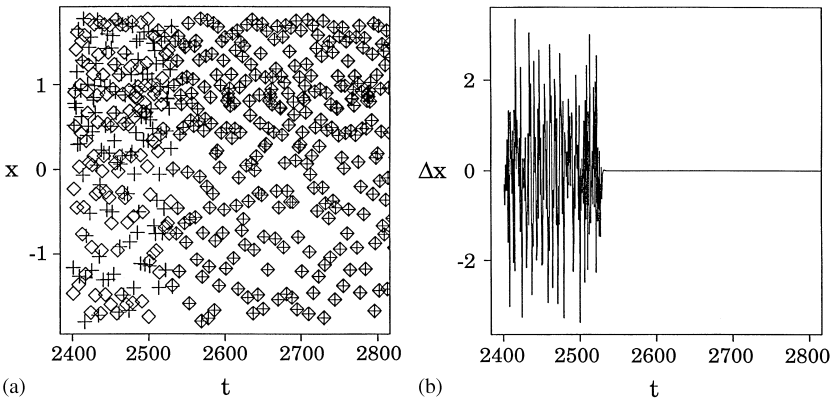

Fig. 14. From Ref. [51]. Synchronizing two Hénon systems $[(x, y) \to (a - x^2 + 0.3y, x)]$. In system A, the parameter a is fixed at $a_0 = 1.4$. In system B, a is allowed to vary in [1.39,1.41]. (a) The uncorrelated and synchronized chaotic trajectories of the two systems before and after the parameter control is turned on and, (b) part of the time series of the difference $\Delta x = x_2 - x_1$ corresponding to (a). The synchronization neighborhood is chosen to be a circle of radius 0.01 (see text).

parameter value ($a = a_0 = 1.4$) which serves as the "target" and, in the other system we adjust a in a small range $(1.39, 1.41)$ according to Eq. (6). At time $t = 0$, we start two systems with different initial conditions: $(x_1, y_1) = (0.5, -0.8)$ and $(x_2, y_2) = (0.0, 0.0)$. The two systems then move in completely uncorrelated chaotic trajectories. At time step 2534, the trajectory points of the two systems come close to each other within a circle of radius of 0.01. When this occurs, we turned on the parameter perturbations calculated from Eq. (6). Note that the radius 0.01 above can be changed slightly (without affecting the synchronization) depending on how we define the "synchronization neighborhood" in which the two trajectories are considered to be close together. In general, the size of such a neighborhood should be chosen to be proportional to δ, the maximum allowed parameter perturbation. Fig. 14a shows part of a time series of the uncorrelated and synchronized chaotic trajectories before and after the control is turned on, respectively, where the crosses and diamonds denote values of x for the two chaotic trajectories. Clearly, after the control is turned on, crosses and diamonds overlap each other, indicating the two chaotic Hénon trajectories evolve completely in phase (synchronization), although they are still chaotic. Fig. 14b shows a time series of $\Delta x(t) = x_2(t) - x_1(t)$, where we see that $\Delta x(t) = 0$ after the control is applied.

In the presence of noise, the two synchronized trajectories can go uncorrelated again (x_2 is "kicked" out of the neighborhood of x_1 by the noise). When $\Delta x(t)$ exceeds a critical value, say 0.01, we turn off the control and let the two systems evolve by themselves. Due to ergodicity, the two trajectories will come close again and be synchronized. To model the effect of noise, we add a term $\varepsilon\sigma(t)$ to the x-component of the two Hénon systems, where σ is a random variable with Gaussian probability distribution of zero mean and unit standard deviation and, ε characterizes the noise amplitude. Figs. 15a and b show part of the time series of $\Delta x(t)$ for $\varepsilon = 3.8 \times 10^{-4}$ and $\varepsilon = 4.18 \times 10^{-4}$, respectively. Clearly, the smaller the noise amplitude is, the longer the two systems are expected to remain synchronized.

In stabilizing unstable periodic orbits, the average transient time to achieve the control is shown to scale with the maximum allowed parameter perturbation δ as $\tau \sim \delta^{-\gamma}$, where γ is given in terms

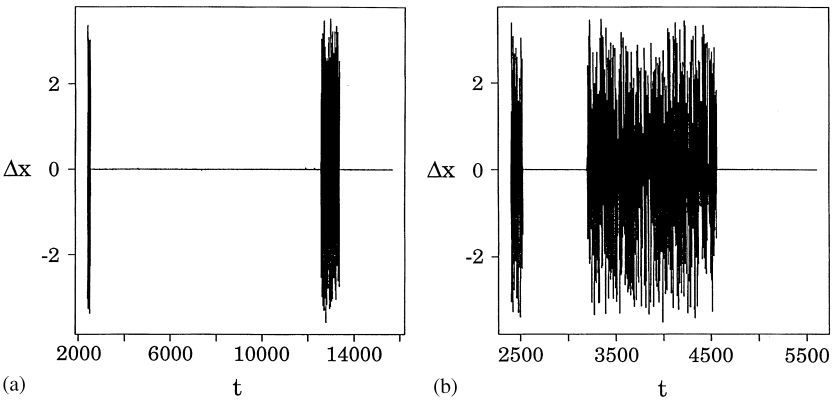

Fig. 15. From Ref. [51]. The influence of noise [of the form $\varepsilon\sigma(t)$, where $\sigma(t)$ is a Gaussian random variable having zero mean and unit standard deviation and, ε is the noise amplitude] on synchronized orbits. (a) $\varepsilon = 3.8 \times 10^{-4}$ and (b) $\varepsilon = 4.18 \times 10^{-4}$. It is clear that noise can make the synchronized orbits uncorrelated by kicking one orbit out of the neighborhood of the other orbit.

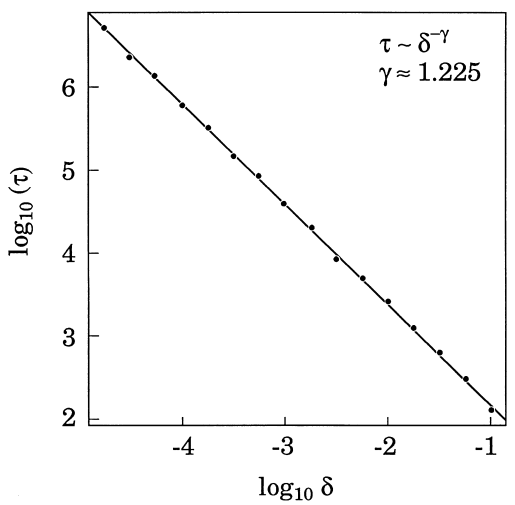

Fig. 16. From Ref. [51]. Average time to achieve synchronization τ versus the size of the synchronization neighborhood δ on a log–log plot. Note that $\tau \sim \delta^{-\gamma}$, where γ is the absolute value of the straight line in the figure.

of the stable and unstable eigenvalues (λ_s and λ_u) of the unstable periodic orbit by [1,23]:

$$\gamma = 1 - \log|\lambda_u|/\log|\lambda_s|\ , \tag{81}$$

if the controlling neighborhood is chosen to be a circle and the process is two dimensional. In the case of synchronization, such a scaling relation still holds, as shown in Fig. 16 for the standard Hénon map, where we plot the average time (with respect to 200 random pairs of initial conditions) to achieve synchronization versus δ on a logarithmic scale. The absolute value of the slope of the

line is the scaling exponent γ, which is approximately 1.23 for Fig. 16. Following the same argument as in Ref. [1,23], it is easy to see that γ is still given by Eq. (81), except that now λ_s and λ_u are the stable and unstable Lyapunov numbers of a *typical chaotic trajectory*. For the standard Hénon map, we found that $\gamma \approx 1.27$ in terms of Eq. (81), which agrees reasonably well with the value obtained from the linear fitting in Fig. 16. Note that the average time to achieve synchronization increases algebraically as δ is decreased. For $\delta \sim 10^{-2}$ in the Hénon map, $\tau \sim 10^3$ [see Figs. 14a, b and 16]. For stabilizing unstable periodic orbits, it has been demonstrated that the average time to achieve control can be greatly reduced by applying small controls to the orbit outside the control neighborhood. This technique is known as "targeting" [35]. Note that in such a case, the target (the unstable periodic orbit) is always fixed. While in the synchronization problem, the target moves chaotically because both trajectories wander on the chaotic attractor and, the actual location where the two trajectories get close to each other depends sensitively on the pair of initial conditions and the size of the synchronization neighborhood.

We remark that one advantage of the OGY method is that it does not require complete knowledge of the system equations [1,23], although it is necessary to "learn" from data to obtain enough knowledge about the unstable periodic orbits to be stabilized in order to control. Here by "knowledge" we mean the Jacobian matrices $\boldsymbol{J}$ [note that $\boldsymbol{f}_{u(n)}$ can be calculated in terms of $\boldsymbol{J}$] and vector $\boldsymbol{K}$ in Eq. (79). A nonlinear time series of the process is enough to extract the necessary parameter perturbations to stabilize a chaotic trajectory around the unstable periodic orbit. In the synchronization problem, the orbit to be stabilized is chaotic. Nonetheless, one can still run the system for enough long time to estimate both $\boldsymbol{J}$ and $\boldsymbol{K}$ at many trajectory points, enough points to practically cover the whole chaotic attractor. Indeed, Newell et al. [97,98] successfully demonstrated that the synchronization method [51] can be realized in experiments where a detailed knowledge of the system's equations is not available. The experiments involved two almost identical chaotic laser diodes. Synchronization was readily achieved when small feedback control was applied to one of them [97,98]. In principle, not only two such lasers can be synchronized, but also an array of almost identical chaotic lasers. This may be potentially useful in engineering applications.

5.1.4. Synchronization of spatiotemporal chaotic systems by control

Spatiotemporal chaotic systems are high-dimensional dynamical systems. Consider such a system that consists of a spatial network of chaotic elements. For the Pecora–Carroll type of synchronism [22] to occur, it may be necessary to use a large number of driving variables spatially distributed among chaotic elements. Nonetheless, it is often the case that the subsystem obtained by excluding only a few driving variables is still chaotic to a similar degree as the original system. That is, the subsystem still has a comparable number of positive Lyapunov exponents as the original system. To illustrate this, consider the coupled logistic map lattice [110] (to be described later) with 20 spatial sites (a 20-dimensional system). In certain parameter regimes, there are 8 positive Lyapunov exponents. Linking one arbitrarily chosen dynamical variable yields a 19-dimensional subsystem that still has 7 positive Lyapunov exponents. While synchronizable non-chaotic subsystem can be obtained by linking sufficient number of dynamical variables, they are difficult to identify due to the high dimensionality of the system. It is difficult to extend the control strategy proposed in Ref. [51] to high-dimensional systems because its success depends on the existence of one stable and an unstable directions at each trajectory point. Spatiotemporal chaotic

systems usually have many unstable and stable directions at each trajectory point in the phase space.

One strategy [111] is to combine the Pecora–Carroll idea [22] and the control idea in Ref. [51] to synchronize two nearly identical spatiotemporal systems. Specifically, by using a certain number of driving variables and by applying appropriately designed *feedback controls*, synchronization can be achieved for the two systems. The choice of driving variables can be done arbitrarily and their number can be as few as *only one*. The feedback control is applied to one of the two systems to be synchronized. The magnitude of the feedback control required can, in general, be very small.

The design of the feedback control in Ref. [111] is based on the principle of Kalmán filter [112] which tracks the system state by measuring a single scalar function of the system state. The Kalmán filter is optimal for linear systems. For nonlinear or chaotic systems, a modified technique was developed in Ref. [113] to deduce and track the state of the system from limited observation. Our design of the synchronization scheme is a direct application of this modified technique. Consider two identical spatiotemporal systems described by the following maps:

$$\boldsymbol{x}_{n+1} = \boldsymbol{F}(\boldsymbol{x}_n), \qquad \hat{\boldsymbol{x}}_{n+1} = \boldsymbol{F}(\hat{\boldsymbol{x}}_n) \ , \tag{82}$$

where $\boldsymbol{x}$ and $\hat{\boldsymbol{x}}$ are N-dimensional state vectors. Following Pecora and Carroll [22], we decompose the system state into two parts: one is the N_d-dimensional driving system which we denote $\boldsymbol{z}$ and $\hat{\boldsymbol{z}}$, and the other is the N_0-dimensional subsystems to be synchronized denoted by $\boldsymbol{y}$ and $\hat{\boldsymbol{y}}$, where $N_d \ll N_0$. In general, we allow the subsystems $\boldsymbol{y}$ and $\hat{\boldsymbol{y}}$ to be chaotic. By definition of "driving", $\boldsymbol{z}$ and $\hat{\boldsymbol{z}}$ are identified, i.e., $\boldsymbol{z} = \hat{\boldsymbol{z}}$. The equations for $\boldsymbol{y}$, $\hat{\boldsymbol{y}}$ and $\boldsymbol{z}$ are as follows:

$$\boldsymbol{y}_{n+1} = \boldsymbol{F}_{(y)}(\boldsymbol{y}_n, \boldsymbol{z}_n), \qquad \hat{\boldsymbol{y}}_{n+1} = \boldsymbol{F}_{(y)}(\hat{\boldsymbol{y}}_n, \boldsymbol{z}_n), \qquad \boldsymbol{z}_{n+1} = \boldsymbol{F}_{(z)}(\boldsymbol{y}_n, \boldsymbol{z}_n) \ , \tag{83}$$

where $\boldsymbol{F} = [\boldsymbol{F}_{(y)}, \boldsymbol{F}_{(z)}]$. In cases where the full system $\boldsymbol{F}$ is chaotic, Pecora and Carroll argued that when the subsystem $\boldsymbol{F}_{(y)}$ has all negative Lyapunov exponents, $\boldsymbol{y}_n$ and $\hat{\boldsymbol{y}}_n$ can be synchronized. Subsystems having only negative Lyapunov exponents are, however, hard to identify when Eq. (82) is spatiotemporally chaotic with many positive Lyapunov exponents and, in principle, we do not know how many. To achieve synchronization of $\boldsymbol{y}_n$ and $\hat{\boldsymbol{y}}_n$, we apply the following feedback control to one of the subsystems $\hat{\boldsymbol{y}}_n$:

$$\hat{\boldsymbol{y}}_{n+1} = \boldsymbol{F}_{(y)}(\hat{\boldsymbol{y}}_n, \boldsymbol{z}_n) - \boldsymbol{C}_n \cdot [\boldsymbol{F}_{(z)}(\hat{\boldsymbol{y}}_n, \boldsymbol{z}_n) - \boldsymbol{F}_{(z)}(\boldsymbol{y}_n, \boldsymbol{z}_n)] \ , \tag{84}$$

where $\boldsymbol{C}_n$ is an $N_0 \times N_d$ control matrix to be evaluated at each time step. The synchronization scheme is schematically shown in Fig. 17. The feedback control $-\boldsymbol{C}_n \cdot [\boldsymbol{F}_{(z)}(\hat{\boldsymbol{y}}_n, \boldsymbol{z}_n) - \boldsymbol{F}_{(z)}(\boldsymbol{y}_n, \boldsymbol{z}_n)]$ is applied only when $\boldsymbol{y}_n$ and $\hat{\boldsymbol{y}}_n$ are close. The linearized dynamics in the neighborhood of $\boldsymbol{y}_n$ can therefore be written as

$$\begin{aligned} \delta\boldsymbol{y}_{n+1} &= \hat{\boldsymbol{y}}_{n+1} - \boldsymbol{y}_{n+1} = \boldsymbol{F}_{(y)}(\hat{\boldsymbol{y}}_n, \boldsymbol{z}_n) - \boldsymbol{F}_{(y)}(\boldsymbol{y}_n, \boldsymbol{z}_n) - \boldsymbol{C}_n \cdot [\boldsymbol{F}_{(z)}(\hat{\boldsymbol{y}}_n, \boldsymbol{z}_n) - \boldsymbol{F}_{(z)}(\boldsymbol{y}_n, \boldsymbol{z}_n)] \\ &= [\boldsymbol{DF}_y(\boldsymbol{y}_n, \boldsymbol{z}_n) - \boldsymbol{C}_n \cdot \boldsymbol{DF}_z(\boldsymbol{y}_n, \boldsymbol{z}_n)] \cdot \delta\boldsymbol{y}_n \equiv \boldsymbol{A}_n \cdot \delta\boldsymbol{y}_n \ , \end{aligned} \tag{85}$$

where $\boldsymbol{DF}_y$ and $\boldsymbol{DF}_z$ are the $N_0 \times N_0$ and $N_d \times N_0$ Jacobian matrices of $\boldsymbol{F}_{(y)}$ and $\boldsymbol{F}_{(z)}$, respectively, evaluated at $\boldsymbol{y}_n$ and $\boldsymbol{z}_n$. Since $\boldsymbol{F}_{(y)}$ is chaotic, $\hat{\boldsymbol{y}}_{n+1}$ will diverge from $\boldsymbol{y}_{n+1}$ exponentially without control. Our goal is to design the control matrix $\boldsymbol{C}_n$ so that $\delta\boldsymbol{y}_n \to 0$ as $n \to \infty$. To achieve this we assume that the subsystem $\boldsymbol{F}_{(y)}$ has N_u positive and N_s negative Lyapunov exponents, where $N_u + N_s = N_0$. Furthermore, we do not assume hyperbolicity for the subsystems $\hat{\boldsymbol{y}}$ and $\boldsymbol{y}$. We

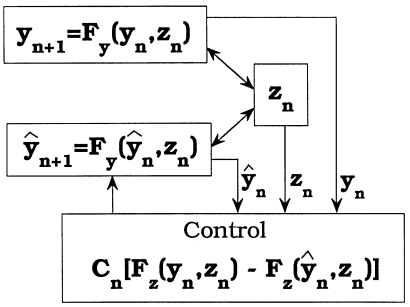

Fig. 17. From Ref. [111]. The scheme of synchronizing two spatiotemporal chaotic systems by driving and feedback control.

require that almost every point but not all on the asymptotic attractor of $\boldsymbol{F}_{(y)}$ has N_{u} unstable and N_{s} stable directions, the stable and unstable subspaces are bounded away from zero [34,39]. The feedback control so designed thus applies to nonhyperbolic dynamical systems [111,113]. Let $\boldsymbol{e}_n^i$ $(i=1,\ldots,N_{\mathrm{u}})$ be the set of base column vectors in the unstable space at $\boldsymbol{y}_n$. If we restrict the control matrix $\boldsymbol{C}_n$ to the unstable space of $\boldsymbol{F}_{(y)}$ at $\boldsymbol{y}_{n+1}$:

$$\boldsymbol{C}_n = \sum_{i=1}^{N_{\mathrm{u}}} \boldsymbol{b}_n^i = \sum_{i=1}^{N_{\mathrm{u}}} [C_1^i \boldsymbol{e}_{n+1}^i \cdot \boldsymbol{v}_1 + \cdots + C_{N_d}^i \boldsymbol{e}_{n+1}^i \cdot \boldsymbol{v}_{N_d}] , \tag{86}$$

where $\{\boldsymbol{v}_j\}$ $(j=1,\ldots,N_d)$ are a complete set of row vector that span the driving system $\boldsymbol{F}_{(z)}$, and $C_1^i, C_2^i, \ldots, C_{N_d}^i$ $(i=1,\ldots,N_{\mathrm{u}})$ are the set of $N_{\mathrm{u}} \times N_d$ control coefficients, then it can be shown [113] that the matrix $\boldsymbol{A}_n[= \boldsymbol{DF}_y(\boldsymbol{y}_n, \boldsymbol{z}_n) - \boldsymbol{C}_n \cdot \boldsymbol{DF}_z(\boldsymbol{y}_n, \boldsymbol{z}_n)]$ reduces to the following upper triangular form:

$$\boldsymbol{A}_n = \begin{pmatrix} \boldsymbol{U}_n & \boldsymbol{W}_n \\ 0 & \boldsymbol{S}_n \end{pmatrix}, \tag{87}$$

where $\boldsymbol{U}_n(\boldsymbol{S}_n)$ is an $N_{\mathrm{u}} \times N_{\mathrm{u}}(N_{\mathrm{s}} \times N_{\mathrm{s}})$ matrix that evolves a vector in the unstable (stable) space at $\boldsymbol{y}_n$ into a vector in the unstable (stable) space at $\boldsymbol{y}_{n+1}$, and $\boldsymbol{W}_n$ is an $N_{\mathrm{u}} \times N_{\mathrm{s}}$ matrix that takes a vector in the stable space at $\boldsymbol{y}_n$ into a vector in the unstable space at $\boldsymbol{y}_{n+1}$. In order to have $|\delta \boldsymbol{y}_n| \to 0$ as $n \to \infty$, it is required that all eigenvalues of the product matrix $\boldsymbol{A}_n \boldsymbol{A}_{n-1} \cdots \boldsymbol{A}_1$ vanish as $n \to \infty$. Since,

$$\boldsymbol{A}_n \boldsymbol{A}_{n-1} \cdots \boldsymbol{A}_1 = \begin{pmatrix} \boldsymbol{U}_n \boldsymbol{U}_{n-1} \cdots \boldsymbol{U}_1 & \sum_{i=1}^{n} \prod_{j=i+1}^{n} \boldsymbol{U}_j \boldsymbol{W}_i \prod_{k=1}^{i-1} \boldsymbol{S}_k \\ 0 & \boldsymbol{S}_n \boldsymbol{S}_{n-1} \cdots \boldsymbol{S}_1 \end{pmatrix}, \tag{88}$$

i.e., the product matrix $\boldsymbol{A}_n \boldsymbol{A}_{n-1} \cdots \boldsymbol{A}_1$ is upper triangular and, since the matrices $\boldsymbol{S}_n$ are already in the stable space along the trajectory (eigenvalues of the matrix product $\boldsymbol{S}_n \boldsymbol{S}_{n-1} \cdots \boldsymbol{S}_1 \to 0$ as $n \to \infty$), the stability of the product $\boldsymbol{A}_n \boldsymbol{A}_{n-1} \cdots \boldsymbol{A}_1$ depends solely on the stability of $\boldsymbol{U}_n \boldsymbol{U}_{n-1} \cdots \boldsymbol{U}_1$. One way to make the product $\boldsymbol{U}_n \boldsymbol{U}_{n-1} \cdots \boldsymbol{U}_1$ stable is to let $\boldsymbol{U}_i$ be lower triangular and be stable, i.e., all diagonal elements of $\boldsymbol{U}_i$ are eigenvalues of $\boldsymbol{U}_i$ and are less than 1. In this way, the product $\boldsymbol{U}_n \boldsymbol{U}_{n-1} \cdots \boldsymbol{U}_1$ is still lower triangular and has vanishing diagonal elements (eigenvalues) [113].

Now define a set of contravariant row vectors $\boldsymbol{f}_{n+1}^i$ $(i=1,\ldots,N_{\mathrm{u}})$ in the unstable space at $\boldsymbol{y}_{n+1}$ such that $\boldsymbol{f}_{n+1}^i \cdot \boldsymbol{e}_{n+1}^j = \delta_{ij}$, where $\delta_{ij} = 0$ if $i \neq j$ and $\delta_{ii} = 1$. The matrix elements of $\boldsymbol{U}_n$ are

given by $U_{ij} = \boldsymbol{f}^i_{n+1} \cdot \boldsymbol{A}_n \cdot \boldsymbol{e}^j_n$ [113]. In order to make the matrices $\boldsymbol{U}_i$ lower triangular, we look at elements U_{ij} of the matrix $\boldsymbol{U}_n$, which can be expressed as follows:

$$\begin{aligned} U_{ij} &= \boldsymbol{f}^i_{n+1} \cdot \boldsymbol{A}_n \cdot \boldsymbol{e}^j_n = \boldsymbol{f}^i_{n+1} \cdot [\boldsymbol{DF}_y(\boldsymbol{y}_n, \boldsymbol{z}_n) - \boldsymbol{C}_n \cdot \boldsymbol{DF}_z(\boldsymbol{y}_n, \boldsymbol{z}_n)] \cdot \boldsymbol{e}^j_n \\ &= \boldsymbol{f}^i_{n+1} \cdot \boldsymbol{DF}_y(\boldsymbol{y}_n, \boldsymbol{z}_n) \cdot \boldsymbol{e}^j_n - \boldsymbol{f}^i_{n+1} \cdot \boldsymbol{b}^i_n \cdot \boldsymbol{DF}_z(\boldsymbol{y}_n, \boldsymbol{z}_n) \cdot \boldsymbol{e}^j_n \ , \end{aligned} \tag{89}$$

where $\boldsymbol{f}^i_{n+1} \cdot \boldsymbol{b}^j_n = 0$ for $i \neq j$ has been used. In order to have $U_{ij} = 0$ for $j > i$, So et al. [113] suggested the following procedure for choosing the unstable base vectors:

$$\begin{aligned} &\lambda^1_n \boldsymbol{e}^1_{n+1} = [\boldsymbol{DF}_y(\boldsymbol{y}_n, \boldsymbol{z}_n)] \cdot \boldsymbol{e}^1_n \ , \\ &\lambda^2_n \boldsymbol{e}^2_{n+1} = [\boldsymbol{DF}_y(\boldsymbol{y}_n, \boldsymbol{z}_n) - \boldsymbol{b}^1_n \cdot \boldsymbol{DF}_z(\hat{\boldsymbol{y}}_n, \boldsymbol{z}_n)] \cdot \boldsymbol{e}^2_n \ , \\ &\cdots = \cdots \\ &\lambda^{N_u}_n \boldsymbol{e}^{N_u}_{n+1} = \left[\boldsymbol{DF}_y(\boldsymbol{y}_n, \boldsymbol{z}_n) - \sum_{i=1}^{N_u - 1} \boldsymbol{b}^i_n \cdot \boldsymbol{DF}_z(\hat{\boldsymbol{y}}_n, \boldsymbol{z}_n) \right] \cdot \boldsymbol{e}^{N_u}_n \ , \end{aligned} \tag{90}$$

where λ^i_n $(i = 1, \ldots, N_u)$ are a set of numbers which can be related to the stretching rate of infinitesimal vectors along the unstable direction $\boldsymbol{e}^i_n$. It can then be shown that elements of the matrix $\boldsymbol{U}_n$ are given by

$$\begin{aligned} &U_{ij} = 0, \quad j > i \ , \\ &U_{ii} = \lambda^i_n - \boldsymbol{f}^i_{n+1} \cdot \boldsymbol{b}^i_n \cdot \boldsymbol{Dh}^i_n \ , \\ &U_{ij} = -\boldsymbol{f}^i_{n+1} \cdot \boldsymbol{b}^i_n \cdot \boldsymbol{Dh}^j_n, \quad j < i \ , \end{aligned} \tag{91}$$

where $\boldsymbol{Dh}^j_n \equiv \boldsymbol{DF}_z(\boldsymbol{y}_n, \boldsymbol{z}_n) \cdot \boldsymbol{e}^j_n$. To make the eigenvalues of the matrix $\boldsymbol{U}_n$ less than one, we can adjust the $N_u \times N_d$ free control parameters C^i_j $(i = 1, \ldots, N_u, j = 1, \ldots, N_d)$ such that all diagonal elements of $\boldsymbol{U}_n$ are less than one. But this only provides N_u conditions, and there are still $N_u(N_d - 1)$ free control parameters we must set. The simplest choice is to set $C^i_j = 0$ for $j > 1$. Then setting the diagonal elements in Eq. (91) zero gives, $C^i_1 = \lambda^i_n / [\boldsymbol{v}_1 \cdot \boldsymbol{Dh}^i_n]$ $(i = 1, \ldots, N_u)$ and consequently, the control matrix is given by

$$\boldsymbol{C}_n = \sum_{i=1}^{N_u} \frac{\lambda^i_n}{\boldsymbol{v}_1 \cdot \boldsymbol{Dh}^i_n} \boldsymbol{e}^i_{n+1} \cdot \boldsymbol{v}_1 \ . \tag{92}$$

In practice, the set of numbers λ^i_n and the set of unstable base vectors $\boldsymbol{e}^i_n$ can be computed by randomly initializing a set of base vectors $\boldsymbol{e}^i_0$ and evolving them in terms of Eq. (90). After a period of transient, the set of vectors so obtained converge to the real unstable directions. To assure that only small perturbations are applied, it is necessary to monitor the magnitude of the term in the denominator of Eq. (92). When $|\boldsymbol{v}_1 \cdot \boldsymbol{Dh}^i_n|$ is below some small threshold, we set $\boldsymbol{C}_n = 0$. This will not result in the loss of control provided it is done only occasionally. We stress that the feedback control is derived under the applicability of linearized dynamics and, hence, the control is applied only when trajectories $\hat{\boldsymbol{y}}$ and $\boldsymbol{y}$ are sufficiently close. No control is applied when they are not close. Also note that the control law Eq. (92) has been derived under the condition of hyperbolicity at almost every point along the trajectory, while there is no guarantee that spatiotemporal chaotic systems are hyperbolic. Nonetheless, as we illustrate below, the control works for spatiotemporal systems modeled by coupled map lattices.

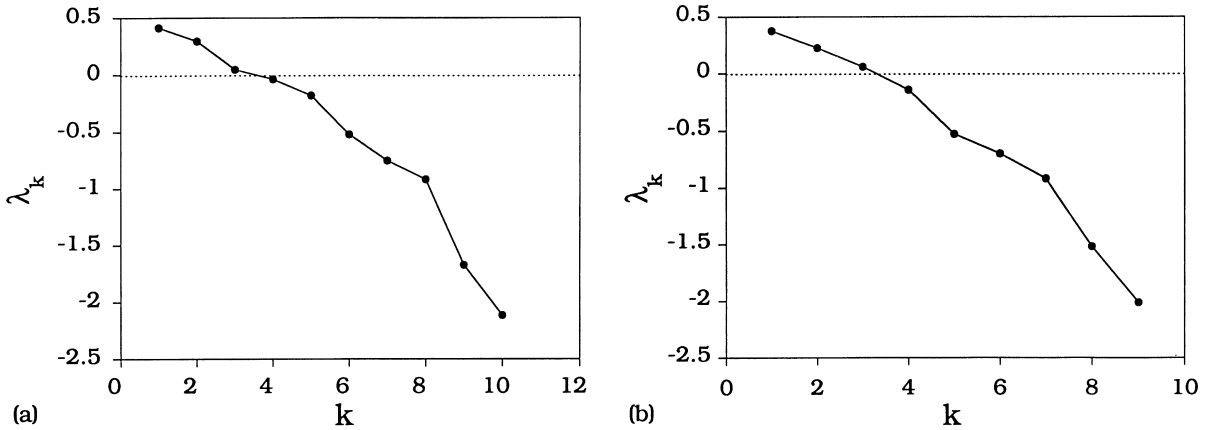

Fig. 18. From Ref. [111]. The Lyapunov spectrum for $N = 10$ and $\varepsilon = 0.7$, (a) of the full system, and (b) of the reduced system by using one site as the driving signal.

To illustrate the applicability of the control method, we consider the following system of diffusively coupled logistic maps [110] as a phenomenological model for spatiotemporal chaotic systems:

$$x_{n+1}(i) = (1-\varepsilon)f[x_n(i)] + \tfrac{1}{2}\varepsilon\{f[x_n(i+1)] + f[x_n(i-1)]\}, \quad i = 1, \ldots, N \ , \tag{93}$$

where i and n denote discrete spatial sites and time, respectively, N is the total number of maps coupled in the lattice, ε denotes the coupling strength, and $f(x)$ is the one-dimensional logistic map $f(x) = ax(1-x)$. We assume periodic boundary condition: $x_n(N+1) = x_n(1)$. Eq. (93) exhibits extremely rich dynamical phenomena seen in real spatiotemporal systems and it is perhaps the most extensively studied model spatiotemporal system so far. In examples, $a = 4$ was chosen [111], the parameter value for which the logistic map has a chaotic attractor.

Our first example is for $N = 10$ and $\varepsilon = 0.7$. At this ε value, there are three positive Lyapunov exponents for Eq. (93). Fig. 18a shows the corresponding Lyapunov spectrum for the full system Eq. (93), in which λ_k versus the index k ($k = 1, \ldots, N$, $\lambda_1 \geq \lambda_2 \geq \cdots \geq \lambda_N$) is plotted. To synchronize two such systems, we choose one of the $x(i)$ ($i = 1, \ldots, 10$) as the driving variable. Choosing a different $x(i)$ does not change the result due to symmetry of Eq. (93) with respect to site index i. The subsystems to be synchronized are therefore nine-dimensional, and still possesses 3 positive Lyapunov exponents, as shown by the corresponding Lyapunov spectrum in Fig. 18b. Thus, the Pecora–Carroll type synchronism will not occur for the nine-dimensional subsystem. The control neighborhood is set to be $|\hat{\boldsymbol{y}} - \boldsymbol{y}| \leq r_0 = 0.015$. The control Eq. (92) is applied only when $|\boldsymbol{v}_1 \cdot \boldsymbol{Dh}_n^j| \geq 10^{-3}$ ($j = 1, 2, 3$). With these control parameter settings, most randomly chosen initial conditions can be controlled. In general, the smaller the control neighborhood, the larger the probability that trajectories resulting from two randomly chosen initial conditions can be synchronized. In cases where one set of initial conditions fails to be synchronized, we disregard them and choose another set of initial conditions. Figs. 19a and b show, when trajectories of the two subsystems resulting from a pair of randomly chosen initial conditions are within r_0, the error Δ_n,

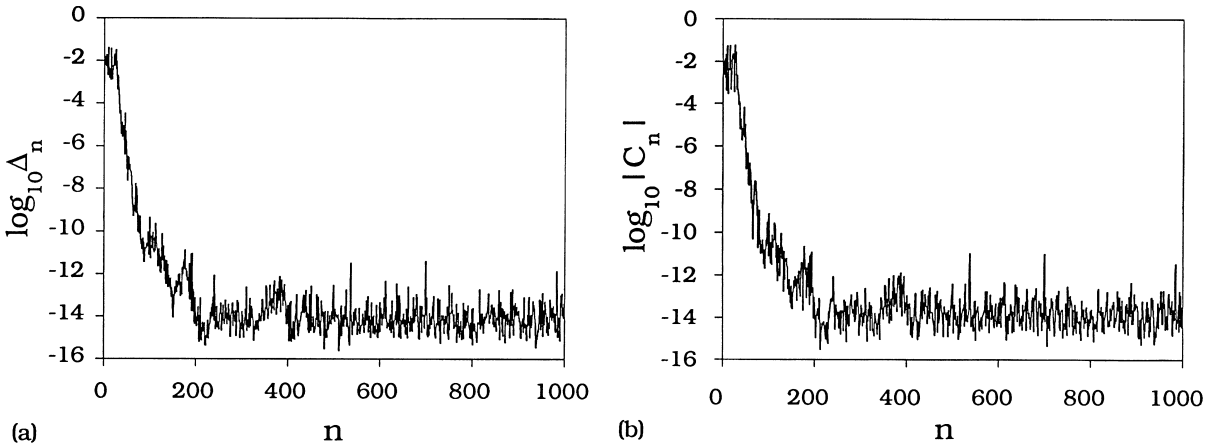

Fig. 19. From Ref. [111]. Synchronization of two logistic map lattices ($N = 10$, $\varepsilon = 0.7$). (a) The synchronization error $\log_{10} \Delta_n$ versus n, and (b) the required feedback control magnitude $\log_{10}(|C_n|)$ versus n. The control neighborhood is set to be 0.015.

defined as

$$\Delta_n = |\hat{\boldsymbol{y}}_n - \boldsymbol{y}_n| \,, \tag{94}$$

and the control magnitude, defined as

$$|\boldsymbol{C}_n| = |\boldsymbol{C}_n \cdot [\boldsymbol{F}_{(z)}(\hat{\boldsymbol{y}}_n, \boldsymbol{z}_n) - \boldsymbol{F}_{(z)}(\boldsymbol{y}_n, \boldsymbol{z}_n)]| \,, \tag{95}$$

versus the time step n after the control is turned on. Clearly, the two trajectories rapidly approach each other to within computer roundoff error ($\sim 10^{-14}$) after the control is applied, and the required feedback control decreases correspondingly to extremely small values.

Under the influence of small random noise, the degree to which two subsystems can be synchronized, or the value of $|\delta \boldsymbol{y}_n|$ is proportional to the amplitude of the noise. Figs. 20a and b show Δ_n and $|C_n|$ versus time step n for the parameter setting of Fig. 19 when a noise term modeled by $h\sigma_n^i$ is added to each site of the lattice, where $h = 10^{-7}$ is the noise amplitude and σ_n^i is a Gaussian random variable with zero mean and unit variance. In general, minimum values of Δ_n and $|C_n|$ have the same order of magnitude as h. Occasionally both Δ_n and $|C_n|$ can have values larger than 10^{-3}, indicating that the degree of synchronization decreases significantly at these time steps. Eventually, the systems lose synchronization due to large amplitude noise in the tail of the Gaussian distribution. When this occurs, we turn off the control and let the systems evolve by themselves. Due to the ergodicity of the chaotic attractor, at some later time the two trajectories will come close to each other and can be controlled again.

To demonstrate the applicability of the control algorithm in higher dimensions, we have performed control using $N = 20$. In this case, we found that for $\varepsilon = 0.5$, there is a unique chaotic attractor with 8 positive Lyapunov exponents. The subsystem obtained by using a driving signal $x_n(i)$, where i can be any number between 1 and 20, has 7 positive Lyapunov exponents, as shown in Fig. 21. In this case, the control neighborhood needs to be smaller for synchronization to occur. Besides, the quantity N_u used in the control algorithm needs to be slightly larger than the actual number of unstable directions. We found that using $N_u = 10$ suffices. Figs. 22a and b show Δ_n and $|C_n|$ versus n, where the control is applied only when $|\delta \boldsymbol{y}_n| \leq 5 \times 10^{-5}$.

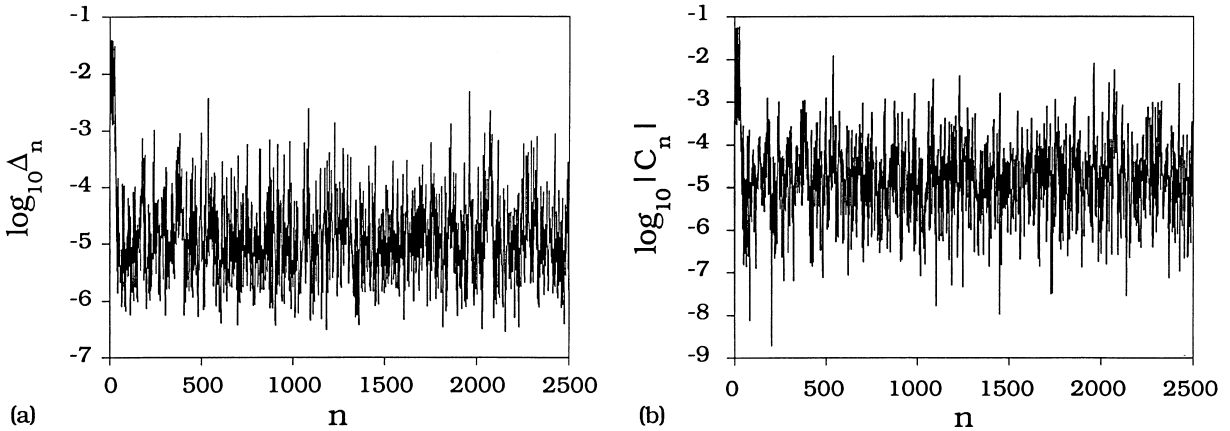

Fig. 20. From Ref. [111]. (a) The synchronization error $\log_{10} \Delta_n$, and (b) the required feedback control magnitude $\log_{10}(|C_n|)$ versus n when a noise term $10^{-7}\sigma_n^i$ is added to each site of the lattice, where σ_n^i is a Gaussian random variable with zero mean and unit variance.

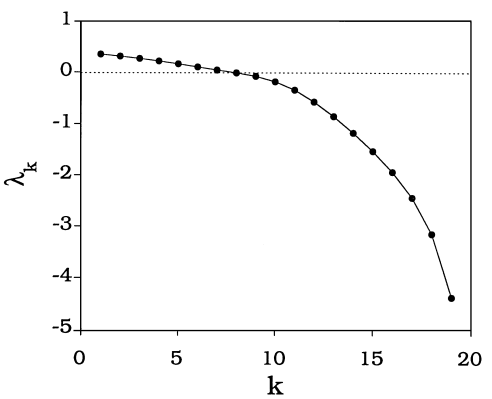

Fig. 21. From Ref. [111]. The reduced Lyapunov spectrum for $N = 20$ and $\varepsilon = 0.5$, where one site of the lattice is used as the driving signal.

As we have demonstrated with Eq. (93), the control neighborhood needs to be reduced as the number of unstable directions increases. Going from 3 unstable directions (Fig. 19, the $N = 10$ case) to 7 unstable directions (Fig. 22, the $N = 20$ case) requires almost three orders of magnitude decrease in the size of the control neighborhood. As the size of control neighborhood is decreased, the average transient time for two trajectories to get close increases algebraically with a scaling exponent determined by the Lyapunov spectrum of the chaotic attractor. Thus, even for spatiotemporal systems with moderate sizes, the transient time required may be very long. The reason that extremely small control neighborhood is needed is not clear, but may be related to the noninvertibility and nonhyperbolicity of the coupled logistic map lattice. For instance, for noninvertible dynamical systems, there may not be unique stable and unstable spaces at every trajectory points, whereas the control algorithm is designed under the assumption that the dynamical systems possess unique and distinct stable and unstable spaces (invertibility and hyperbolicity).

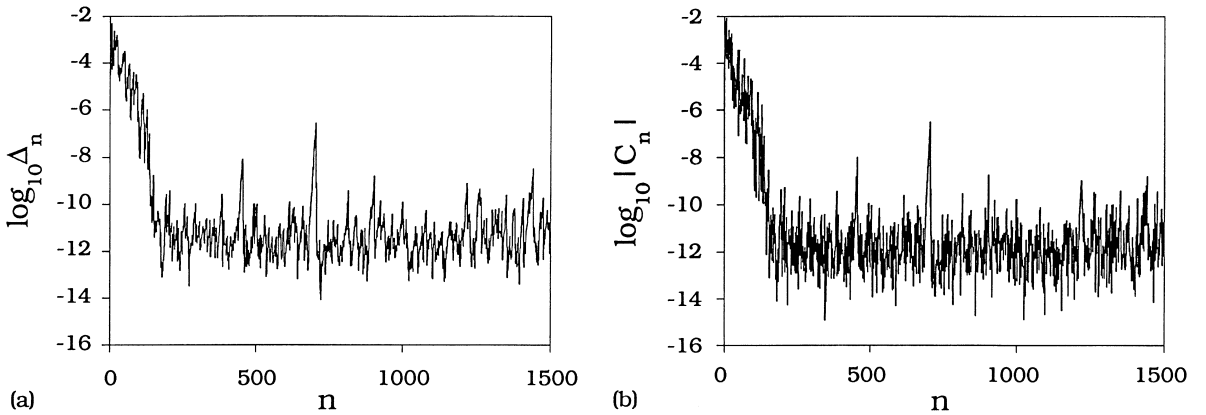

Fig. 22. From Ref. [111]. (a) The synchronization error $\log_{10} \Delta_n$, and (b) the required feedback control magnitude $\log_{10}(|C_n|)$ versus n for $N = 20$ and $\varepsilon = 0.5$. The control neighborhood needs to be reduced to 5×10^{-5} in order to achieve the control.

5.1.5. Remarks

Stabilizing a chaotic orbit has other applications as well. Here we briefly discuss an application to select a desirable chaotic phase from a chaotic attractor that contains two interconnected components. In the study of chaotic systems, there are situations where orbits switch intermittently between distinct chaotic phases. For example, a dynamical system in parameter regime after a bifurcation called the "interior crisis" [32,114] exhibits such intermittent chaotic behavior. The phenomenology of interior crisis is as follows. Before the crisis, there is a chaotic attractor and a coexisting nonattracting chaotic saddle in the phase space. The chaotic attractor and the chaotic saddle are separated from each other and, hence, trajectories originating from almost all initial conditions eventually asymptote to the chaotic attractor. At the crisis, the chaotic saddle collides with the chaotic attractor so that the original nonattracting chaotic saddle becomes part of the combined attractor, whose phase-space extent is larger than the original chaotic attractor. After the crisis, trajectories wander on the whole combined larger attractor, in such a way that the trajectories visit both parts, which correspond to the original chaotic attractor and the chaotic saddle, in an intermittent fashion. As a consequence, time series recorded from such a trajectory exhibits distinct intermittent chaotic phases. It has been demonstrated [53] that it is possible to keep trajectories in one of the chaotic phases by applying only small parameter perturbations to the system. We remark that similar intermittent chaotic signals also arise in biomedical systems [53].

5.1.6. Encoding digital messages using chaos control

Recent development in nonlinear dynamics and chaos has led to the idea of encoding digital information by using chaos [21,24,54–57]. In particular, it has been demonstrated both theoretically and experimentally by Hayes et al. [21,24] that a chaotic system can be manipulated, via arbitrarily small time-dependent perturbations, to generate controlled chaotic orbits whose symbolic representation corresponds to the digital representation of a desirable message. Imagine

a chaotic oscillator that generates a large amplitude signal consisting of an apparently random sequence of positive and negative peaks. A possible way to assign a symbolic representation to the signal is to associate a positive peak with a one, and a negative peak with a zero, thereby generating a binary sequence. The use of small perturbations to an accessible system parameter or variable can then cause the signal to follow an orbit whose binary sequence encodes a desirable message which one wishes to transmit [21,24]. One advantage of this type of message-encoding strategy is that the nonlinear chaotic oscillator that generates the waveform for transmission can remain simple and efficient, while all the necessary electronics controlling encoding of the signal can remain at low-powered microelectronic level most of the time.[5]

A central issue in any digital communication device concerns with the *channel capacity* [115,116], a quantity that measures the amount of information that the device can encode. For a chaotic system, channel capacity is equivalent to the *topological entropy* because it defines the rate at which information is generated by the system [117]. To give a concrete example, consider symbol sequences consisting of a string of n symbols generated by the dynamics. For a completely random process, one expects to be able to observe all 2^n possible symbol sequences. In this case, the topological entropy is

$$h_T = \lim_{n\to\infty} \frac{\ln 2^n}{n} = \ln 2 \ ,$$

which is the maximum possible value for processes defined by two symbols. A deterministic chaotic system is, however, not purely random. Thus, if its symbolic dynamics requires only two symbols, the topological entropy of the chaotic attractor is in general[6] less than $\ln 2$.

In a digital communication scheme, it is highly desirable to have the channel capacity as large as possible to maximize the amount of information that can be encoded. It has been pointed out recently [118] that in nonlinear digital communication, it is generally more advantageous to use *transient chaos naturally arising in wide parameter regimes of nonlinear systems* as information sources from the standpoint of channel capacity. Dynamically, transient chaos is generated by nonattracting chaotic saddles in the phase space [119,120]. A general observation is that, typically, a nonlinear system can generate chaotic attractors (corresponding to sustained chaos) and chaotic saddles in different parameter regimes. As a system parameter changes, a chaotic attractor can abe converted into a chaotic saddle via a dynamical event such as crisis [32]. The orbital complexity associated with trajectories on a chaotic saddle can be greater than that of trajectories on a chaotic

[5] The basic principle that makes digital encoding with chaos possible lies in the fundamental link between chaos and information. The evolution of a chaotic system is unpredictable in long terms. In communication, it was realized by Shannon in 1948 that a sequence of events conveys information if the events are not fully predictable [115,116]. Thus, the fundamental unpredictability of chaos implies that chaotic systems can be regarded as sources that naturally generate digital communication signals. By manipulating a chaotic system in an intelligent way, digital information can be encoded.

[6] There are chaotic attractors with topological entropies $\ln 2$, such as the logistic map $f(x) = rx(1 - x)$ at $r = 4$. But such situations are rare.

attractor because, crisis is generally a complexity-increasing event.[7] As such, if one measures the topological entropy of the system as a single parameter changes through the crisis point, one usually finds that the entropy is a nondecreasing function of the system parameter. For a symbolic dynamics of two symbols observed in typical low-dimensional chaotic systems, the maximum allowed value of the topological entropy, ln 2, is often realized in a parameter regime where there is transient chaos. Thus, it is highly desirable to design a chaotic system operating in a transient chaotic regime for digital encoding.

In what follows, we first develop a theoretical and numerical framework for encoding digital information using transient chaos. We provide numerical evidence that the topological entropies of chaotic saddles are usually greater than those of chaotic attractors. We then detail a procedure for encoding digital messages into trajectories that live on chaotic saddles. We argue that digital encoding with chaotic saddles can be robust against environmental noise, thereby significantly reducing the probability of bit error in encoding. Finally, we describe message encoding using two-dimensional symbolic dynamics.

5.1.7. The channel capacity

In general, the topological entropy associated with transient chaos is greater than that with permanent chaos. Although at present there is no rigorous proof for this statement, is was observed in several chaotic systems: (1) Hamiltoniian maps [121,122]; and (2) the Hènon map [123]. For illustrative purpose, we demonstrate how transient chaos can be utilized to encode digital information by using the one-dimensional logistic map: $x_{n+1} = f(x_n) = rx_n(1 - x_n)$. The map exhibits chaotic attractors and stable periodic attractors for $r_F < r \leq r_c = 4$, where $r_F \approx 3.58$ is the Feigenbaum point of the transition to chaos via the route of period-doubling bifurcations [124]. At $r = r_c$, crisis occurs [32] so that the chaotic attractor is converted into a chaotic repeller.[8] Thus, for $r > r_c$, what is typically observed is transient chaos. That is, a trajectory starting from a random initial condition in $x \in [0, 1]$ behaves chaotically for a period of time and then asymptotes to $x = -\infty$. The average transient time depends on the parameter difference $(r - r_c)$ and scales with it algebraically: $\tau \sim (r - r_c)^{-1/2}$ [32].

The existence of a chaotic repeller for $r > 4$, which is in fact a fractal Cantor set in the unit interval, can be easily seen in the map function in Fig. 23a. Letting $s \equiv (r/4 - 1)$ we see that there is a primary gap of size $\sqrt{s/(1 + s)}$. Initial conditions from this gap maps out of the unit interval in

[7] A crisis that destroys a chaotic attractor and converts it into a nonattracting chaotic saddle is called a boundary crisis [32]. It is triggered by the collision of the attractor with the basin boundary. Dynamically, a crisis is induced by a homoclinic or a herteroclinic tangency of stable and unstable manifolds of some unstable periodic orbits in the phase space. In the case of boundary crisis, the two colliding sets are, (1) the chaotic attractor which lives in the closure of the unstable manifold of an unstable periodic orbit on the basin boundary, and (2) the basin boundary which is the stable manifold of the periodic orbit on the boundary. Accompanying a homoclinic or a heteroclinic tangency and the subsequent homoclinic or heteroclinic crossing of stable and unstable manifolds is a horseshoe type of dynamics, which creates an infinite number of new unstable periodic orbits, and consequently increases the complexity of the resulting chaotic set.

[8] Chaotic repellers are one-dimensional analogies of chaotic saddles in two-dimensional maps or in three-dimensional flows, because one-dimensional noninvertible maps can be regarded as the limiting case of two-dimensional invertible maps when the determinant of the Jacobian matrix tends to zero (e.g., logistic map versus the Hènon map).

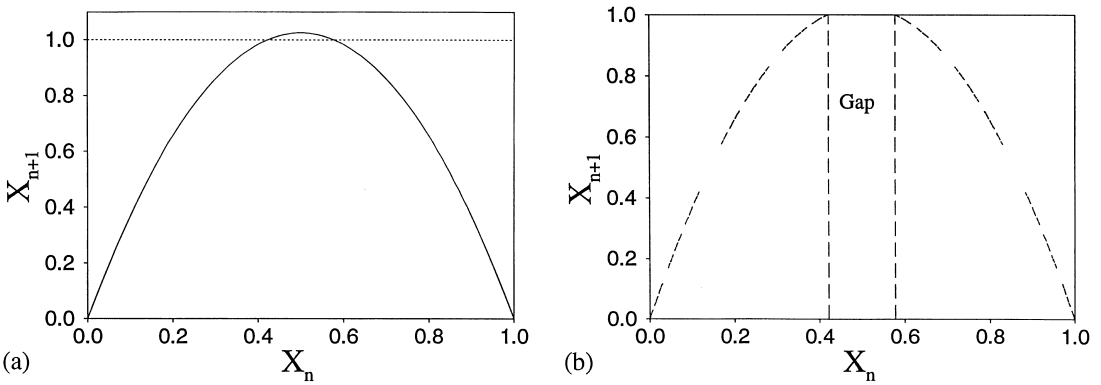

Fig. 23. (a) The logistic map for $r > 4$. (b) For $r = 4.1$, a numerical trajectory of 10 000 points on the chaotic repeller. Apparently, the chaotic repeller exhibits a fractal structure.

one iteration and goes to $x = -\infty$. There are two (2^n) preimages of the primary gap in which initial conditions map out of the unit interval in two $[(n+1)]$ iterations. Taking the limit $n \to \infty$, we see that almost all initial conditions in the unit interval eventually escape from it except for a set of Lebesgue measure zero. This set, by construction, is a fractal Cantor set. Fig. 23b shows, for $r = 4.1$, a numerical trajectory of 10 000 points on the Cantor set [33]. The fractal structure of the set is apparent from the figure.

A symbolic dynamics for the logistic map can be defined by setting the symbolic partition at the critical point $x_c = 0.5$. A trajectory point x bears a symbol **0** if $x < x_c$ and a symbol **1** if $x > x_c$. A trajectory in the phase space thus corresponds to a symbol sequence in the symbolic space. The topological entropy h_T quantifies how random such a symbol sequence can be. To compute h_T, we generate a large number of symbol sequences of length n from many trajectories in the phase space and count $N(n)$, the number of possible symbol sequences. In general, $N(n)$ scales with n as $N(n) \sim e^{h_T n}$ and, hence, h_T is given by

$$h_T = \lim_{n \to \infty} \frac{\ln N(n)}{n} . \tag{96}$$

In practice, we plot $\ln N(n)$ versus n for say, $1 \leq n \leq 16$. The slope of such a plot is approximately h_T.

We now discuss the topological entropy of the logistic map in different parameter regimes. For $r < r_F$, the asymptotic invariant sets are stable periodic orbits so that $h_T = 0$ because there is no randomness in the trajectory. As r is increased from r_F, chaos can arise so that the topological entropy starts increasing from zero. For $r = 4$, the logistic map is topologically equivalent to the tent map whose symbolic dynamics is a Bernoulli shift, the topological entropy of which is $\ln 2$. Thus, as r is increased from r_F to $r_c = 4$, the topological entropy h_T continuously increases from zero to $\ln 2$ except when r falls in one of the infinite number of parameter intervals of periodic windows. In each window, there is an attracting set (periodic or chaotic) and a chaotic repeller. The topological entropy of the chaotic repeller remains constant in the window, where the constant is the value of h_T at the beginning of the window. Since $\ln 2$ is the maximally realizable value of the

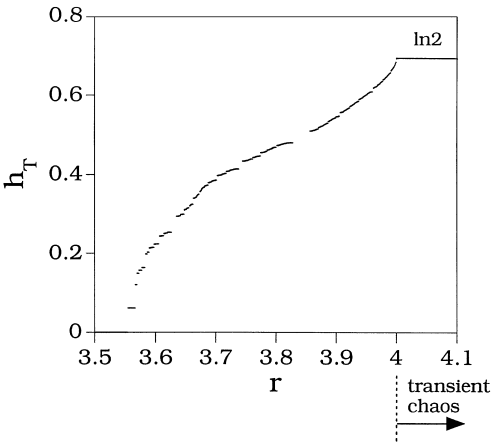

Fig. 24. For the logistic map, the topological entropy $h_T(r)$ versus r for $3.5 < r < 4.1$. We see that for $r > 4$, h_T remains at $\ln 2$, the maximum possible value for a symbolic dynamics of two symbols.

topological entropy for a symbolic dynamics of two symbols, and since a crisis occurs at r_c, we see that for $r > 4$, the entropy remains at $\ln 2$. These behaviors are shown in Fig. 24, a plot of $h_T(r)$ versus r for $3.5 < r < 4.1$. Thus, for the logistic map, whose dynamical behaviors are seen in a large class of deterministic chaotic systems, the largest possible value of the topological entropy, or the channel capacity, is achieved in a parameter regime of transient chaos where the invariant sets are chaotic repellers. This can be quite advantageous because message encoding, an essential task in any communication scheme, becomes quite straightforward for transient chaos as there are no forbidden words associated with the symbolic dynamics. In communication terminology, such a communication channel is unconstrained.

5.1.8. Message encoding, control scheme, and noise immunity

To encode an arbitrary binary message into a trajectory that lives on the chaotic repeller, it is necessary to use small perturbations to an accessible system parameter or a dynamical variable. For the logistic map we choose to perturb the state variable x. Say we wish to apply only small perturbations on the order of 2^{-m}. Our procedure is as follows. First, we convert the message into a binary sequence by using the ASCII code and store the sequence into a symbol registor. Next, we choose an initial condition whose trajectory stays near the chaotic repeller for certain number, say, n_c ($n_c > m$) iterations. This is practically feasible as one can run the system and pre-determine the phase space regions, from which initial conditions chosen yield trajectories whose lifetimes (the times trajectories spend near the chaotic repeller) are at least n_c. We then determine all m symbols corresponding to m points on the trajectory starting from x_0 and check to see if the mth symbol agrees with the first message bit in the symbol registor. If yes, we iterate x_0 once to get x_1 and determine the mth symbol from x_1 [equivalently the $(m+1)$th symbol from x_0] to see if it matches the second message bit in the symbol registor. If no, we apply a small perturbation to x_0 so that the mth symbol from it matches the first message bit. This process continues until all the message bits in the symbol registor are encoded into the chaotic trajectory.

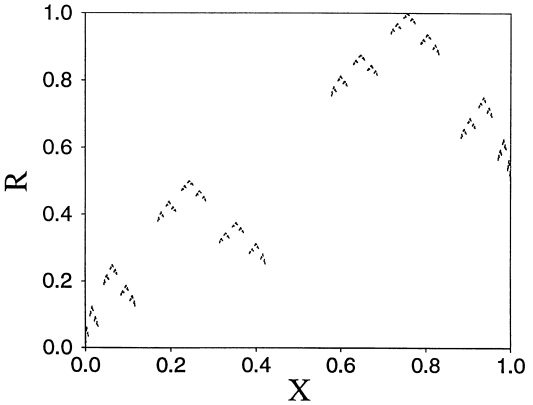

Fig. 25. The coding function $R(x)$ for the logistic map at $r = 4.1$. We see that indeed, R can assume any value between 0 and 1, but there are many gaps on the x-axis, due to the fact that the chaotic repeller is a fractal Cantor set on the x-axis.

To compute the parameter perturbation, we make use of the *coding function* [24,21], which can be determined as follows. We divide the unit interval in x into N bins of size $\delta x = 1/N$, where $\delta x \ll 1/2^m$ and $1/2^m$ is the maximally allowed perturbation. We then choose a point from each bin, iterate it for m times, and determine the corresponding symbol sequence of length m: $a_1 a_2 \ldots a_m$, where a_i can be either zero or one. If a point leaves the unit interval in less than m iterations, we simply disregard it. For those points x for which a symbol sequence of length m can be defined, we compute the following symbolic value:

$$R = \sum_{i=1}^{m} a_i/2^i \,, \tag{97}$$

where $0 \leq R \leq 1$. This thus gives the coding function $R(x)$ for points on the chaotic repeller. Since the chaotic repeller has a topological entropy ln 2, R can, in principle, have any value between 0 and 1. Fig. 25 shows the coding function for the logistic map at $r = 4.1$, where $\delta x = 2 \times 10^{-4}$. We see that indeed, R can assume any value between 0 and 1, but there are many gaps on the x-axis, due to the fact that the chaotic repeller is a fractal Cantor set on the x-axis.

Given the coding function, the determination of the state perturbations is quite straightforward. Let the natural m-bit symbol sequence from x_0 be $a_1 a_2 \ldots a_{m-1} a_m$ (produced by iterating the map directly) and let the first message bit to be encoded be b_1. We compare the natural symbol sequence $a_1 a_2 \ldots a_{m-1} a_m$ with the desirable symbol sequence $a_1 a_2 \ldots a_{m-1} b_1$ and compute $\delta R = (a_m - b_1)/2^m$. From the coding function $R(x)$, we can then compute the perturbation δx. This is done by locating pairs of points with same values of δR in the computer representation of the coding function $R(x)$ and choosing the one that yields the smallest value of δx. Thus, by applying δx to the initial condition x_0, the trajectory point after m iterations will correspond to a symbol which is the first message bit. Note that if a_m is identical to the message bit b, no perturbation is necessary. To encode the next message bit, we iterate the perturbed initial condition once to obtain x_1. Let $x'_0 = x_1$. The natural m-bit symbol sequence of x'_0 is $a'_1 a'_2 \ldots b_1 a'_m$, where $a'_1 = a_2, a'_2 = a_3, \ldots$, and a'_m is the binary symbol corresponding to the trajectory point $f^{(m)}(x'_0)$. We now compare a'_m and

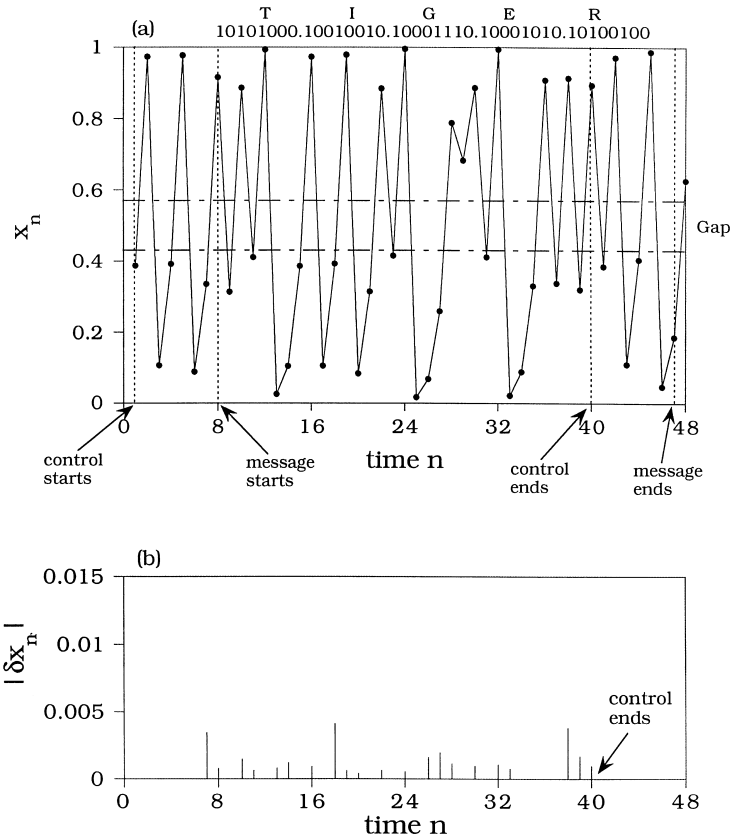

Fig. 26. Encoding the word "TIGER" into a trajectory on the chaotic repeller at $r = 4.1$ for the logistic map. The binary representation of the word is shown on the top of the figure. Shown is a time series where small control is initiated at $n = 1$ and the first binary bit of the message is encoded into the trajectory at $n = 8$. Time dependent perturbations are applied at subsequent iterations so that the entire message "TIGER" can be encoded into the trajectory. The magnitudes of the control perturbations required are shown in (b).

b_2 to determine the next perturbation to be applied to x'_0. Continuing this procedure, we can encode an arbitrary message into the chaotic trajectory $\{x_n\}$.

Fig. 26a shows an example of encoding the word "TIGER" into a trajectory on the chaotic repeller at $r = 4.1$ for the logistic map. The binary (ASCII) representation of the word is shown on the top of the figure. Assuming that perturbations of magnitude of 2^{-8} are to be applied, we generate a set of initial conditions whose lifetimes in the unit interval under the map are at least 8. Shown in Fig. 26a is a time series where small control is initiated at $n = 1$ and the first binary bit of the message is encoded into the trajectory at $n = 8$. Time dependent perturbations are applied at subsequent iterations so that the entire message "TIGER" can be encoded into the trajectory. Fig. 26b shows the magnitude of the control perturbations applied at different time steps. We see that the perturbations required are small. No control perturbation is required for the first six time steps because for this initial condition, the natural symbols corresponding to the trajectory points from $n = 8$ to $n = 13$ happen to coincide with the first six bits of the message.

Some features of the above control scheme are as follows. Note that since the channel capacity of the chaotic repeller is $\ln 2$, there are no forbidden symbol sequences. Thus, in the above encoding scheme, any binary sequences can be produced by a typical trajectory near the chaotic repeller. Since we use the coding function $R(x)$ to compute the perturbation δx, we see that once the perturbation is turned on, the trajectory is then automatically confined in the vicinity of the chaotic repeller because the coding function is defined with respect to trajectories on the chaotic repeller. Suppose that small perturbations on the order of 2^{-m} are to be applied. To encode a message, we only need to identify a set of initial conditions which can stay near the chaotic repeller for m iterations. Since the typical value of m is, say, 10, it is actually fairly easy to identify a large number of such initial conditions. In practice, before encoding, we can run the system to produce a set of initial conditions whose lifetimes are greater than m. Together with the coding function which also needs to be determined beforehand, one can in principle encode any binary sequences into a dynamical trajectory on the chaotic repeller. We mention that utilizing the symbolic dynamics as described above may in turn provide an alternative way to control transient chaos, which has been a challenging problem in the study of controlling chaos.

Besides possessing the maximum topological entropy $\ln 2$, the chaotic repellers of the logistic map for $r > 4$ also have the property of strong noise immunity. To see this, we contrast a chaotic repeller, such as the one shown in Fig. 23b, with the chaotic attractor at $r = 4$. For the chaotic repeller, we see that there is a gap of size $\sim \sqrt{s}$, where $s = r/4 - 1$, about the partition point $x_c = 1/2$. For the chaotic attractor there is no such gap. A trajectory on the chaotic attractor can then come arbitrarily close to the partition point. In a noisy environment, this may cause a bit error. Say the trajectory point is to the immediate right side of x_c. This point thus has a symbol **1**. Due to noise, the trajectory can be kicked through x_c and thus assumes a wrong symbol **0**. For a trajectory on the chaotic repeller, this situation is much more improved. In so far as the noise amplitude is smaller than the size of the gap across the partition point x_c, the symbolic dynamics is immune to noise. This is of tremendous value to practical implementation of communication with chaos [56,57].

Since all chaotic repellers for $r > 4$ in the logistic map have the same topological entropy $\ln 2$, it appears that it is more advantageous to use chaotic repellers at large r because they possess larger gaps across x_c and thus their corresponding symbolic dynamics are more robust against noise. We note, however, as r increases, the sizes of the gaps increase so that it becomes more difficult to generate trajectories that can stay near the chaotic repeller for sufficiently long time. In general, when choosing an optimal chaotic repeller for digital encoding, there is a trade-off between the degree of difficulty of generating a trajectory near the chaotic repeller and the noise immunity [56,57].

5.1.9. Message encoding using two-dimensional symbolic dynamics

We consider message encoding by controlling symbolic dynamics in two-dimensional maps (equivalently three-dimensional flows) [125]. Our motivation comes from the fact that, although the principle of utilizing chaotic symbolic dynamics for communication is quite general, most examples illustrating this idea exclusively utilize chaotic systems whose dynamics can be approximated by one-dimensional maps [24,25]. Many chaotic systems encountered in practice, however,

cannot be described by one-dimensional dynamics. It is thus of interest to study whether communicating using controlled symbolic dynamics can be realized in higher dimensions.

The major difficulty when two-dimensional maps are utilized for communication is to locate a generalized partition so that a good symbolic dynamics can be defined. This difficulty arises due to nonhyperbolicity. In smooth, noninvertible two-dimensional maps such as those arising on the Poincaré surface of section of three-dimensional autonomous flows, nonhyperbolicity is typically characterized by the existence of an infinite number of points embedded in a chaotic attractor at which the stable and unstable directions coincide – the set of tangency points. Analogous to the critical point in one-dimensional chaotic maps [e.g., $x_c = 1/2$ in the logistic map $f(x) = rx(1 - x)$], which is naturally the generating partition point for defining symbolic dynamics, in two dimensions the generating partition is a zig-zag curve, the curve connecting all primary tangency points in the chaotic attractor [126,127]. It is generally quite difficult to locate precisely the partition curve even for well studied two-dimensional systems such as the Hénon map [40]. To overcome this difficulty, in Ref. [125], a general solution is proposed: one exploits various *hyperbolic chaotic invariant sets* embedded in the nonhyperbolic chaotic attractors. Due to hyperbolicity, it is straightforward to locate a generating partition for trajectories restricted to these saddles.[9] One can choose the chaotic saddles so that the symbolic dynamics are robust against small random noise. Thus, utilizing hyperbolic chaotic saddles for communication also provides a solution to overcome the influence of noise [56,57].

We briefly describe symbolic partitions in two dimensions. The fundamental requirement that qualifies a chaotic system for communication is whether a good symbolic dynamics can be defined which faithfully represents the dynamics in the phase space. That is, there should be a one-to-one correspondence between points in the phase space and those in the symbolic space. To generate a symbolic dynamics, one first partitions the phase space into cells C_i $(i = 1, 2, \ldots, m)$ covering the entire attractor and then assigns symbols s_i to cells C_i, respectively. Consider a point $\boldsymbol{x}$ in the cell C_i, together with a segment of its unstable manifold. Let $\boldsymbol{a}$ and $\boldsymbol{b}$ be the two intersecting points of the unstable manifold segment with the cell boundaries, as shown in Fig. 27. A primary condition for a good symbolic dynamics is that the images of $\boldsymbol{a}$ and $\boldsymbol{b}$ under the map $\boldsymbol{F}(\boldsymbol{x})$, denoted by $\boldsymbol{F}(\boldsymbol{a})$ and $\boldsymbol{F}(\boldsymbol{b})$, respectively, should still be at the cell boundaries within which the curve $\boldsymbol{F}(\boldsymbol{a})\boldsymbol{F}(\boldsymbol{b})$ lies, as shown in Fig. 27a. However, for an arbitrary partition, situation may arise where one of the end points, say $\boldsymbol{b}$, is no longer on a cell boundary, thus creating a "dangling end", as shown in Fig. 27b. Dangling ends may also occur for the stable manifold of $\boldsymbol{x}$ under the inverse map $\boldsymbol{F}^{-1}$. In both cases, there is no one-to-one correspondence between points in the phase space and those in the symbolic space. Such an ill-defined symbolic representation of phase-space points is not desirable for communication application, as ambiguities will arise when one attempts to assign symbols to different cells. Nonetheless, if the chaotic attractor is hyperbolic, the partition into cells can be chosen in such a way that the situation of dangling ends depicted in Figs. 27b does not occur [128]. Such partitions are called Markov partitions [129], the dynamics of which is schematically illustrated in Fig. 27a. The partition is *generating* if every infinitely long symbol sequence created by the partition corresponds to a single point in the phase space [126,127].

[9] Strictly speaking, the hyperbolic subsets do not cover the entire attractor and, hence, the corresponding "generating partition" is not the generating partition for the original map but for a "truncated" map.

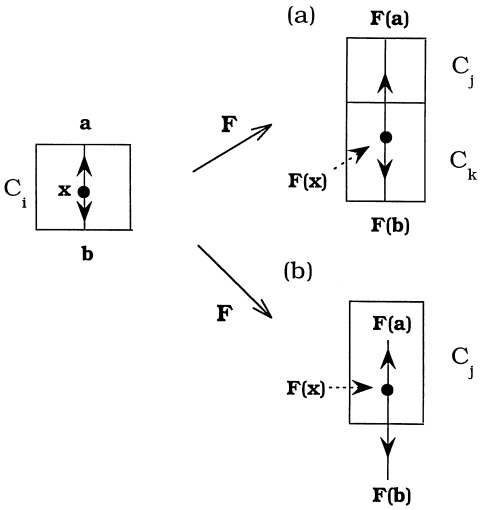

Fig. 27. From Ref. [125]. (a) The forward dynamics of a Markov partition. (b) For an arbitrary partition, a "dangling end" of the unstable manifold. This dangling end destroys the one-to-one correspondence between the phase space and the symbolic space.

Since chaotic attractors arising in most two-dimensional maps are nonhyperbolic, the key issue becomes how to find hyperbolic subsets embedded in the attractor. To illustrate the principle, we use the Hénon map [40]: $(x, y) \to (1.4 - x^2 + 0.3y, x)$, which is widely believed to admit a chaotic attractor. The partition is a zig-zag curve connecting all primary tangency points in the phase space, which lies near $y = 0$ [126,127]. Trajectory points above the curve bear symbol **1** and those below bear symbol **0**. This curve is a generating partition but it is difficult to compute. To overcome this difficulty while preserving the generating partition, we look for chaotic saddles embedded in the attractor with a gap region, or a forbidden region, defined by $y = \pm s/2$, which covers the partition curve. Due to the gap, a trajectory restricted to the chaotic saddle will never visit the vicinity of the zig-zag partition curve. The partition for the chaotic saddles thus becomes easy to locate: it is the gap itself. In particular, trajectory points above the gap bear symbol **1** and those below bear symbol **0**, and this partition is *generating*. Fig. 28a shows such a chaotic saddle with gap size $s = 0.2$. The chaotic saddles are numerically computed by the *Proper-Interior-Maximum triple* (PIM-triple) procedure [33]. Since the forbidden region contains *all* the primary tangency points, the chaotic saddle in Fig. 28a is apparently *hyperbolic*: it does not contain any tangency points between the stable and unstable manifolds. As such, a Markov partition can be defined for such a hyperbolic saddle, which naturally admits a good symbolic dynamics. In fact, there are infinitely many gap sizes s which correspond to different hyperbolic chaotic saddles embedded in the attractor.

The hyperbolic chaotic saddle shown in Fig. 28a is a subset embedded in the chaotic attractor and, hence, its topological entropy cannot be larger than that of the attractor. A question is then, how severe is the reduction in the topological entropy. This question is important for communication because the topological entropy of a chaotic set characterizes, quantitatively, how much information can be encoded into the trajectories on the set (the channel capacity) [24,55–57,115]. To address this, we compute the topological entropy $h_T(s)$ of the chaotic saddle as the gap size s

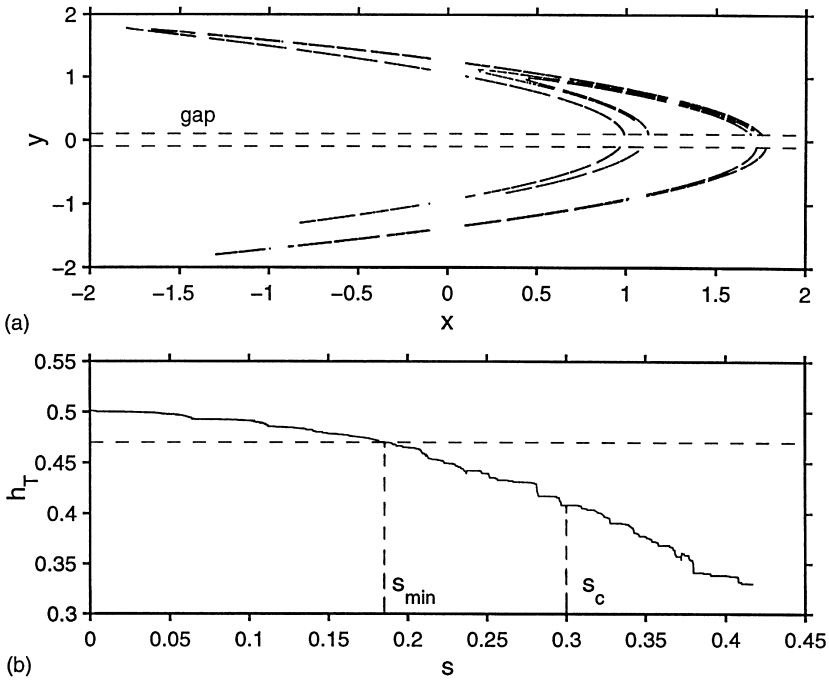

Fig. 28. From Ref. [125]. (a) A hyperbolic chaotic saddle embedded in the Hénon attractor with gap size $s = 0.2$. (b) The topological entropy $h_T(s)$ of the chaotic saddle as a function of the gap size s.

is increased from zero [56,57], as shown in Fig. 28b for $0 \leq s < s_{\max} \approx 0.42$, where the dashed horizontal line at $h_T = 0.466$ defines the minimum gap size $s_{\min}$ above which the generating partition for the chaotic saddle is simply[10] $y = 0$. We see that as s increases from 0, h_T decreases slowly at first, and then faster. The slowly decreasing behavior warrants a relatively large regime $s < s_c \approx 0.3$ in which h_T decreases only slightly (less than 10% reduction in h_T). The key implication is that utilizing chaotic saddles with gap size smaller than s_c but larger than $s_{\min}$ seems to be practically beneficial in communication applications: the specification of the symbolic dynamics is straightforward, yet the channel capacity is close to that obtained when one utilizes the original chaotic attractor. It was conjectured [125] that the function of h_T versus s is a devil's staircase, a statement that can be made rigorous for certain one-dimensional maps [56,57].

[10] When the noise-gap size is small so that the zigzag generating partition curve cannot be covered entirely, utilizing $y = 0$ as the partition line for the symbolic dynamics leads to an error ΔN in $N(n)$, the number of possible symbol sequences of length n. The values of h_T for $s = 0$ (the chaotic attractor) were compared [125]: (i) by counting $N(n)$, with x-axis as the partition line; and (ii) by using a procedure developed by Newhouse and Pignataro [130]. The counting method (i) yields $h_T(s = 0) \approx 0.500$, while the Newhouse–Pignataro algorithm (ii) gives $h_T(s = 0) \approx 0.466$. This suggests that when a chaotic saddle has entropy less than about 0.466, its noise-resisting gap has already covered the zigzag generating partition of the attractor. This, in turn, gives an estimation for the value $s_{\min}$ in Fig. 28b, the minimum gap size for which a good symbolic dynamics can be defined by simply using $y = 0$ as the partition.

In general, it is advantageous to use chaotic saddles, such as the ones depicted in Fig. 28a, for communication, because the symbolic dynamics on the chaotic saddle are immune to small noise. If the system is in a noisy environment, and the original chaotic attractor is used to encode messages, then a bit error (i.e., **0** becomes **1** or vice versa) may occur whenever the trajectory comes close to the partition curve, because noise can kick the trajectory over the curve in both directions. However, trajectories on the chaotic saddles do not come close to the partition point because of the forbidden region. Thus, the possibility for bit error due to noise can be substantially reduced when a chaotic saddle is utilized to encode messages if the noise amplitude is smaller than $s_{\min}$. Generally, there is a trade-off between the channel capacity and noise resistance.

We now give an example of coding a specific message. Suppose we wish to encode the message "BEAT ARMY!" into a trajectory in the chaotic saddle in Fig. 28a. The message "BEAT ARMY!" has the following ASCII representation:

$$\overbrace{1000010}^{B}\ \overbrace{1100101}^{E}\ \overbrace{1100001}^{A}\ \overbrace{1110100}^{T}\ \overbrace{0100000}^{\text{space}}\ \overbrace{1000001}^{A}\ \overbrace{1110010}^{R}\ \overbrace{1101101}^{M}\ \overbrace{1111001}^{Y}\ \overbrace{0100001}^{!}.$$

If the chaotic saddle were equivalent to the fullshift grammar symbolic dynamics, i.e., no grammatical restrictions, then we could simply find a trajectory in the x, y plane such that its y itinerary exactly follows the above digital message. However, the symbolic dynamics of the chaotic saddle are subshift-type because its topological entropy is less than $\ln 2$.

Dynamics on the saddle is representable by the Bernoulli shift map, on a bi-infinite symbol space Σ of two symbols [126,127,131]. A bi-infinite symbol sequence is a point in the symbolic space: $\sigma = \ldots \sigma_{-2}\sigma_{-1}\sigma_0 \cdot \sigma_1\sigma_2\sigma_3 \ldots \in \Sigma$, where $\sigma_i = \mathbf{0}$ or $\mathbf{1}$, and σ_i is the position of $(x_i, y_i) \in \mathbf{R}^2$, relative to a partition curve, on the ith (pre)iterate for $(i < 0)$ $i \geq 0$. Shifting the decimal to the right represents a forward iteration, and shifting the decimal to the left represents an inverse iteration. To quantify the correspondence between a point $\boldsymbol{x}$ in the phase space and a point (points) in the symbolic space, it is necessary to use a vector function (the so-called coding function [24], corresponding to the "symbolic plane" discussed in Ref. [131]): $\boldsymbol{G} = (\delta, \gamma)$, where δ and γ are determined by

$$\delta = 1 - 0.d_1 d_2 \cdots d_\infty \equiv 1 - \sum_{k=1}^{\infty} d_k 2^{-k},$$

$$\gamma = 0.c_1 c_2 \cdots c_\infty \equiv \sum_{k=1}^{\infty} c_k 2^{-k}, \tag{98}$$

where $d_k = \sum_{i=1}^{k} (1 - a_{-i}) \bmod(2)$ and $c_k = \sum_{i=1}^{k} a_i \bmod(2)$. The phase-space dynamics can then be represented by the following map in the coding space: $(\delta_{n+1}, \gamma_{n+1}) = D(\delta_n, \gamma_n)$, where $D(\delta, \gamma) = \{(1 - \delta)/2, 2\gamma\}$ if $\gamma < 1/2$ and $D(\delta, \gamma) = \{(1 + \delta)/2, 2 - 2\gamma\}$ if $\gamma \geq 1/2$. A trajectory of 50 000 points in the symbolic plane corresponding to the chaotic saddle in Fig. 28a is shown in Fig. 29. The forbidden points (blank regions) in the symbolic plane is generated by the *pruning front* [131]. Fig. 29 thus determines, completely, the grammar on the chaotic saddle, from which a controlling scheme can be derived to encode messages into the trajectories in the chaotic saddle. We note that the pruning front of an embedded chaotic saddle must be ordered less than or equal to the pruning front of the full chaotic attractor, following the fact that the subshift grammar of the chaotic saddle

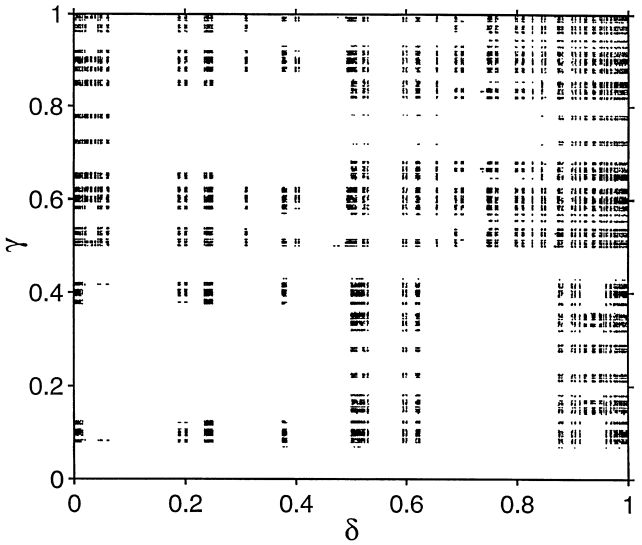

Fig. 29. From Ref. [125]. The symbolic plane for the hyperbolic chaotic saddle in Fig. 28a.

must be a subset of the subshift grammar of the attractor. Furthermore, the pruning front must be a monotone nonincreasing curve (i.e., receding), as a function of the increasing gap. This corresponds to the fact that we observe a monotone nonincreasing topological entropy.

In what follows we present a practical method to learn the grammar and then to encode digital messages. In physical or numerical experiments, only finite precision can be achieved and, hence, it is reasonable to choose an n-bit precision approximation (subshift of finite type). A way to represent the transitions between the allowed n-bit words is to use the directed-graph method in Ref. [55] which was originally discussed for one-dimensional noninvertible chaotic maps (with an infinite shift space). The directed-graph representation is, however, more general: two-dimensional invertible maps (with a bi-infinite shift space) requires little modification, for n-bit words, or truncations of the bi-infinite symbol sequences, which represent $n/2$ pre-iterates and $n/2$ future iterates. The main point of a symbol dynamics representation is that each (x, y) state in phase space occupies a neighborhood which corresponds to an n-bit code, labeled as a node on the graph. There are two possible situations: (1) either a **0** or a **1** may be shifted into the n-bit register, and this choice means that one of the message bits may be controlled; or alternatively, (2) only a **0** or a **1** exclusively may be shifted in to the bit register, and this must be a nonmessage bearing "buffer-bit" *even if the bit happens to coincide with the next message bit* because according to Shannon's information theory [115], an event only carries information if that event is not pre-determined. It is exactly this time spent transmitting the buffer-bits which causes decreased channel capacity, as measured by the topological entropy. The more of the n-bit words which have the two possible outcomes, **0** or **1**, the higher the channel capacity. In numerical experiments, we approximate the symbolic dynamics of the chaotic saddle by using 12-bit words. By using the method outlined in Ref. [55], we encode the message into a trajectory on the chaotic saddle, where the actual phase-space trajectory is shown in Fig. 30a and the corresponding time series y_n is shown

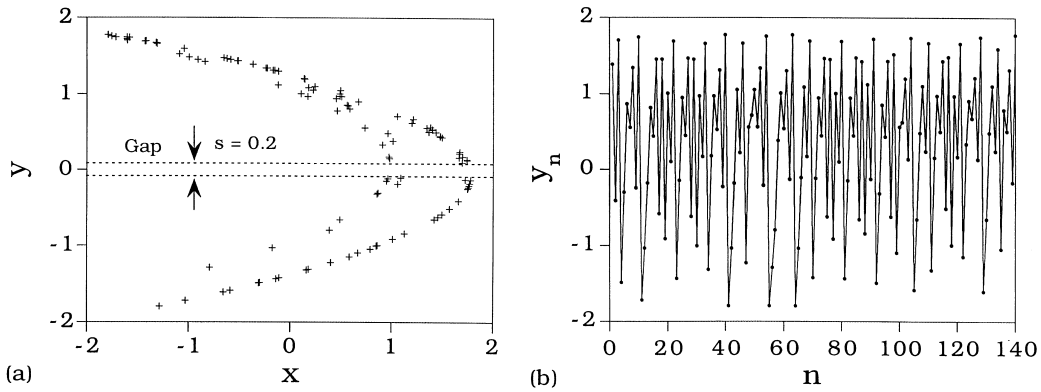

Fig. 30. From Ref. [125]. Example of encoding a message into a chaotic saddle: (a) controlled trajectory in the phase space; and (b) the corresponding time series.

in Fig. 30b. The receiver can completely recover the original message, given the time-series, the location of the symbol partition $y = 0$, and the grammar in the form of the 2^n list of transitions.

We remark that an alternative method to record the grammar of a two-dimensional map is to use the pruning fronts [131] which was orginally developed for the Hénon map as the analogy in the symbol plane to the one-dimensional kneading theory of Milnor and Thurston [132]. Both theories give a partial order for the symbol representation of a given point, relative to a "maximum" grammatically allowed word. Given a particular n-bit sequence, it is only necessary to check whether both possibilities are grammatically permitted. In the case of the kneading theory, one checks, in the Gray-code ordering, whether both shifting in a **0** and a **1** give new n-bit words which are also below the kneading sequence, which is the maximum sequence corresponding to the symbolic code of the critical point. In the case of the two-dimensional pruning-front theory, one must check that both **0** and **1** lead to symbolic codes ordered "below" the pruning front; if either shift, say a **0** (or **1**), is greater than the pruning front, then that word is grammatically forbidden on the chaotic saddle, and therefore the alternative shift, say the **1** (or **0**), is determined. In either case, just as with the directed-graph method of book-keeping the grammar, information theory demands that when the two possible outcomes are permitted, the message bit can be transmitted, but when one of the alternatives (**0** or **1**) leads to a symbolic code ordered larger than the pruning front, the transmitted bit must be a non-message bearing buffer bit.

5.1.10. Discussions

Nonlinear digital communication using chaos has become a field of recent interest. There are two different approaches to the problem. One is to use the principle of synchronous chaos[11] to embed and transmit digital information. Another is to extend the principle of controlling chaos [1,23] to dynamical systems with well-defined symbolic dynamics to encode information [21,24,54–57]. The latter approach makes explicit use of the fundamental principle that chaotic

[11] For an overview of the field of chaos control and synchronization, see the focus issue of Chaos **7**(4), 1997.

systems are natural information sources. By manipulating the symbolic dynamics of a chaotic system in an intelligent way, the system produces trajectories in which digital information is embedded. The methodology reviewed here is within the scope of the second approach. Specifically, we address the problem of controlling the symbolic dynamics of chaotic systems. We argue, by explicit computation of the topological entropy, that a dynamical system operating in parameter regimes of transient chaos on nonattracting chaotic saddles usually possess a greater information-bearing capability as compared with the same system in regimes of sustained chaos on attractors. We detail a procedure, which is applicable to chaotic systems described by one-dimensional maps, to encode digital information into typical trajectories wandering in the vicinity of the chaotic saddle.

Using transient chaos for message encoding has the advantage of strong noise immunity. This notion has been recently pointed out from the perspective of finding an optimal coding scheme for communicating using chaotic attractors [56,57]. In such a case, a code is necessary for message encoding in order to accommodate the grammar of the chaotic attractor whose topological entropy is typically less than $\ln 2$. It is argued [56,57] that a code always yields a chaotic saddle *embedded* in the chaotic attractor. The topological entropy of such a chaotic saddle is smaller than that of the original chaotic attractor, although the symbolic dynamics restricted to the chaotic saddle also has noise immunity. Thus, in digital encoding using sustained chaos on attractors, the trade-off between channel capacity and noise immunity becomes a critical issue. The chaotic saddles considered here are those *naturally* arising in wide parameter regimes of a nonlinear system. The characteristic difference between a natural chaotic saddle and one embedded in a chaotic attractor is that the former usually has the maximally allowed value of the topological entropy. As such, coding is *not* necessary for communicating with these natural chaotic saddles, while strong noise immunity can be achieved. As transient chaos arises commonly in many situations of physical interest [119,120], we expect the main point and its implications reviewed here to be a major considering factor in designing practical communication schemes.

The observation that the topological entropy is greater for transient chaos also seems to hold for some well studied high-dimensional chaotic systems. For instance, it is known that for the Hénon map [40]: $(x, y) \to (a - x^2 + by, x)$, the topological entropy increases as a system parameter changes from regimes with chaotic attractors to regimes with transient chaos (see Fig. 2 in Ref. [123]). Communicating with high-dimensional chaotic symbolic dynamics is itself an interesting problem. The main difficulty is to define a generating partition in the phase space so that a good symbolic dynamics can be defined [126,131]. Here we wish to point out that utilizing transient chaos may greatly simplify the task of symbolically partitioning the phase space. Take the Hénon map as an example. When the parameter b is fixed at 0.3, it is believed that the map generates a chaotic attractor at $a = 1.4$. In this case, the generating partition is a zigzag curve connecting all primary tangencies between the stable and unstable manifolds, a good computation of which is highly nontrivial [126]. In contrast, for $a = 3.0$, the dynamical invariant set is a hyperbolic chaotic saddle. The symbolic dynamics can be described by two symbols on a full shift, and the generating partition is simply the straight line $y = 0$. With the advantage of having the maximum topological entropy $\ln 2$, the hyperbolic chaotic saddles can serve as excellent information sources for digital encoding in noisy environment.

We also remark that the procedure of controlling symbolic dynamics can be effectively utilized for controlling transient chaos [133–136], which is still a challenging problem in the field of chaos

control. By encoding an arbitrary but random symbol sequence, the trajectory of the system remains in the vicinity of the chaotic saddle. Insofar as the encoding continues, the chaotic trajectory is stabilized. This may be of value to the important problem of maintaining chaos [52,136–140].

Finally, we have reviewed the feasibility of utilizing two-dimensional symbolic dynamics for communicating with chaos. The main difficulty for chaotic attractors in two-dimensional invertible maps, arising from three-dimensional flows, is that due to nonhyperbolicity, the generating partition for defining a good symbolic dynamics is extremely difficult to compute. Our idea is that there typically exists an infinite number of hyperbolic chaotic saddles embedded in the chaotic attractor for which the generating partition can be easily specified. The hyperbolic chaotic saddles have the additional property that their symbolic dynamics are immune to small environmental noise. When chosen properly, the topological entropies of the chaotic saddles can be close to that of the original attractor. These advantages make dynamical systems described by two-dimensional invertible maps potential candidates for nonlinear digital communication.

5.2. The adaptive synchronization of chaos for secure communication

In the previous section, we have described how the OGY idea can be implemented for the control of chaotic behaviors, with applications to the process of communicating with chaos. Here, we show that the adaptive technique introduced for the stabilization of UPOs can, in fact, be successfully applied to the problem of synchronization of chaos. The process of synchronizing two identical chaotic systems starting from different initial conditions [22] consists in linking the trajectory of one system to the same values as the other so that they remain in step with each other, through the transmission of a signal.

We have already described in details the possibility of encoding a message within a chaotic dynamics [21], and we have pointed out that synchronization of chaos provides a good tool for communicating between a sender and a receiver. In this section, we highlight that the use of a chaotic carrier for the transmission of a message can give rise to security in the communication.

Several problems arise in order to assure security. The main one is due to the fact that the sender must transmit to the receiver a part of the information on the dynamical system (in the Pecora–Carroll case [22] this is realized by means of the transmission of one of the system variables). As a result, a clever spy intercepting the communications can try to reconstruct the whole dynamics, hence decoding the message. To prevent reconstructions of the message, Cuomo and Hoppenheim [106] have proposed to use chaos to hide messages, by transmitting a signal which consists in the sum of a chaotic signal and of a given message. Later, Perez and Cerdeira [107] have shown that messages masked by low-dimensional chaotic processes can be intercepted and extracted. Therefore, the attention was directed to the implementation of the Pecora and Carrols (PC) idea to higher dimensional systems [141] with the hope that increased unpredictability could improve security in the communication.

Another problems using the PC procedure is that the subsystem to be synchronized must show negative subLiapunov exponents [22]. In other words, synchronization occur in a linear sense, and, because of this requirement, an additive signal used to hide the real message should be an infinitesimal perturbation of the signal itself, while masking messages with large signals could lead to problems in the synchronization.

Enrichments of the PC method has been provided an alternative approaches to synchronization based on nonreplica subsystems have been proposed [142], but still the problem of security in the communication is an hot issue.

Ref. [65] describes the application of the adaptive scheme for chaos synchronization, and shows how some of the above difficulties can be overcome, leading to a reliable level of security against external interceptions even in the case of low dimensional chaotic systems.

The communication scheme in Ref. [65] consists of a message sender (Alice), a receiver (Bob) and a spy (James) ready to intercept and decode all communications between Alice and Bob. Alice consists of two identical chaotic systems

$$\dot{\boldsymbol{x}}_1 = \boldsymbol{f}(\boldsymbol{x}_1, \mu), \qquad \dot{\boldsymbol{x}}_2 = \boldsymbol{f}(\boldsymbol{x}_2, \mu)\ , \tag{99}$$

where μ is a set of control parameters chosen in such a way as to produce chaos, $\boldsymbol{x}_1, \boldsymbol{x}_2$ are two D-dimensional vectors ($D \geq 3$) and $\boldsymbol{f}$ is a nonlinear function. Bob consists of a third identical system

$$\dot{\boldsymbol{x}}_3 = \boldsymbol{f}(\boldsymbol{x}_3, \mu)\ . \tag{100}$$

The three systems start from different initial conditions, and therefore produce unsynchronized dynamics. Ref. [65] considers the Lorenz system, where the vectors $\boldsymbol{x}_j = (x_j, y_j, z_j), (j = 1, 2, 3)$ obey the equations:

$$\dot{x}_j = \tilde{\sigma}(y_j - x_j), \quad \dot{y}_j = r x_j - y_j - x_j z_j, \quad \dot{z}_j = -bz_j + x_j y_j\ . \tag{101}$$

The scheme for the communication is reported in Fig. 31. With this scheme, one supposes to have encripted a message within the vector $\boldsymbol{x}_1$ (with the use, e.g. of the encoding techniques described in Section 5.1). The point is how to transmit the message to Bob in a secure way, so as to avoid a possible reconstruction by James.

The first step is to produce synchronization between $\boldsymbol{x}_2$ and $\boldsymbol{x}_3$. Bob sends to Alice the variables $y_3(t)$ which is replaced into the equations for x_2 and z_2. Synchronization (in the PC sense) is here assured by the fact that the sub-Liapunov exponents for the subsystem (x_2, z_2) are both negative (for $\tilde{\sigma} = 10, b = \frac{8}{3}$ and $r = 60$ they are -2.67 and -9.99, respectively [22]).

This way, Alice knows the actual dynamical state of Bob and can transmit the perturbation $U(t)$ to be applied to the x_3 equation in order for Bob to synchronize the system $\boldsymbol{x}_3$ to $\boldsymbol{x}_1$. Alice makes use of the adaptive method to slave the system $\boldsymbol{x}_2$ to the goal dynamics $\boldsymbol{x}_1$.

Precisely, the same algorithm of Eqs. (54)–(57) is used with actual dynamics $x_2(t)$ and goal dynamics $x_1(t)$.

The perturbation $U(t)$ is then given by

$$U(t) = K(t)(x_1(t) - x_2(t))\ . \tag{102}$$

The effectiveness of this scheme is illustrated in Fig. 32, which reports the temporal behavior of $\Delta x = |x_1 - x_3|$, measuring the synchronization between Alice and Bob for $\tilde{\sigma} = 10$, $b = \frac{8}{3}$ and $r = 60$. Similar results hold also for $|y_1 - y_3|$ and $|z_1 - z_3|$. As a consequence, the message encoded within $\boldsymbol{x}_1$ is received by Bob.

Let us move to discuss the problem of security. James intercepts the two communication signals $U(t)$ and $y_3(t)$. No information on $\boldsymbol{x}_1$ can be retrieved from $U(t)$ since $U(t)$ vanishes as soon as Alice and Bob reach synchronization, and the weighting factor $K(t)$ is not decided a priori, but it is continuously changed by the adaptive algorithm. This is equivalent to have a time variable decoding key.

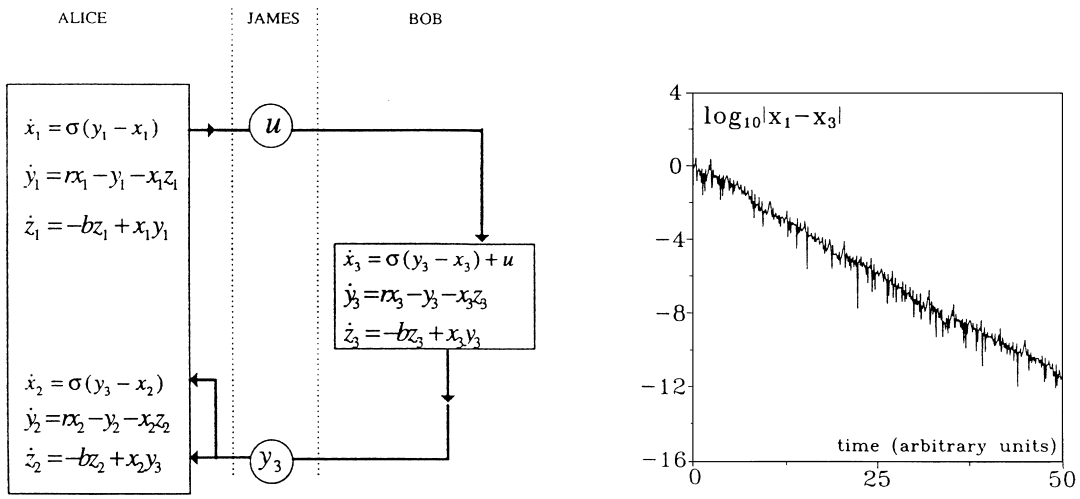

Fig. 31. The scheme for adaptive synchronization. Bob sends to Alice the variable y_3 to synchronize $\boldsymbol{x}_2$ and $\boldsymbol{x}_3$. Alice sends to Bob the adaptive correction $U(t)$ to be added to the evolution equation for x_3. James intercepts both $U(t)$ and y_3.

Fig. 32. From Ref. [65]. Temporal evolution of the quantity $\log_{10}(|x_1 - x_3|)$ measuring the synchronization between $\boldsymbol{x}_1$ and $\boldsymbol{x}_3$. $\tilde{\sigma} = 10$, $b = \frac{8}{3}$, $r = 60$, $K_0 = 10$, $\sigma = 0.011$.

However, from the knowledge of y_3, James can reconstruct the whole chaotic attractor corresponding to $\boldsymbol{x}_3$ through standard embedding techniques, and can easily decode the message once $\boldsymbol{x}_3$ and $\boldsymbol{x}_1$ become synchronized.

To prevent for this, Ref. [65] introduces the following trick. Alice and Bob agree on a given accuracy θ in the message reception. Once such an accuracy is reached. (Alice can test on it), Bob stops sending y_3 for a given while T_0. During this time lag the two systems $\boldsymbol{x}_2$ and $\boldsymbol{x}_3$ evolve separately. After T_0 Bob starts again sending y_3 to Alice. Now, if T_0 exceeds the decorrelation time $\tilde{\tau}$ of the system (which is defined as the reciprocal of the maximum Liapunov exponent Λ), then the effective signal sent by Bob results in the sum of uncorrelated temporal subsequences, and the embedding technique fails. Therefore, no reconstruction of $\boldsymbol{x}_3$ is possible by James in this case.

Fig. 33 reports the results for $T_0 = 1$ and $\theta = 10^{-5}$ (notice that in the present case $\Lambda \simeq 1.41$, hence $T_0 > \tilde{\tau} \simeq 0.71$). The synchronization scheme maintains the stipulated accuracy (Fig. 33a) even when the signal sent by Bob is affected by large holes (Fig. 33b) preventing external reconstructions of $\boldsymbol{x}_3(t)$. Finally, Fig. 33c shows the controlling signal which remains confined within a range negligible with respect to the x_1 dynamics (x_1 variations from -28 to 28).

6. Experimental evidences and perspectives of chaos control

6.1. Introduction

The large body of the theoretical proposal on chaos control has stimulated different applications in experimental systems whose natural behavior showed chaos. The stabilization of a dynamical

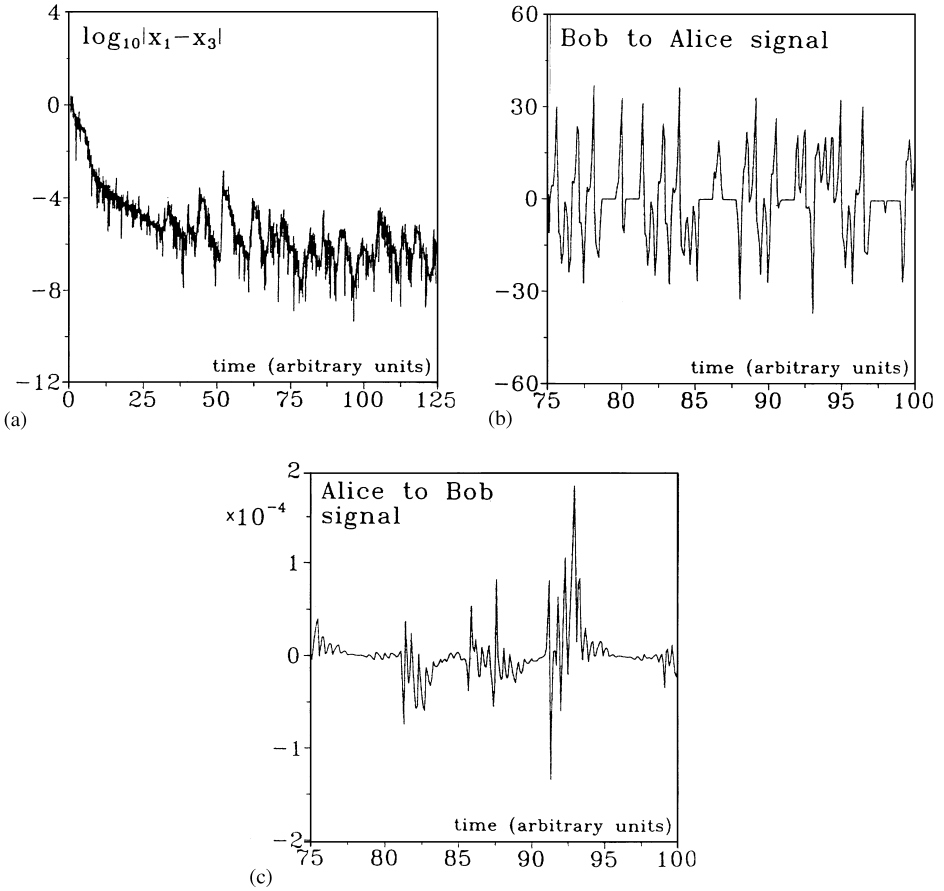

Fig. 33. From Ref. [65]. (a) Temporal evolution of $\log_{10}(|x_1 - x_3|)$ for $\theta = 10^{-5}$ and $T_0 = 1 > 1/\Lambda \simeq 0.71$. The stipulated accuracy in the transmission is perserved in time even though (b) the syncronization signal Bob sends to Alice is affected by large holes which prevent any reconstruction of the message, and (c) the controlling signal $U(t)$ is kept within a range negligible with respect to the dynamics. Other parameters as in Fig. 5.

system toward a state of controlled periodicity allows a lot of possible technological applications, thus motivating the interest for the experimental demonstration of the reliability of the different theoretical techniques, in practical situations where often a mathematical model for the system is unknown, or very detailed dynamical features are practically impossible to be extracted from the outputs.

Stabilization and control are old engineering problems [42,143]. Open loop methods and closed loop negative feedback approaches has been developed long time ago and are still extensively used.

All experimental systems need some kind of stabilization to give safe operation and outputs. To avoid irregular fluctuations in a system, normal procedure include adding dissipativity to lower the gain, or redesigning the operating parameters so as to find a safe operating point, or filtering with narrow band the desired output, or other similar techniques.

In particular, in nonlinear devices where irregular fluctuations are normally obtained, there is a strong practical interest in obtaining an output intensity or a frequency free of irregular

behaviors. This is the main reason why a lot of different stabilization and control techniques have been used.

Stabilization and control in our context means achieving safe operations of a chaotic system onto some unstable orbits giving the possibility of choosing (and changing) a controlled, complex, multiperiodic desired behavior without hard changes in the parameter space of the system.

In general, we cannot claim that a control method is better than others for practical experimental implementations. Rather, the performances of the different proposed techniques depend on the particular situation under study.

What can be surely affirmed is that, in order to exploit all the advantages of a control chaos method, one needs an algorithm which takes profit of the possibilities offered by the chaotic attractor. Therefore, if the control will be performed on a variable, a parameter, modulating the pump or adding negative feedback, mainly depends on the particular problem to be faced.

In the following, we will consider some relevant experimental achievements that, in our opinion, may guide the reader toward a family of other works, which use similar or related techniques. We are aware that it would be unrealistic to pretend covering all the body of experimental works which are offered in the literature nowadays, and it has been necessary to concentrate our treatment only on few prototypic experiments, duly referring to the other literature on similar matter.

Along this line here we want to illustrate both experiments designed to verify some theoretical aspects, and others that intend, within the state of art, to solve some real technological problems.

Under this methodology, we will attempt to keep the chronological order.

6.2. Nonfeedback methods

Before the OGY method, Lima and Pettini [59] proposed a perturbative technique of stabilizing the chaotic system toward a periodic state. In this case, the periodicity is fixed by the frequency of a control signal perturbing the parameter space. Such a technique was called "suppression of chaos" by the same authors. Its implementation, however, can be complicated by the fact that it needs a preliminary learning task of the system response to possible perturbations of variable amplitude.

The effects of parametric perturbations was first studied by Azevedo and Rezende in Ref. [14], in a control experiment with a system of spin waves excited by microwaves. The experimental system consisted in a sample of yttrium iron garnet (YIG) localized within a waveguide, which was syntonized with the mode TE_{102}. In these conditions, the system behavior becomes chaotic as far as an external field H perturbs the YIG sample in the direction perpendicular to the field h of the cavity.

The authors did not develop a systematic study of the system dynamics as a function of control parameters. Rather, they limited to the introduction of a periodic modulation in H ($H = H_0 + \delta H \cos(2\pi f t)$), with amplitude δH about four orders of magnitude smaller than the continuous component H_0. In this case, the operator suitably scans a large frequency band in f, in order to individuate those forcing frequencies leading to a global periodic behavior of the system. Once the frequencies have been selected, the operator acts on the respective amplitudes in order to get the best control conditions. This experiment should be considered as pioneering, insofar as it demonstrated for the first time that a suitable periodic perturbation may produce mode-locking, thus restoring a periodic state for control parameter values much above the threshold of the

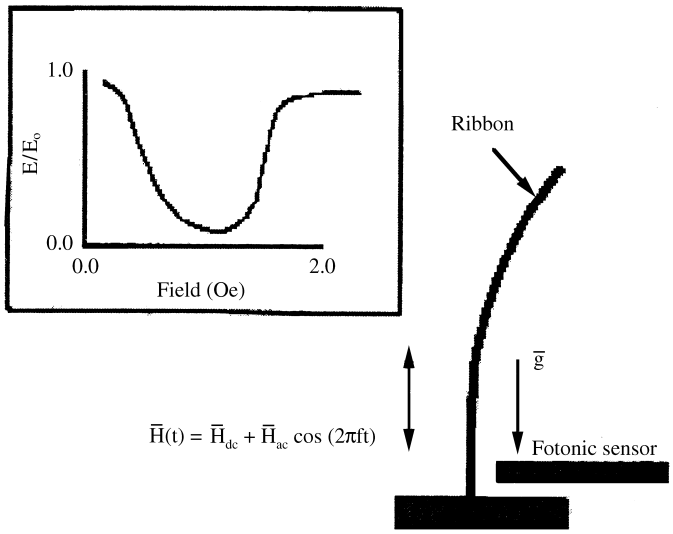

Fig. 34. Experimental setup of the magnetoelastic ribbon control experiment.

appearance of chaos. In other words, it is here experimentally demonstrated that a synchronization mechanism between a chaotic attractor and a periodic perturbation can be considered as a reliable control method in various circumstances.

Among the various experimental application of this technique, we here mention the results by Fronzoni et al. [144], who have shown the elimination of chaotic oscillations of a bistable magnetoelastic system, actually represented by the Duffing–Holmes equation. Recently this technique has been also applied for stabilizing periodic orbits in a single mode CO_2 laser with modulated losses [146]. The authors applied a slow nonresonant (or near-resonant) parametric modulation to the cavity detuning. The addition of the "control signal" is able to reduce the periodicity of the periodic orbit (e.g. from period four to period two and to period one) and even to control unstable periodic orbits [147].

6.3. Control of chaos with OGY method

The first experimental application of the OGY control method was realized by Ditto et al. at the end of 1990 [9]. In this paper, the authors obtained the stabilization of period one oscillations in the dynamics of a magnetoelastic ribbon. The experimental setup consisted of an amorphous magnetoelastic ribbon of thickness 25 μm, width 3 mm and length 100 mm. The first 35 mm were fixed at the basis, allowing only the remaining part of the ribbon to perform horizontal displacements. The choice of the material was carefully done, since amorphous materials allow large variations of their Young modulus for relatively small changes in the applied magnetic field H. The system was put inside three Helmoltz reels (perpendicular to each other) in order to compensate for the earthly magnetic field. The setup is reported in Fig. 34.

In order to force the appearance of the oscillations, a forcing field $H = H_{dc} + H_{ac}\cos(2\pi ft)$ was applied, where H_{dc} (H_{ac}) is the amplitude of a continuous (alternate) magnetic field. The deter-

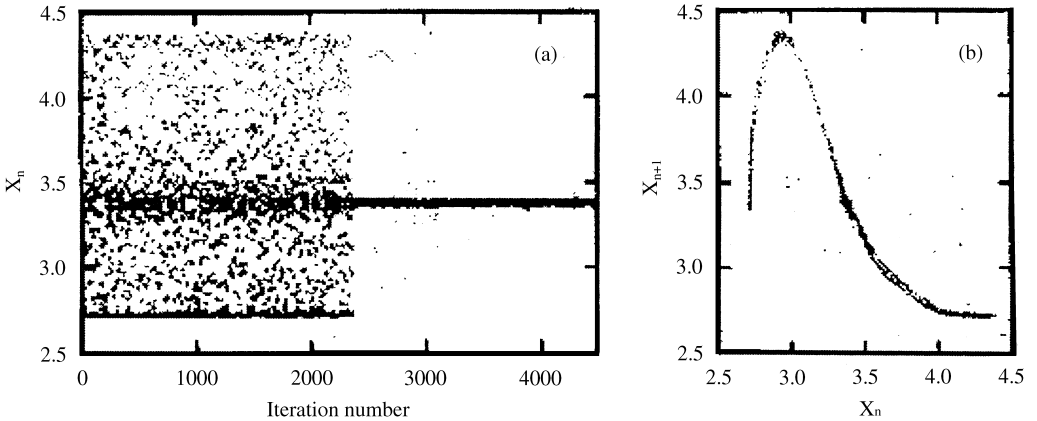

Fig. 35. From Ref. [9]. (a) Time series of $X_n = V(t_n)$ before and after the control was switched ON. (b) The first return map (X_{n+1} versus X_n) for the uncontrolled system (in gray) and the controlled output when the control is turned ON (in black).

mination of the dynamics was done by measuring the horizontal displacements of the ribbon by means of a photonic sensor pointing at a height of 6 mm with respect to the basis of the system.

The dynamics of such displacements shows interesting chaotic features. For a detailed discussion on the structure of the chaotic attractor, we here address the reader to Ref. [145].

The application of the OGY to such a system required the localization of a saddle fixed point within the attractor set, with a neighborhood wherein the local dynamics could be considered linear in the perturbations introduced in some control parameter. Ditto et al. then constructed experimentally the time series $X_n = V(t_n)$ (t_n being the natural sampling time corresponding to the forcing period) of the voltages out from the photodetector. In Fig. 35, this time series was used to construct the return map, for 2350 points, $H_{dc} = 0.112$ Oe, $H_{ac} = 2.050$ Oe and $f = 0.85$ Hz.

In this framework the period one orbit is individuated by the condition $X_{n+1} = X_n$, which was said to be fulfilled within the experimental resolution (in the present case, the error in the measure of the voltage was ± 0.005 V). For each pair of points, it is possible to construct a local linear map $\boldsymbol{M}$, and to extract the values of stable (λ_s) and unstable (λ_u) eigenvalues, and the corresponding eigenvectors ($\boldsymbol{e}_s, \boldsymbol{e}_u$).

By slightly varying a control parameter (in this case it was the continuous magnetic field H_{dc}), the authors were able to estimate the variation in the fixed point position, and by the use of OGY technique, to control the desired fixed point. In the present case, the whole execution time of the control line was about three orders of magnitude smaller than the characteristic time of the system oscillations, thus allowing a real time on line control. Within the parameter range of Fig. 35, the authors were able to stabilize the period one orbit for more than 200 000 iterations (about 64 h), using a maximum perturbation of 9% of the unperturbed dynamics. By using the second return map of the experimental time series, the authors were also able to stabilize the period two orbit, with the same limitation in the perturbation strength.

This experiment constituted the first robust evidence of the reliability of the OGY technique, insofar as it was shown that the control over chaos persisted inspite the presence of experimental

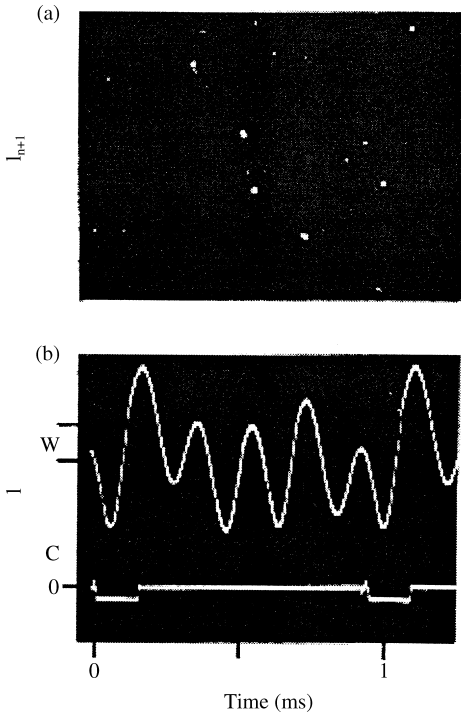

Fig. 36. From Ref. [15]. (a) First return map (I_{n+1} versus I_n) for the uncontrolled system. Bright points correspond to the controlled orbit. (b) The current through the resonator versus time, with the control window "W". The control signal (lower trace) is turned ON only when a peak of the signal enters within the window.

noise, which affects the determination of the map $\boldsymbol{M}$, thus of the estimate of the eigenvalues and eigenvectors.

6.4. Control of electronic circuits

The two experiments by Azevedo and Rezende [14] and Ditto et al. [9], even though realized with different methods, have a common underlying idea, which is that of forbidding large parameter variations in the control procedure. A qualitative change in this framework was performed by Hunt in Ref. [15], where the perturbations were allowed to be quite large, thus permitting the control of more complicated periodic behaviors, associated with higher periodic orbits of period as large as 23 times the characteristic oscillation period.

In this experiment, a simple electronic circuit is used, based on a diode resonator. A p–n junction is excited by an harmonic voltage, and the system shows a series of period doubling bifurcation, eventually entering a chaotic regime. Because of its extreme simplicity, the system comes out to be well described by a bidimensional mappings, which can be directly constructed by means of the experimental observations of the maxima of the current traveling through the junction (see Fig. 36a).

By exploiting such a preliminary learning process, the system is fed back with a control signal proportional to the distance between the measured maximum and the expected one for the periodic

orbit. Due to this procedure, the method itself was called *Occasional Proportional Feedback* (OPF). Even though the basic concept does not differ from the OGY one, here the author does not consider explicit limitations for the perturbation strength (which, instead, are peculiar of the formal OGY technique). As a result, the chaotic attractor comes out to be slightly distorted as a consequence of the large variations in the control parameters.

Precisely, Hunt defines a window in the neighborhood of the current value corresponding to the desired orbit. The width of this window also defines the maximum strength of the perturbation. This process is simply realized by the use of a current–voltage converter, which sends the output signal to an electronic comparator, which eventually delivers the control pulse. The duration of the pulse can be adjusted to achieve robustness in the control, but it is always limited to be a rather small fraction of the characteristic oscillation time.

The results of Ref. [15] show that small perturbations (about 0.5%) are able to stabilize lower periodic orbits, whereas the process leading to the control of higher periodic orbits is associated with a larger perturbation strength (about 10%). Such large perturbations may induce important modifications in the controlled orbits, as it appears evident in Fig. 36b, where a period 5 controlled orbit is shown. If one compares the coordinates of the controlled orbits with those of the unperturbed signal in the first return map, the former appear to be quite displaced, thus meaning that a slight deformation of the orbit has been produced.

The robustness of the method is highlighted by the control of very large periodic orbits, as large as period 21. In this case, the perturbation is even stronger, and the consequent deformation is more evident. The relevance of such an experiment is due to the first evidence of robust control of very high periodic behaviors.

6.5. Control of chemical chaos

Occasional Proportional Feedback method was introduced independently by Peng et al. [148] in order to control a model of chemical reactions. Chemical chaos generally correspond to a unpredictable variation in the concentration of some components that enter an oscillatory reaction. The most popular chaotic chemical system is the Belousov–Zhabotinsky (BZ) reaction, where a cerium ion-catalyzed oxidation malonic acid is produced by acidified bromate [149] in a continuous-flow stirred-tank reactor. The first control experiment in chemical chaos was implemented in a BZ reaction by the group of Showalter [17]. The authors here applied the so called single map based algorithm to an oscillatory BZ reaction continuously excited, feedbacking the control signal "$\Delta\mu$" of the cerium and bromide solutions entering the reaction tank.

The perturbation in the control signal $\Delta\mu = (A_n - A_s)/g$ can be directly calculated as a function of A_n (the potential in a Bromide electrode), and A_s (the fixed point value obtained by the first return map), while the weighting factor g can be evaluated by measuring the horizontal distance between two maps extracted from a suitable model of the reaction (Fig. 37a) [148,150]. This calculation allows a very precise estimate of the perturbation value necessary for the system to stabilize the desired periodic orbit.

In Fig. 37b the potential of bromide electrode as a function of time is presented. The control algorithm was switched on to control a period one orbit ($t = 27\,800$ s until $t = 29\,500$ s) and a period two orbit ($t = 30\,000$ s until $t = 32\,100$ s). The control range was set at ± 30 mV.

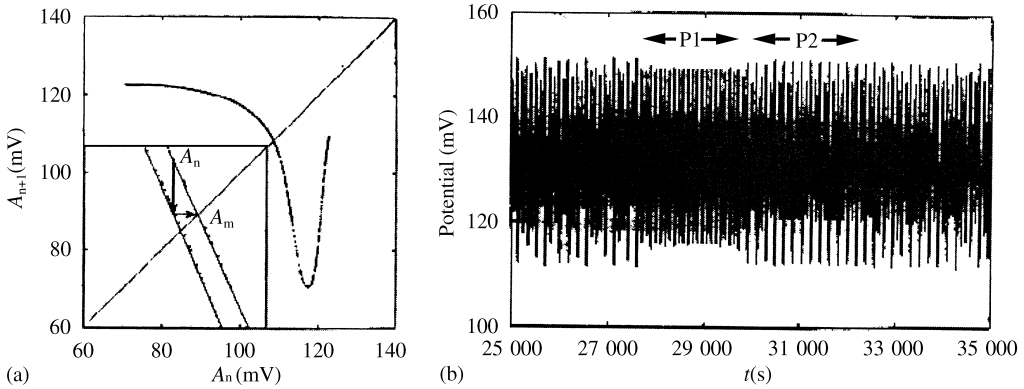

Fig. 37. Reprinted by permission from Nature 361, p. 242, copyright (1993) Macmillan Magazines Ltd. (a) First return map of the concentrations used in the experiment calculated from the Györyi-Field model. The system is directed to the stable fixed point applying a change $\Delta\mu = (A_n - A_s)/g$. (b) Bromide electrode potential versus time. The control algorithm was switched on at $t = 27\,800$ s unit $t = 29\,500$ s for controlling a period 1 orbit (p1) and from $t = 30\,000$ s until $t = 32\,100$ s for the control trial of a period 2 orbit (p2). The control range was set at $\pm$ 30 mV.

The map-based control algorithm has been also implemented for tracking unstable periodic orbits in the same BZ reaction [151].

6.6. Control of chaos in lasers and nonlinear optics

The control of stability in lasers and nonlinear optical devices is frequently necessary.

Indeed, from the beginning of laser industry a crucial point was to improve the performance in frequency and intensity, motivated by many problems inherent to the presence of several longitudinal and transverse modes (pulling and pushing of laser modes), couplings in nonlinear internal devices, nonlinearities in amplifiers and other issues related to the generation of laser radiation or due to interaction of laser with matter.

A crucial issue is connected with the important irregular intensity fluctuations that appear in the generation of second harmonic with an intracavity nonlinear device. The nonlinear couplings between modes that are produced in nonlinear crystals give rise to irregular fluctuations in the optical cavity. These fluctuations are amplified from the beginning by the quality factor Q of the laser cavity and by the presence of the laser amplifier media.

Strong fluctuations appear then in the laser intensity. This is clearly a nondesirable situation for practical applications. To give an example of what discussed above, the second harmonic generation (green light) in a diode-pumped intracavity doubled Nd:YAG laser (1.06 μm) [152], is normally accompanied with strong intensity fluctuations. The irregular behavior in this kind of systems was largely investigated [153] and attributed to the destabilization of relaxation oscillations, always present in this kind of lasers, due to the nonlinear coupling of longitudinal modes. Several experimental works have been devoted to eliminate such a chaotic behavior [154].

In the context of chaos control, Roy et al. [16], in a very important experiment, used the Occasional Proportional Feedback method for selecting a series of perturbations of limited durations ("kicks") to the driver of the Nd:YAG pump diodes. The feedback pulses drive the

injection current of the pump diodes at periodic intervals and they are proportional to the difference between the chaotic output signal and a given reference value.

The interval T between successive kicks was adjusted to be roughly the period of the relaxation oscillations. The control parameters of the experiments are, together with the duration of the kick, its amplitude and the reference level.

The results are remarkable in the case of a weak chaotic regime. The authors first prepare the laser as to operate in that regime, by an appropriated orientation of the nonlinear crystal (KTP). The results can be regarded in Fig. 38. The control of period 2, 4 and 9 periodic orbits was obtained in all cases with small amplitude perturbations (a few percents) operating near threshold.

A weak chaotic regime means small output intensity generated in the green frequency (second harmonic). If a significative amount of green light is generated, the regime becomes strongly chaotic and the system is unable to stabilize the output. The authors reported that, by adjusting the reference level to the mean of the chaotic fluctuations and by adjusting the period T to the relaxations oscillations period, the dynamics comes out to realize a stable output. The control voltage fluctuations become very small once the steady state is achieved.

The strong green output case represents a new situation, insofar as here if some parameter (like pump intensity) is changed after the steady state is reached, then the control is lost. The control variables need to be adjusted to stabilize the new operation conditions. Several attempts have been made to overcome this problem by means of a systematic tracking of periodic orbits [155].

By tracking and stabilization techniques [156], a stable output is presented in a pump range very far from threshold (as far as three time above threshold). This implies a strong improvement, even though the results are presented here on the 1.06 μm output (that is on the infrared range).

Besides the interest of the obtained results, there are two qualitative differences between the experiments realized by Ditto et al. and those realized by the group of Roy. The first one is the number of degrees of freedom involved in the dynamics of the system under control. In the case of the magnetoelastic ribbon, the dynamic is conveniently described by few strongly localized modes, whereas in the case of the multimode laser, the system is itself highly dimensional. The second difference is the order of magnitude of temporal scales on which control must be performed. While in the first case the characteristic time scale of oscillations was few seconds, a time sufficient to allow a complicated off line control scheme, in the second case the time scale is of the same order, or even smaller, than the algorithmic time necessary for the calculation of the control signal.

The same group of Roy has later proved experimentally the possibility of synchronizing chaotic lasers [157], with possible application to digital communication [158]. More recently, experiments on communicating with chaos has been carried out in the same group, showing the possibility of encoding and decoding messages with chaotic lasers [159], and the possibility of transmitting a desired message in a very fast way using high-dimensional chaotic waveforms [160,161]. An exhaustive review of different experimental setups for the communication of chaos with time-delayed optical systems is available in Ref. [162].

6.7. Control of chaos in fluids

The first control experiments on a convective fluid were reported by Singer and Bau [12,13]. In these experiments, a fluid is confined in a toroidal cell in a vertical position. The lower half of the cell is surrounded by a heater, whereas the upper part is maintained at a lower temperature

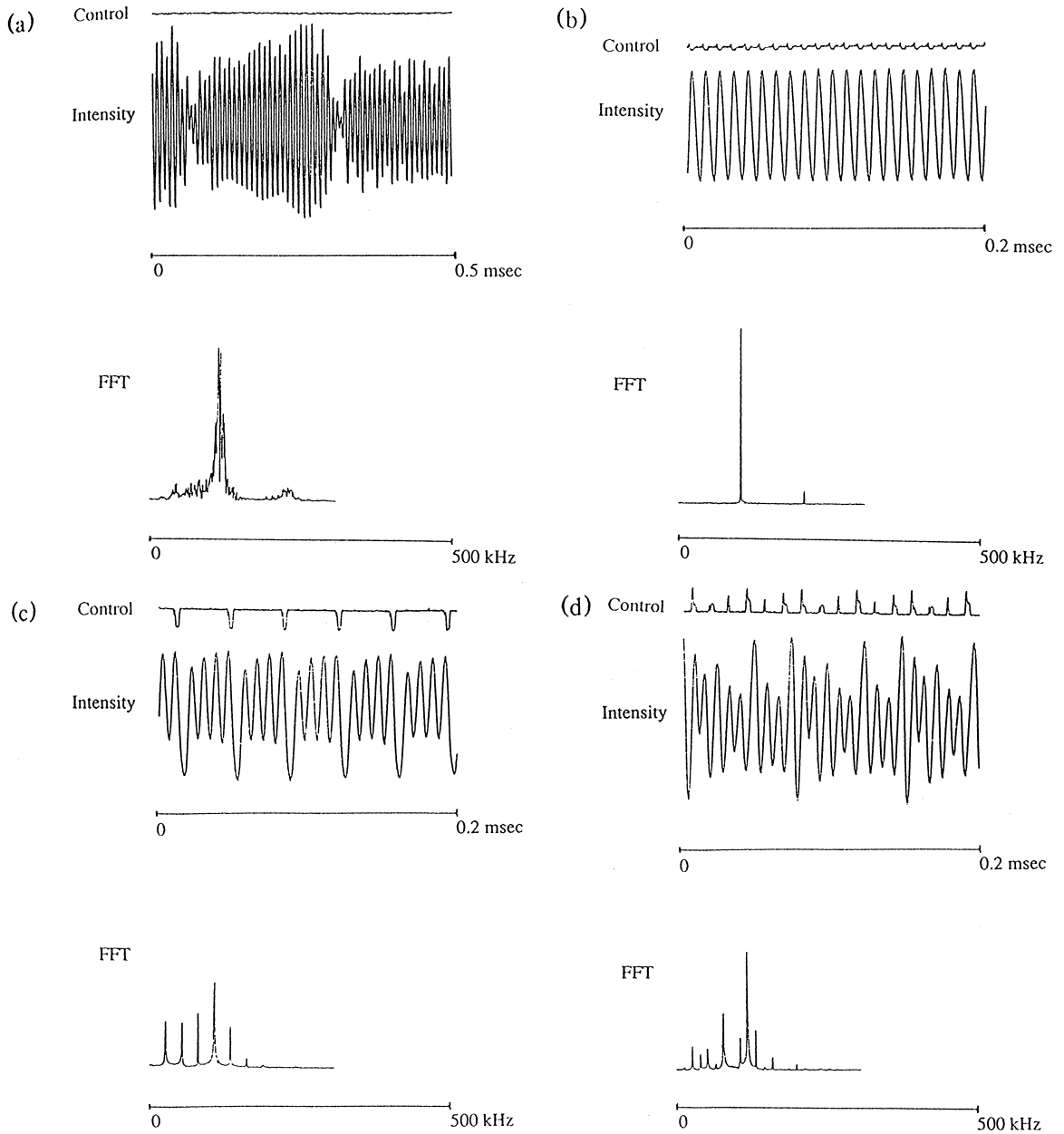

Fig. 38. From Ref. [16]. Temporal traces of the output intensity, control signal and FFT corresponding to (a) no control, (b) period 1, (c) period 4 and (d) period 9.

through a thermal bath. This particular system give rise to a dynamics which can be reduced to the Lorenz model [163]. The chaotic regime is constituted by jumps between two possible basins of attraction, corresponding to the two possible orientations in the rotation direction of the flux inside the convective cell.

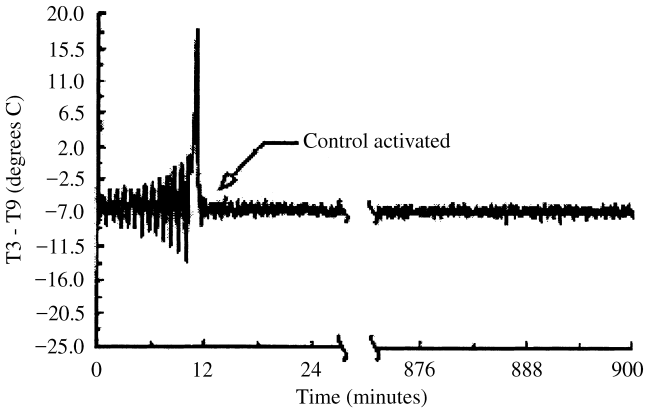

Fig. 39. Temperature difference between positions 3 and 9 o'clock around the loop. the change in the sign corresponds to an inversion in the flow direction.

Chaotic oscillations of the temperature arise associated to the convective flux. The control parameter for this system is the power supplied to the heater. The used control algorithm consisted in a negative feedback acting on the same heater by a perturbation proportional to the temperature difference between the regions where the flux passes from the upper to the lower part of the cell. In Fig. 39 one can clearly see that the chaotic regime is realized by means of oscillations of increasing amplitude intermittently jumping between the two basins of attraction due to the change in the direction of the main convective flux. Such chaotic oscillations are suppressed when the control is turned on.

Another relevant experiment on convective systems was reported by Petrov et al. [164]. In this case, the authors controlled the oscillations inside of a liquid bridge of 3 mm width suffering a temperature difference of about 15°. The relevance of this work is due to the fact that the authors show the effectiveness in the control of an unstable isolated solution in the phase space. This is the case of toroidal trajectories corresponding to a quasiperiodic attractor. This particular solution is encountered in the unperturbed system for sufficiently high temperature difference across the bridge. The control was implemented in two stages. First of all, the authors study the system response against localized temperature perturbations inside the liquid gap. In the second stage, this learning process is used to select the right perturbation able to drive the system toward the desired state. Fig. 40 shows the toroidal regime and the controlled periodic state. In this case it has been shown how a low-dimensional space–time chaotic dynamics can be conveniently controlled by means of localized perturbations.

6.8. Control of chaos in biological and biomechanical systems

Another application of the techniques for chaos control was developed for biomechanical systems. The first experiment on chaos control in this framework was reported by Garfinkel et al. [10,11]. Here, the authors use the OGY method on a preparation of rabbit cardiac muscle. The peculiarity of this case is that the perturbation, instead of acting on the amplitude of the signal, is

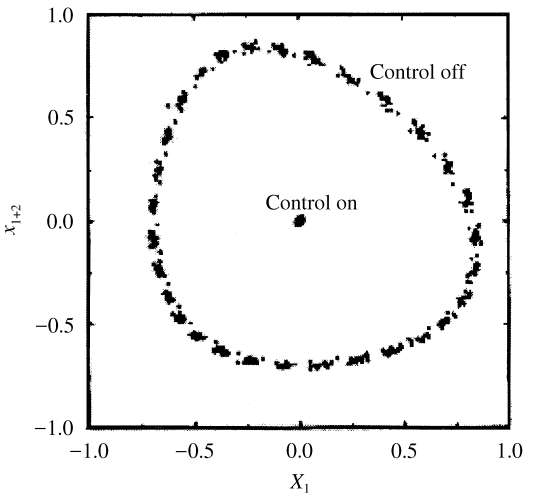

Fig. 40. From Ref. [164]. Second return map constructed from the experimental time series of the temperature measured approximately at the medium of the liquid bridge and near to the free surface. In the figure can be seen the quasiperiodic regime, and the controlled unstable periodic orbit.

applied to vary the interbeat intervals. Fig. 41 shows the control of period 3 periodic orbit. It should be remarked that the intrinsic difficulty here is constituted by the fact that the perturbation must act unidirectionally, insofar as the operator can reduce but cannot increase the natural duration of the pulse, due to the presence of refractoriness in the experimental system.

Another example of control (or *anti*control) of chaos in biological system is the control of the neuronal activity of hippocampal slices realized by Schiff et al. [165]. An interesting suggestion here is that one can, in fact, try to maintain the chaotic state, which sometimes can be preferable. For example, since the epileptic processes are associated with a periodic synchronization of the neuronal tissue, in order to avoid the primer of epilepsis, one can actually implement a technique similar to OGY in order to *anticontrol* the chaos, that is in order to maintain a chaotic state wherever the system would naturally be pushed onto a periodic one.

6.9. Experimental control of chaos by time delay feedback

Another important branch of experimental control of chaos is constituted by different implementations of the method originally introduced by Pyragas [2], that is by the application of a continuous time delayed feedback.

The first experimental evidences of this type of control was reported by Pyragas and Tamasevicius [166]. The experimental setup was an externally driven nonlinear oscillator with a tunnel diode as negative resistance device. Bielawski et al. [167] use essentially the same diode resonator which was used in the experiment by Hunt [15], but with a higher frequency (about 10.3 MHz). The control signal is selected by comparing the output signal with the same signal delayed by a time τ corresponding to the period of the desired orbit. In these conditions, the authors were able to stabilize orbits of different periodicity in the system.

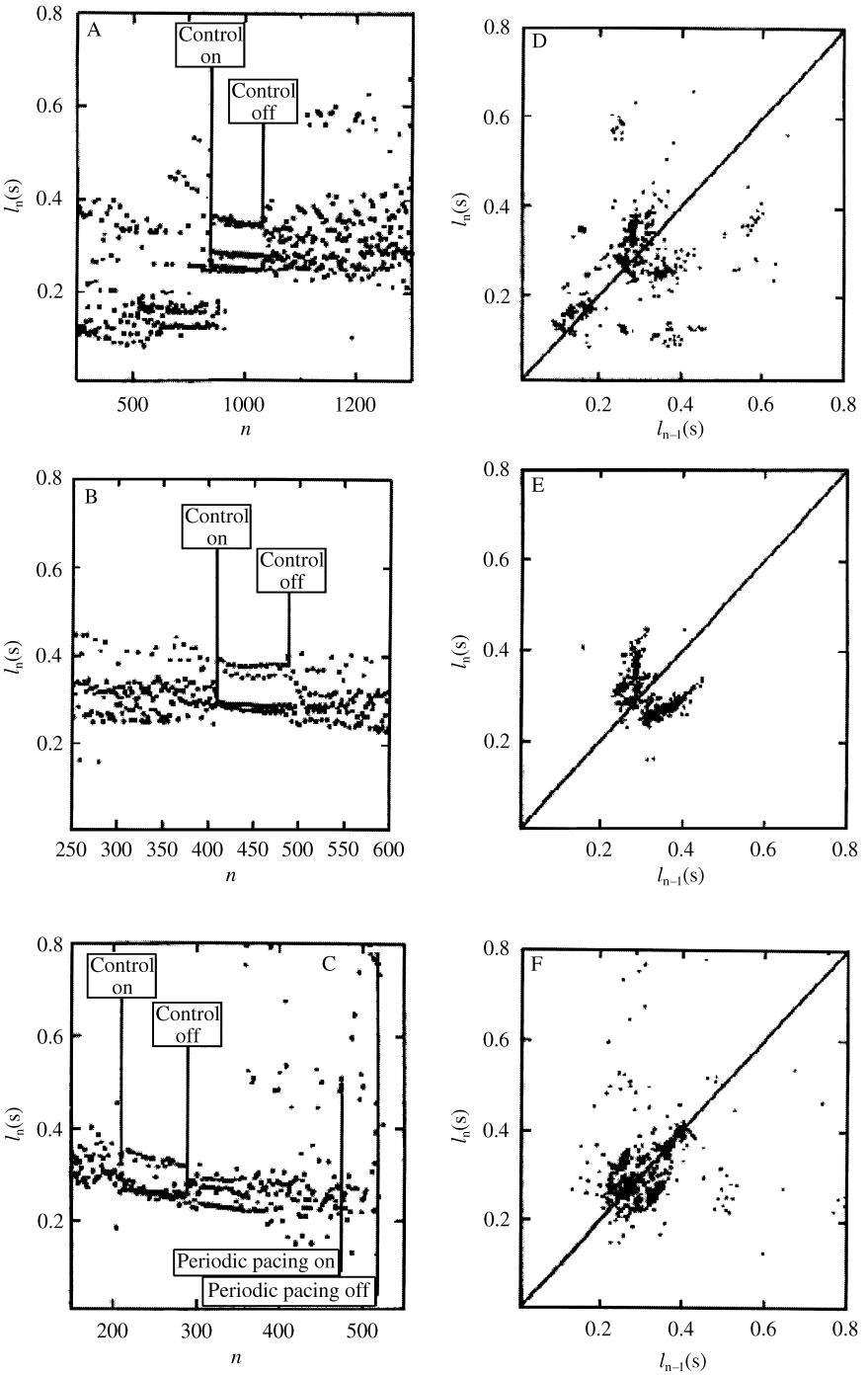

Fig. 41. Reprinted with permission from Science 257, p. 1230, copyright (1992) American Association for the Advancement of Science. (a–c) Interbeat interval I_n versus the beat number during the chaotic phases. (d–f) Corresponding Poincaré sections.

The same technique was later successfully used for the control of laser systems [168], namely in the case of a CO_2 laser with intracavity electro optical modulator.

Another interesting application of feedback control is the implementation of the so called *washout filter*, which was used for the control of the chaotic dynamics generated by both autonomous [169,170] and nonautonomous [171] systems. In both cases the system under control was a CO_2 laser with cavity losses modulated by an electro-optical crystal driven by an external sinusoidal voltage. The control signal is represented by a feedback on such a crystal, with amplitude of the order of few percent of the driving signal.

In chemical systems, the implementation of Pyragas' technique has been provided for the Belouzov–Zhabotinski reaction [172,173] and in enzymatic reactions [174].

6.10. Other experiments

It should be here mentioned the large body of experimental realizations of chaos control in laser systems, posterior to the first evidence by the group of Roy mentioned in Section 6.5. Control of chaos was realized by means of weak parametric perturbations [175], negative feedback of subharmonic components [171,176,177], proportional feedback with delay [178], addition of a weak second periodic signal in a modulated multimode laser [179–181]. Other recent experiments in lasers are reported in Refs. [182,183].

In mechanical systems, the possibility of improving the OGY method has been shown by the use of a Neural Network for the optimization of the interpretation of the experimental results with the aim of finding the different unstable periodic orbits [184]. The OGY method has also been optimized by In et al. [185] through an adaptive technique. Furthermore, OGY has been also used by Kiss et al. [186] for the control of the electrodissolution of a rotating copper disk in a phosphoric acid electrolite. A recent electrochemical experiment is reported in Ref. [187]. Moreover, control of chaos was realized in ionization waves that appear in a periodically excited neon glow discharge [188,189].

More recently, chaos control in experimental high-dimensional systems was realized, namely in a double pendulum [190] and in a two coupled diode resonators [191].

In electronics, the most recent achievements are reported in Refs. [192–195].

Finally, two recent review papers contain discussions and References on some experimental applications of the control of chaos [196,197].

Acknowledgements

The authors are grateful to F.T. Arecchi, E. Barreto, G. Basti, E. Bollt, A. Farini, R. Genesio, A. Giaquinta, S. Hayes, E. Kostelich, A.L. Perrone, F. Romeiras and T. Tél for many fruitful discussions. SB acknowledges financial support from the EEC Contract no. ERBFMBICT983466. CG was supported by DOE and by a joint Brasil-USA grant (CNPq/NSF-INT). YCL was supported by AFOSR under Grant No. F49620-98-1-0400 and by NSF under Grant No. PHY-9722156. HM and DM acknowledge financial support from Ministerio de Educacion y Ciencia (Grant N. PB95-0578) and Universidad de Navarra, Spain (PIUNA).

References

[1] E. Ott, C. Grebogi, J.A. Yorke, Phys. Rev. Lett. 64 (1990) 1196. ***
[2] K. Pyragas, Phys. Lett. A 170 (1992) 421. **
[3] S. Boccaletti, F.T. Arecchi, Europhys. Lett. 31 (1995) 127; ibid. Physica 96D (1996) 9. **
[4] T. Kapitaniak (Ed.), Special Issue: Controlling Chaos, Chaos Solitons and Fractals 8 (9) (1997).
[5] W.L. Ditto, K. Showalter (Eds.), Focus Issue: Control and Synchronization of Chaos, Chaos 7 (4) (1997).
[6] C. Grebogi, Y.-C. Lai, S. Hayes, Int. J. Bifurcation Chaos 7 (1997) 2175.
[7] F.T. Arecchi, S. Boccaletti, M. Ciofini, C. Grebogi, R. Meucci (Eds.), Theme Issue: Control of Chaos: New Perspectives in Experimental and Theoretical Nonlinear Science, Part I, Int. J. Bifurcation Chaos 8 (8) (1998).
[8] F.T. Arecchi, S. Boccaletti, M. Ciofini, C. Grebogi, R. Meucci (Eds.), Theme Issue: Control of Chaos: New Perspectives in Experimental and Theoretical Nonlinear Science, Part II, Int. J. Bifurcation Chaos 8 (9) (1998).
[9] W.L. Ditto, S.N. Rauseo, M.L. Spano, Phys. Rev. Lett. 65 (1990) 3211. **
[10] A. Garfinkel, M. Spano, W. Ditto, J. Weiss, Science 257 (1992) 1230.
[11] A. Garfinkel, J. Weiss, W. Ditto, M. Spano, Trends Cardiovasc. Med. 5 (1995) 76.
[12] J. Singer, H.H. Bau, Phys. Fluids A 3 (1991) 2859.
[13] J. Singer, Y.-Z. Wang, H.H. Bau, Phys. Rev. Lett. 66 (1991) 1123.
[14] A. Azevedo, S. Rezende, Phys. Rev. Lett. 66 (1991) 1342.
[15] E.R. Hunt, Phys. Rev. Lett. 67 (1991) 1953. **
[16] R. Roy, T. Murphy, T. Maier, Z. Gills, Phys. Rev. Lett. 68 (1992) 1259. **
[17] V. Petrov, V. Gáspár, J. Masere, K. Showalter, Nature 361 (1993) 240. **
[18] A.N. Kolmogorov, Dokl. Akad Nauk 119 (1958) 861; ibid., Dokl. Akad. Nauk 124 (1959) 754.
[19] S. Newhouse, Ergodic Theory Dynamical Systems 8 (1988) 283.
[20] S. Newhouse, Ann. Math. 129 (1989) 215.
[21] S. Hayes, C. Grebogi, E. Ott, A. Mark, Phys. Rev. Lett. 73 (1994) 1781. *
[22] L.M. Pecora, T.L. Carroll, Phys. Rev. Lett. 64 (1990) 821. **
[23] E. Ott, C. Grebogi, J.A. Yorke, in: D. Campbell (Ed.), CHAOS/XAOC, Soviet-American Perspective on Nonlinear Science, American Institute of Physics, New York, 1990, pp. 153–172.
[24] S. Hayes, C. Grebogi, E. Ott, Phys. Rev. Lett. 70 (1993) 3031. *
[25] Y.-C. Lai, Controlling chaos, Comput. Phys. 8 (1994) 62.
[26] F. Takens, Detecting strange attractors in turbulence, in: D.A. Rand, L.-S. Young (Eds.), Dynamical Systems and Turbulence, Lecture Notes in Mathematics, Vol. 898, Springer, New York, 1980, pp. 366–381. ***
[27] N. Packard, J. Crutchfield, J.D. Farmer, R. Shaw, Phys. Rev. Lett. 45 (1980) 712.
[28] K.T. Alligood, T.D. Sauer, J.A. Yorke, Chaos: An Introduction to Dynamical Systems, Springer, New York, 1997.
[29] J.D. Farmer, E. Ott, J.A. Yorke, Physica D 7 (1983) 153.
[30] J.-P. Eckmann, D. Ruelle, Rev. Mod. Phys. 57 (1985) 617. ***
[31] C. Grebogi, E. Ott, J.A. Yorke, Phys. Rev. Lett. 48 (1982) 1507.
[32] C. Grebogi, E. Ott, J.A. Yorke, Physica D 7 (1983) 181.
[33] H.E. Nusse, J.A. Yorke, Physica D 36 (1989) 137.
[34] Y.-C. Lai, C. Grebogi, J.A. Yorke, I. Kan, Nonlinearity 6 (1993) 779.
[35] T. Shinbrot, E. Ott, C. Grebogi, J.A. Yorke, Phys. Rev. Lett. 65 (1990) 3215.
[36] E.J. Kostelich, C. Grebogi, E. Ott, J.A. Yorke, Phys. Rev. E 47 (1993) 305. *
[37] E.M. Bollt, J.D. Meiss, Phys. Lett. A 204 (1995) 373.
[38] E.M. Bollt, J.D. Meiss, Physica D 81 (1995) 280.
[39] C. Grebogi, E. Ott, J.A. Yorke, Phys. Rev. A 37 (1988) 1711.
[40] M. Hénon, Comm. Math. Phys. 50 (1976) 69.
[41] F.J. Romeiras, C. Grebogi, E. Ott, W.P. Dayawansa, Physica D 58 (1992) 165.
[42] K. Ogata, Modern Control Engineering, 2nd Edition, Prentice-Hall, Englewood, NJ, 1990.
[43] C. Grebogi, E. Ott, F.J. Romeiras, J.A. Yorke, Phys. Rev. A 36 (1987) 5365.
[44] C. Grebogi, E. Kostelich, E. Ott, J.A. Yorke, Physica D 25 (1987) 347.
[45] U. Dressler, G. Nitsche, Phys. Rev. Lett. 68 (1992) 1.

[46] D.P. Lathrop, E.J. Kostelich, Phys. Rev. A 40 (1989) 4028.
[47] D. Auerbach, P. Cvitanović, J.-P. Eckmann, G. Gunaratne, I. Procaccia, Phys. Rev. Lett. 58 (1987) 2387. ***
[48] D. Auerbach, C. Grebogi, E. Ott, J.A. Yorke, Phys. Rev. Lett. 69 (1992) 3479.
[49] P. Chossat, M. Golubitsky, Physica D 32 (1988) 423.
[50] W. Chin, C. Grebogi, I. Kan, Random Comput. Dyn. 1 (1992) 349.
[51] Y.-C. Lai, C. Grebogi, Phys. Rev. E 47 (1993) 2357.
[52] Y.-C. Lai, C. Grebogi, Phys. Rev. E 49 (1994) 1094.
[53] Y. Nagai, Y.-C. Lai, Phys. Rev. E 51 (1995) 3842.
[54] E. Rosa, S. Hayes, C. Grebogi, Phys. Rev. Lett. 78 (1997) 1247.
[55] E. Bollt, M. Dolnik, Phys. Rev. E 55 (1997) 6404.
[56] E. Bollt, Y.-C. Lai, C. Grebogi, Phys. Rev. Lett. 79 (1997) 3787.
[57] E. Bollt, Y.-C. Lai, Phys. Rev. E 58 (1998) 1724.
[58] B.B. Plapp, A.W. Huebler, Phys. Rev. Lett. 65 (1990) 2302; E.A. Jackson, A.W. Huebler, Physica D 44 (1990) 407.
[59] R. Lima, M. Pettini, Phys. Rev. A 41 (1990) 726. *
[60] Y. Braiman, J. Goldhirsch, Phys. Rev. Lett. 66 (1991) 2545.
[61] G.B. Mindlin, X.-J. Hou, H.G. Solari, R. Gilmore, N.B. Tufillaro, Phys. Rev. Lett. 64 (1990) 2350; P. Cvitanovic, G.H. Gunaratne, I. Procaccia, Phys. Rev. A 38 (1988) 1503; G.H. Gunaratne, P.S. Linsay, M.J. Vinson, Phys. Rev. Lett. 63 (1989) 1; N.B. Tufillaro, H.G. Solari, R. Gilmore, Phys. Rev. A 41 (1990) 5717.
[62] D.J. Gauthier, D.K. Sukow, H.M. Concannon, J.E.S. Socolar, Phys. Rev. E 50 (1994) 2343; J.E.S. Socolar, D.K. Sukow, D.J. Gauthier, Phys. Rev. E 50 (1994) 3245.
[63] K. Pyragas, Phys. Lett. A 206 (1995) 323.
[64] F.T. Arecchi, G. Basti, S. Boccaletti, A.L. Perrone, Europhys. Lett. 26 (1994) 327. *
[65] S. Boccaletti, A. Farini, F.T. Arecchi, Phys. Rev. E 55 (1997) 4979.
[66] S. Boccaletti, A. Farini, E.J. Kostelich, F.T. Arecchi, Phys. Rev. E 55 (1997) R4845.
[67] S. Boccaletti, A. Giaquinta, F.T. Arecchi, Phys. Rev. E 55 (1997) 5393.
[68] S. Boccaletti, D. Maza, H. Mancini, R. Genesio, F.T. Arecchi, Phys. Rev. Lett. 79 (1997) 5246. *
[69] F.T. Arecchi et al., Phys. Rev. A 45 (1992) R4225; G. Giacomelli et al., Phys. Rev. Lett. 73 (1994) 1099.
[70] G. Giacomelli, A. Politi, Phys. Rev. Lett. 76 (1996) 2686.
[71] J.D. Farmer, Physica D 4 (1982) 366; K. Ikeda, M. Matsumoto, J. Stat. Phys. 44 (1986) 955.
[72] F. Plaza, M.G. Velarde, F.T. Arecchi, S. Boccaletti, M. Ciofini, R. Meucci, Europhys. Lett. 38 (1997) 85.
[73] E. Villermaux, E.J. Hopfinger, Physica D 72 (1994) 230.
[74] E. Villermaux, Phys. Rev. Lett. 75 (1995) 4618.
[75] E. Villermaux, Nature 371 (1994) 24.
[76] H. Mancini, D. Maza, Phys. Rev. E 55 (1997) 2757.
[77] R. Montagne, E. Hernández-Garcia, M. San Miguel, Phys. Rev. Lett. 77 (1996) 267; A. Torcini, Phys. Rev. Lett. 77 (1996) 1047.
[78] C. Grebogi, S.W. McDonald, E. Ott, J.A. Yorke, Phys. Lett. A 99 (1983) 415.
[79] S.W. McDonald, C. Grebogi, E. Ott, J.A. Yorke, Physica D 17 (1985) 125.
[80] F.C. Moon, G.-X. Li, Phys. Rev. Lett. 55 (1985) 1439.
[81] E.G. Gwinn, R.M. Westervelt, Phys. Rev. A 33 (1986) 4143.
[82] H.B. Stewart, Y. Ueda, Proc. Roy. Soc. London A 432 (1991) 113.
[83] J.M.T. Thompson, H.B. Stewart, Y. Ueda, Phys. Rev. E 49 (1994) 1019.
[84] L.M. Pecora, T.L. Carroll, Phys. Rev. A 44 (1991) 2374.
[85] Y.-C. Lai, Phys. Lett. A 221 (1996) 375.
[86] C. Grebogi, H.E. Nusse, E. Ott, J.A. Yorke, Basic sets: sets that determine the dimension of basin boundaries, in: J.C. Alexander (Ed.), Lecture Notes in Mathematics, Vol. 1342, Springer, New York, 1988, pp. 220–250.
[87] C. Grebogi, E.J. Kostelich, E. Ott, J.A. Yorke, Physica D 25 (1987) 347.
[88] Y.-C. Lai, R.L. Winslow, Phys. Rev. Lett. 72 (1994) 1640.
[89] Y.-C. Lai, R.L. Winslow, Physica D 74 (1994) 353.
[90] J.C. Alexander, J.A. Yorke, Z. You, I. Kan, Int. J. Bifurcation Chaos 2 (1992) 795.
[91] I. Kan, Bull. Am. Math. Soc. 31 (1994) 68.

[92] E. Ott, J.C. Alexander, I. Kan, J.C. Sommerer, J.A. Yorke, Physica D 76 (1994) 384.
[93] Y.-C. Lai, C. Grebogi, Phys. Rev. E 52 (1995) R3313.
[94] J.F. Heagy, T.L. Carroll, L.M. Pecora, Phys. Rev. Lett. 73 (1994) 3528.
[95] P. Ashwin, J. Buescu, I.N. Stewart, Phys. Lett. A 193 (1994) 126.
[96] P. Ashwin, J. Buescu, I.N. Stewart, Nonlinearity 9 (1996) 703.
[97] T.C. Newell, P.M. Alsing, A. Gaverielides, V. Kovanis, Phys. Rev. Lett. 72 (1994) 1647.
[98] T.C. Newell, P.M. Alsing, A. Gavrielides, V. Kovanis, Phys. Rev. E 51 (1995) 2963.
[99] T. Shinbrot, E. Ott, C. Grebogi, J.A. Yorke, Phys. Rev. A 45 (1992) 4165. *
[100] T. Shinbrot, W. Ditto, C. Grebogi, E. Ott, M. Spano, J.A. Yorke, Phys. Rev. Lett. 68 (1992) 2863.
[101] T. Shinbrot, C. Grebogi, E. Ott, J.A. Yorke, Phys. Lett. A 169 (1992) 349.
[102] T. Shinbrot, C. Grebogi, E. Ott, J.A. Yorke, Nature 363 (1993) 411.
[103] E. Barreto, E.J. Kostelich, C. Grebogi, E. Ott, J.A. Yorke, Phys. Rev. E 51 (1995) 4169.
[104] D. Gligorosky, D. Dimovsky, V. Urumov, Phys. Rev. E 51 (1995) 1690.
[105] O.E. Rössler, Phys. Lett. A 57 (1976) 397.
[106] K.M. Cuomo, A.V. Oppenheim, Phys. Rev. Lett. 71 (1993) 65.
[107] G. Pérez, H.A. Cerdeira, Phys. Rev. Lett. 74 (1995) 1970.
[108] L. Kocarev, U. Parlitz, Phys. Rev. Lett. 74 (1995) 5028.
[109] N.J. Metha, R.M. Henderson, Phys. Rev. A 44 (1991) 4861.
[110] K. Kaneko, Focus issue on coupled map lattices, Chaos 2 (1992). *
[111] Y.-C. Lai, C. Grebogi, Phys. Rev. E 50 (1994) 1894.
[112] B.D. Anderson, J.B. Moore, Optimal Filtering, Prentice-Hall, Englewood Cliffs, NJ, 1990, pp. 193–211.
[113] P. So, E. Ott, W.P. Dayawansa, Phys. Rev. E 49 (1994) 2650.
[114] Y.-C. Lai, C. Grebogi, J.A. Yorke, Sudden change in the size of chaotic attractors: how does it occur?, in: J.H. Kim, J. Stringer (Eds.), Applied Chaos, Wiley, New York, 1992.
[115] C.E. Shannon, W. Weaver, The Mathematical Theory of Communication, University of Illinois Press, Urbana, 1964.
[116] R.E. Blahut, Principles and Practice of Information Theory, Addison-Wesley, Reading, MA, 1988.
[117] R.L. Adler, A.G. Konheim, M.H. McAndrew, Trans. Am. Math. Soc. 114 (1965) 309.
[118] S. Taherion, Y.-C. Lai, Encoding digital information using transient chaos, preprint, 1998.
[119] T. Tél, Transient chaos, in: B.-L. Hao (Ed.), Directions in Chaos, Vol. 3, World Scientific, Singapore, 1990.
[120] T. Tél, Transient chaos: a type of metastable state, in: B.-L. Hao (Ed.), STATPHYS 19, World Scientifc, Singapore, 1996.
[121] P. Gaspard, S.A. Rice, J. Phys. Chem. 93 (1989) 6947.
[122] I. Burghardt, P. Gaspard, Chem. Phys. 225 (1997) 259.
[123] Q. Chen, E. Ott, L. Hurd, Phys. Lett. A 156 (1991) 48.
[124] M.J. Feigenbaum, J. Stat. Phys. 19 (1978) 25. ***
[125] Y.-C. Lai, E. Bollt, C. Grebogi, Communicating with chaos using two-dimensional symbolic dynamics, preprint, 1988.
[126] P. Grassberger, H. Kantz, Phys. Lett. A 113 (1985) 235.
[127] P. Grassberger, H. Kantz, U. Moenig, J. Phys. A: Math. Gen. 22 (1989) 5217.
[128] R. Bowen, Equilibrium States and the Ergodic Theory of Anosov Diffeomorphisms, Springer, Berlin, 1975.
[129] J. Guckenheimer, P. Holmes, Nonlinear Oscillations, Dynamical Systems, and Bifurcations of Vector Fields, Springer, New York, 1983.
[130] S. Newhouse, T. Pignataro, J. Stat. Phys. 72 (1993) 1331.
[131] P. Cvitanovic, G. Gunaratne, I. Procaccia, Phys. Rev. A 38 (1988) 1503.
[132] J. Milnor, R. Thurston, On Iterated Map of Interval, Princeton University Press, Princeton, 1977.
[133] T. Tél, J. Phys. A: Math. Gen. 24 (1991) L1359.
[134] Y.-C. Lai, T. Tél, C. Grebogi, Phys. Rev. E 48 (1993) 709.
[135] Y.-C. Lai, C. Grebogi, T. Tél, Controlling transient chaos in dynamical systems, in: Towards the Harnessing of Chaos, the 7th TOYOTA Conference, Elsevier, Amsterdam, 1994, pp. 153–167.
[136] M. Dhamala, Y.-C. Lai, Phys. Rev. E 59 (1999) 1646.

[137] S.J. Schiff, K. Jerger, D.H. Duong, T. Chang, M.L. Spano, W.L. Ditto, Nature 370 (1994) 615.
[138] V. In, S. Mahan, W.L. Ditto, M.L. Spano, Phys. Rev. Lett. 74 (1995) 4420.
[139] W. Yang, M. Ding, A.J. Mandell, E. Ott, Phys. Rev. E 51 (1995) 102.
[140] V. In, M. Spano, M. Ding, Phys. Rev. Lett. 80 (1998) 700.
[141] J.H. Peng, E.J. Ding, M. Ding, W. Yang, Phys. Rev. Lett. 76 (1996) 904.
[142] M. Ding, E. Ott, Phys. Rev. E 49 (1994) R945.
[143] J.J. D'azzo, C.H. Houpis, Feedback Control System Analysis and Synthesis, McGraw-Hill, New York, 1969.
[144] L. Fronzoni, M. Giacondo, M. Pettini, Phys. Rev. A 43 (1991) 6483.
[145] W. Ditto, S. Rauseo, R. Cawley, C. Grebogi, G. Hsu, E. Kostelich, E. Ott, H. Savage, R. Segnan, M. Spano, J. Yorke, Phys. Rev. Lett. 63 (1989) 923.
[146] A.N. Pisarchick, V.N. Chizhevsky, R. Corbalán, R. Vilaseca, Phys. Rev. E 55 (1997) 2455.
[147] A.N. Pisarchick, B.F. Kuntsevich, R. Corbalán, Phys. Rev. E 58 (1998) R2697.
[148] B. Peng, V. Petrov, K. Showalter, J. Phys. Chem. 95 (1991) 4957.
[149] B.P. Belousov, Sbornik Referatov po Radiatsinnoi Meditsine, 145 (Medgiz, Moscow, 1958). A.M. Zhabotinsky Biofizika 9 (1964) 306 (in Russian).
[150] V. Petrov, B. Peng, K. Showalter, J. Chem. Phys. 96 (1992) 7506.
[151] V. Petrov, M. Crowley, K. Showalter, Phys. Rev. Lett. 72 (1994) 2955.
[152] T. Baer, J. Opt. Soc. Am. B 3 (1986) 1175.
[153] C. Bracikovski, R. Roy, Chaos 1 (1991) 49.
[154] R. Roy, Z. Gills, K.S. Thornburg, Opt. Photon. News 5 (1994) 9.
[155] I. Schwartz, I. Triandaf, Phys. Rev. A 46 (1992) 7439; T. Carroll et al., Phys. Rev. A 46 (1992) 6189.
[156] Z. Gills et al., Phys. Rev. Lett. 69 (1992) 3169.
[157] R. Roy, K. Scott Thornburg, Phys. Rev. Lett. 72 (1994) 2009.
[158] P. Colet, R. Roy, Opt. Lett. 19 (1994) 2056.
[159] P.M. Alsing, A. Gavrielides, V. Kovanis, R. Roy, K. Scott Thornburg, Phys. Rev. E 56 (1997) 6302.
[160] G.D. Van Wiggeren, R. Roy, Science 279 (1998) 1198. *
[161] G.D. Van Wiggeren, R. Roy, Phys. Rev. Lett. 81 (1998) 3547.
[162] G.D. Van Wiggeren, R. Roy, Chaotic communication with time-delayed optical systems, Int. J. Bifurcation Chaos (1999), to appear.
[163] W. Malkus, Mem. Soc. Roy. Sci. Liege Collet 4 (1972) 125.
[164] V. Petrov, M. Schatz, K. Muehlner, S. VanHook, W. McCormick, J.B. Swift, H. Swinney, Phys. Rev. Lett. 77 (1996) 3779. *
[165] S. Schiff, K. Jerger, D. Duong, T. Chang, M. Spano, W. Ditto, Nature 370 (1994) 615.
[166] K. Pyragas, T. Tamasevicius, Phys. Lett. A 180 (1993) 99.
[167] S. Bielawski, D. Derozier, P. Glorieux, Phys. Rev. E 49 (1994) R971.
[168] S. Bielawski, M. Bouazaoui, D. Derozier, P. Glorieux, Phys. Rev. A 47 (1993) 3276.
[169] R. Meucci, M. Ciofini, R. Abbate, Phys. Rev. E 53 (1996) R5537.
[170] M. Ciofini, A. Labate, R. Meucci, Phys. Lett. A 227 (1997) 31.
[171] R. Meucci, A. Labate, M. Ciofini, Phys. Rev. E 56 (1997) 2829.
[172] F. Schneider, R. Blittersdorf, A. Foster, T. Hauck, D. Lebender, J. Müller, J. Phys. Chem. 97 (1993) 12,244.
[173] A. Guderian, A. Münster, M. Kraus, F. Schneider, J. Phys. Chem. 102 (1998) 5059.
[174] A. Lekebusch, A. Föster, W. Schneider, J. Phys. Chem. 99 (1995) 681.
[175] R. Meucci, W. Gadosmki, M. Ciofini, F.T. Arecchi, Phys. Rev. E 49 (1994) R2528.
[176] R. Meucci, W. Gadomski, M. Ciofini, F.T. Arecchi, Phys. Rev. E 52 (1995) 4676.
[177] M. Ciofini, R. Meucci, F.T. Arecchi, Phys. Rev. E 52 (1995) 94.
[178] J.M. Perez, J. Steinshnider, R. Stallcup, A. Aviles, Appl. Phys. Lett. 65 (1994) 1216.
[179] K. Otsuka, J. Chern, J. Lih, Opt. Lett. 22 (1997) 292.
[180] M. Tsunekane, N. Taguchi, H. Inaba, Opt. Lett. 22 (1997) 1000.
[181] M. Basso, R. Genesio, M. Stanghini, A. Tesi, Chaos Solitons Fractals 8 (1997) 1449.
[182] V. Chizhevsky, R. Vilaseca, R. Corbalán, Int. J. Bifircation Chaos 8 (1998) 1777.
[183] A. Pisarchik, R. Corbalán, V. Chizhevsky, R. Vilaseca, B. Kuntsevich, Int. J. Bifurcation Chaos 8 (1998) 1783.

[184] R. Bakker, J. Schouten, F. Takens, Cor M. van den Bleek, Phys. Rev. E 54 (1996) 3545.
[185] V. In, W. Ditto, M. Spano, Phys. Rev. E 51 (1995) R2689.
[186] I.Z. Kiss, V. Gaspar, L. Nyikos, P. Parmananda, J. Phys. Chem. A 101 (1997) 8668.
[187] M. Rhode, R. Rollings, H. Dewald, Chaos 7 (1997) 653.
[188] K. Weltmann, T. Klinger, C. Wilke, Phys. Rev. E 52 (1995) 2106.
[189] T. Braun, Int. J. Bifurcation Chaos 8 (1998) 1739.
[190] D. Christini, J. Collins, P. Linsay, Phys. Rev. E 54 (1996) 4824.
[191] M. Löcher, E. Hunt, Phys. Rev. Lett. 79 (1997) 63.
[192] D. Sukow, M. Bleich, D. Gauthier, J. Socolar, Chaos 7 (1997) 560.
[193] Z. Galias, C. Murphy, M. Kennedy, M. Ogorzalek, Chaos Solitons Fractals 8 (1997) 1471.
[194] C. Hwang, J. Hsieh, R. Lin, Chaos Solitons Fractals 8 (1997) 1517.
[195] S. Rajasekar, K. Murali, M. Lakshmanan, Chaos Solitons Fractals 8 (1997) 1545.
[196] F.T. Arecchi, S. Boccaletti, M. Ciofini, R. Meucci, C. Grebogi, Int. J. Bifurcation Chaos 8 (1998) 1643.
[197] P. Glorieux, Int. J. Bifurcation Chaos 8 (1998) 1749.